AD-A121 487 RYDBERG STATES OF 7LI(2) BY PULSED OPTICAL-OPTICAL DOUBLE RESONANCE SPECT..(U) PENNSYLVANIA STATE UNIV UNIVERSITY PARK APPLIED RESEARCH LAB.. T L TIPTON 1/2

UNCLASSIFIED 12 AUG 82 ARL/PSU/TM-82-181 F/G 20/6 NL

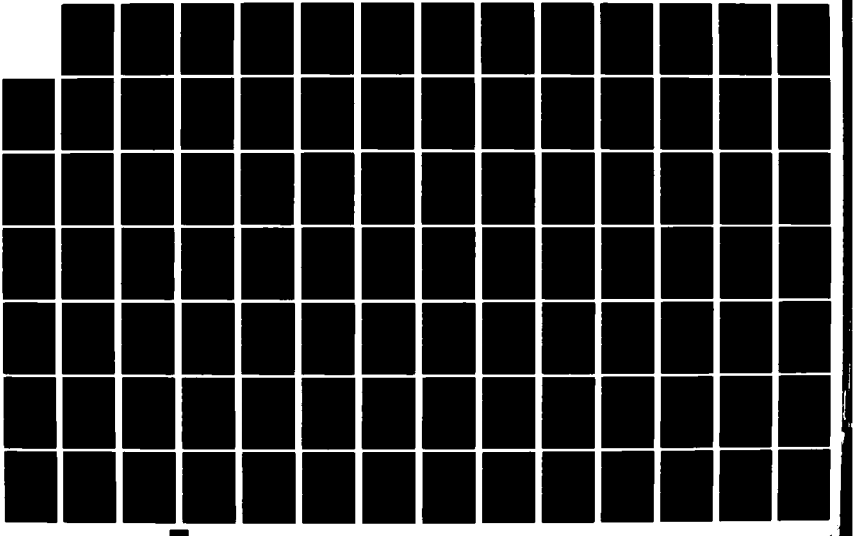

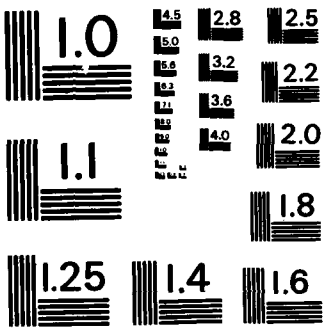

MICROCOPY RESOLUTION TEST CHART

NATIONAL BUREAU OF STANDARDS - 1963 - A

(6)

RYDBERG STATES OF $^7Li_2$ BY PULSED OPTICAL-OPTICAL DOUBLE RESONANCE SPECTROSCOPY

Terence L. Tipton

Technical Memorandum
File No. TM 82-181
August 12, 1982
Contract No. N00024-79-C-6043

Copy No. 6

The Pennsylvania State University
Intercollege Research Programs and Facilities
APPLIED RESEARCH LABORATORY
Post Office Box 30
State College, PA 16801

NAVY DEPARTMENT

NAVAL SEA SYSTEMS COMMAND

UNCLASSIFIED

SECURITY CLASSIFICATION OF THIS PAGE *(When Data Entered)*

REPORT DOCUMENTATION PAGE		READ INSTRUCTIONS BEFORE COMPLETING FORM
1. REPORT NUMBER 82-181	2. GOVT ACCESSION NO. A121487	3. RECIPIENT'S CATALOG NUMBER
4. TITLE *(and Subtitle)* RYDBERG STATES OF $^7Li_2$ BY PULSED OPTICAL-OPTICAL DOUBLE RESONANCE SPECTROSCOPY		5. TYPE OF REPORT & PERIOD COVERED Ph.D. November 1982 6. PERFORMING ORG. REPORT NUMBER 82-181
7. AUTHOR(s) Terence L. Tipton		8. CONTRACT OR GRANT NUMBER(s) N00024-79-C-6043
9. PERFORMING ORGANIZATION NAME AND ADDRESS The Pennsylvania State University Applied Science Laboratory, P.O. Box 30 State College, Pa. 16801		10. PROGRAM ELEMENT, PROJECT, TASK AREA & WORK UNIT NUMBERS
11. CONTROLLING OFFICE NAME AND ADDRESS Naval Sea Systems Command Department of the Navy Washington, DC 20362		12. REPORT DATE August 12, 1982 13. NUMBER OF PAGES 183 pages
14. MONITORING AGENCY NAME & ADDRESS*(if different from Controlling Office)*		15. SECURITY CLASS. *(of this report)* Unclassified, Unlimited 15a. DECLASSIFICATION/DOWNGRADING SCHEDULE

16. DISTRIBUTION STATEMENT *(of this Report)*

Approved for public release, distribution unlimited,
per NSSC (Naval Sea Systems Command), 9/22/82

17. DISTRIBUTION STATEMENT *(of the abstract entered in Block 20, if different from Report)*

18. SUPPLEMENTARY NOTES

19. KEY WORDS *(Continue on reverse side if necessary and identify by block number)*

thesis, lithium, spectroscopy

Sigma Pi

20. ABSTRACT *(Continue on reverse side if necessary and identify by block number)*

Three Rydberg series of electronic states of $^7Li_2$ have been characterized by pulsed optical-optical double resonance spectroscopy. The observed Rydberg states, which include the previously reported $E\,^1\Sigma_g^+$ and $G\,^1\Pi_g$ states, have been identified as 3-10s$\sigma\,^1\Sigma_g^+$, and 3-10d$\sigma\,^1\Sigma_g^+$, and 3-15d$\pi\,^1\Pi_g$. The molecular constants for several of the upper members of each of the above

DD FORM 1 JAN 73 1473 EDITION OF 1 NOV 65 IS OBSOLETE UNCLASSIFIED

SECURITY CLASSIFICATION OF THIS PAGE *(When Data Entered)*

series have been used to deduce the ionization potential of $^7Li_2$ and molecular constants for the $X^2\Sigma_g^+$ state of $^7Li_2^+$. The former was determined to be $T_o(\infty)=41496 \pm 4$ cm^{-1}. The latter, were found to be in good agreement with recent ab initio calculations.

Low-order Dunham coefficients that describe at least the range v=0-2 are reported for twenty-eight previously uncharacterized gerade states of $^7Li_2$. All but one of these states were determined to be correlated with a Li(2s) + Li(ns) or Li(2s) + Li(nd) atomic configuration. Improved results for the previously examined $E^1\Pi_g^+$ (or $3s\sigma^1\Sigma_g^+$) state are also presented. Special attention is given to the $E^1\Sigma_g^+$ state because: 1) a disproportionately large data base (v=0-12) was obtained; 2) a singular experimental arrangement was used; 3) accurate ab initio calculations are available; and 4) a double minimum may exist in the potential as a result of a strong interaction with the $^7Li_2$ (±) ion pair potential.

RKR potentials were derived from the above Dunham coefficients for all states that appeared to be unperturbed. Franck-Condon factors were then calculated from transitions from the intermediate $A^1\Sigma_u^+$ state to each of the excited gerade states.

A large number of both homogeneous and heterogeneous perturbations were observed. These included intensity anomalies in $ns\sigma^1\Sigma_g^+ \leftrightarrow A^1\Sigma_u^+$ transitions resulting from $\Delta\Lambda=\pm1$ interactions. Deperturbations of the mutually perturbing $9d\pi^1\Pi_g$ and $10d\pi^1\Pi_g$ states were performed, yielding results that are described accurately by a model previously used for H_2.

Two significant revisions were made in experimental procedures reported earlier. First, a versatile new laser dye mixture was discovered and successfully utilized in the investigation of the Rydberg states of $^7Li_2$. Second, a computer-based data collection system was used in place of chart reading as the means of obtaining spectral line frequencies from raw d.c. voltage data.

Abstract

Three Rydberg series of electronic states of $^7Li_2$ have been characterized by pulsed optical-optical double resonance spectroscopy. The observed Rydberg states have been identified as 3-10s$\sigma\,^1\Sigma_g^+$, 3-10d$\sigma\,^1\Sigma_g^+$, and 3-15d$\pi\,^1\Pi_g$. The molecular constants for several of the upper members of each of the above series have been used to deduce the ionization potential of $^7Li_2$ and molecular constants for the $X^2\Sigma_g^+$ state of $^7Li_2^+$. The former was determined to be $T_o(\infty)$= 41496±4 cm^{-1}. The latter were found to be in good agreement with recent ab initio calculations.

Low-order Dunham coefficients that describe at least the range v=0-2 are reported for twenty-eight previously uncharacterized gerade states of $^7Li_2$. All but one of these states were determined to be correlated with a Li(2s)+Li(ns) or Li(2s)+Li(nd) atomic configuration. Improved results for the previously examined $E^1\Sigma_g^+$ (or 3s$\sigma\,^1\Sigma_g^+$) state are also presented. Special attention is given to the $E^1\Sigma_g^+$ state because: 1) a disproportionately large data base (v*=0-12) was obtained; 2) a singular experimental arrangement was used; 3) accurate ab initio calculations are available; and 4) a double minimum may exist in the potential as a result of a strong interaction with the $^7Li_2(+,-)$ ion pair potential.

RKR potentials were derived from the above Dunham coefficients for all states that appeared to be unperturbed Franck-Condon factors were then calculated for transitions from the intermediate $A^1\Sigma_u^+$ state to each of the excited gerade states.

A large number of both homogeneous and heterogeneous perturbations were observed. These included intensity anomalies in $ns\sigma\,^1\Sigma_g^+ \leftarrow A\,^1\Sigma_u^+$ transitions resulting from $\Delta\Lambda=\pm1$ interactions. Deperturbations of the mutually perturbing $9d\pi\,^1\Pi_g$ and $10d\pi\,^1\Pi_g$ states were performed, yielding results that are described accurately by a model previously used for H_2.

Two significant revisions were made in experimental procedures reported earlier. First, a versatile new laser dye mixture was discovered and successfully utilized in the investigation of the Rydberg states of $^7Li_2$. Second, a computer-based data collection system was used in place of chart reading as the means of obtaining spectral line frequencies from raw d.c. voltage data.

TABLE OF CONTENTS

LIST OF TABLES

LIST OF FIGURES

ACKNOWLEDGMENTS

The author gratefully acknowledges the guidance and support of Professor L. Peter Gold and Professor Robert A. Bernheim.

Special thanks is given to Dr. Peter B. Kelly, Dr. D. Kirk Veirs, and Mr. Carter Kittrell for setting up the experimental apparatus that was used in this work and for instructions regarding the operation of laser laboratory equipment.

The author also wishes to thank Mr. James Balz for aid with computer programming, Mr. Paul Jarmotz for construction of electronic equipment, Ms. Barbara Itinger and Ms. Deb Burling for typing the thesis, and Ms. Carol Tomczyk and Mr. James Qualey for additional assistance.

This work was supported by the National Science Foundation, the Donors of the Petroleum Research Fund, administered by the American Chemical Society, and the U. S. Naval Sea System Command under contract with The Pennsylvania State University Applied Research Laboratory.

I. INTRODUCTION

The lithium molecule is of considerable interest to both experimentalists and theoreticians since it is the simplest stable homonuclear diatomic molecule after H_2. However, during the first fifty years of experimental investigations of $^7Li_2$ (1928-1978), only five electronic states were examined (1). This slow rate of progress was due to the inherent complexity of spectra that are obtained by single-photon excitation methods. Such spectra are particularly complex for $^7Li_2$ because of the combined effects of the weak Li-Li bond and the elevated temperature at which this molecule must be studied.

A new era in the study of $^7Li_2$ began in 1979 with the first application of pulsed optical-optical double resonance (OODR) spectroscopy to this molecule (2). The double resonance process consists of the sequential absorption of two photons by a molecule (or atom) via a real intermediate state. The first and second steps of this process are called "pump" and "probe" excitations, respectively. A double resonance spectrum is produced by continuously varying the frequency of the probe light while monitoring the radiation emitted by molecules that have undergone two-step excitations. The term "OODR" is reserved for double resonance processes in which the pump and probe photons are in the visible or ultraviolet frequency ranges. The OODR method, which is described in detail in chapter II, results in electronic spectra that are simple and vastly easier to assign than spectra obtained by

conventional single-photon or nonresonant two-photon (3) spectroscopy. OODR excitations can be detected either by monitoring decreases in fluorescence from the intermediate state or by using an ultraviolet bandpass filter to observe emission from levels at which the double excitation terminates.

Although the OODR technique was first applied in 1963 (4), it did not become a versatile spectroscopic tool until after commercial tunable dye lasers became available. The first experiment in which two such lasers were applied to the investigation of a diatomic molecule was performed by Gottscho et al. in 1978 (5). A further improvement in this technique has been made at The Pennsylvania State University by using a pulsed laser system in which a time delay (6,7) controls the amount of rotational relaxation that takes place in the intermediate state of OODR excitations before the second step of the OODR process occurs.

The pulsed OODR investigation of $^7Li_2$ has gone through two distinct phases thus far. The first consisted of a study of the $E\,^1\Sigma_g^+$, $F\,^1\Sigma_g^+$, and $G\,^1\Pi_g$ states (2,6-11); the second consisted of a systematic investigation of several Rydberg series (12,13). This thesis covers the latter part of the first phase (namely, the study of the $E\,^1\Sigma_g^+$ state) and all of the second phase. The theses of Kelly (6) and Viers (7) describe the work done on the $F\,^1\Sigma_g^+$ and $G\,^1\Pi_g$ states and provide detailed information regarding the experimental technique and equipment. A review of the experimental and theoretical work that was conducted on $^7Li_2$ prior to 1978 has been presented by Hessel and Vidal (14).

The intent of the first phase of the OODR work was to demonstrate the usefulness of pulsed OODR and to obtain accurate potential energy curves of excited gerade states of $^7Li_2$ for comparison with theoretical calculations. The intent of the second phase was to: 1) perform the first systematic study of Rydberg states of $^7Li_2$; 2) obtain an accurate ionization potential for $^7Li_2$; and 3) derive the first experimental spectroscopic constants for the ground state of $^7Li_2^+$.

The first successful analysis of a Rydberg series was performed on the hydrogen atom by Balmer in 1885 (15). This event was of great historical significance since it was one of the first steps leading to the development of quantum mechanics. Balmer discovered that the wavelengths of four lines in the visible spectrum of the hydrogen atom can be accurately represented by the empirical formula:

$$\lambda = bm^2/(m^2-n^2) \qquad (1)$$

where m and n are integers and b is a constant. Years later, Bohr recognized that the dependence of the hydrogen atom wavelengths on integers is evidence that some type of quantum phenomenon is involved. Using the quantum concepts of Planck and Einstein, Bohr developed a quantum theory of atomic structure from which Balmer's formula can be derived.

Balmer's formula was modified by Rydberg in 1889 to account for the wavelengths of spectral lines of all types of atoms. In modern notation, the Rydberg formula is:

$$E(n,\ell)=E(\infty,\ell)-R(n-\delta(n,\ell))^{-2} \qquad (2)$$

where $E(n,\ell)$ is the energy of an atomic level having principal quantum number n, and azimuthal quantum number ℓ; $E(\infty,\ell)$ is the atomic ionization potential; $\delta(n,\ell)$ is the quantum defect; and R is the Rydberg constant (109737 cm^{-1} for a nucleus of infinite mass).

The above form of the Rydberg formula applies also to molecules since the interaction of a molecular core with a distant Rydberg electron is quasi-hydrogenic. The principal quantum number is meaningful for a molecule in a Rydberg state since the united atom model is applicable in this case.

Although an abundance of data is now available for atomic Rydberg series, little such information exists for diatomic molecules. Analyses of diatomic Rydberg series are hampered by two major factors: 1) Rydberg spectra are extraordinarily complex when obtained by conventional absorption or emission spectroscopy since the density of electronic states becomes large as the ionization limit is approached; and 2) perturbations increase both in number and in magnitude as the total excitation energy increases since there is an increasingly greater probability that a given state will lie close in energy to a perturbing state. Examples of diatomic molecules whose Rydberg states have been studied extensively include NO, N_2, H_2, He_2, Na_2, and now Li_2 (1). The Rydberg states of the first four of these molecules have been investigated by conventional single-photon methods, while those

of the last two have been examined by OODR spectroscopy (12,13,16-19). The work done on Na_2 and Li_2 has demonstrated the vast superiority of OODR over single-photon excitation methods.

II. THE APPLICATION OF THE OODR METHOD TO Li_2

The OODR process is shown schematically in figure 1 for Li_2. The first step of the excitation consists of a single $A^1\Sigma_u^+$ (v',J') $\leftarrow X^1\Sigma_g^+$ (v'',J'') transition excited by a tunable pulsed dye laser. Further excitations to a number of (v*,J*) levels are then induced by scanning a second pulsed dye laser. An optical delay may be introduced into the path of the probe laser to allow time for substantial rotational relaxation to take place in the $A^1\Sigma_u^+$ state before the probe laser pulse arrives. This feature enlarges the amount of data collected on a single scan without significantly complicating the task of assigning quantum numbers to the spectral transitions.

The OODR method has several important features which make it a valuable tool for the study of $^7Li_2$: 1) OODR spectra are easy to assign and are much less dense than spectra resulting from single-photon excitations; 2) access is obtained to transitions that are forbidden by single-photon selection rules; 3) single-photon fluorescence can be easily filtered out of the detection system without significantly reducing the high-frequency fluorescence from the high-lying states; and 4) the number of excited states that are accessible by tunable dye lasers is greatly increased.

OODR spectra can be obtained for Li_2 by pumping either $A^1\Sigma_u^+ \leftarrow X^1\Sigma_g^+$ or $B^1\Pi_u \leftarrow X^1\Sigma_g^+$ transitions but only the former have been used in practice. The assignments of lines in the $A^1\Sigma_u^+ \leftarrow X^1\Sigma_g^+$ bands can be determined from the accurate molecular constants of Kusch and

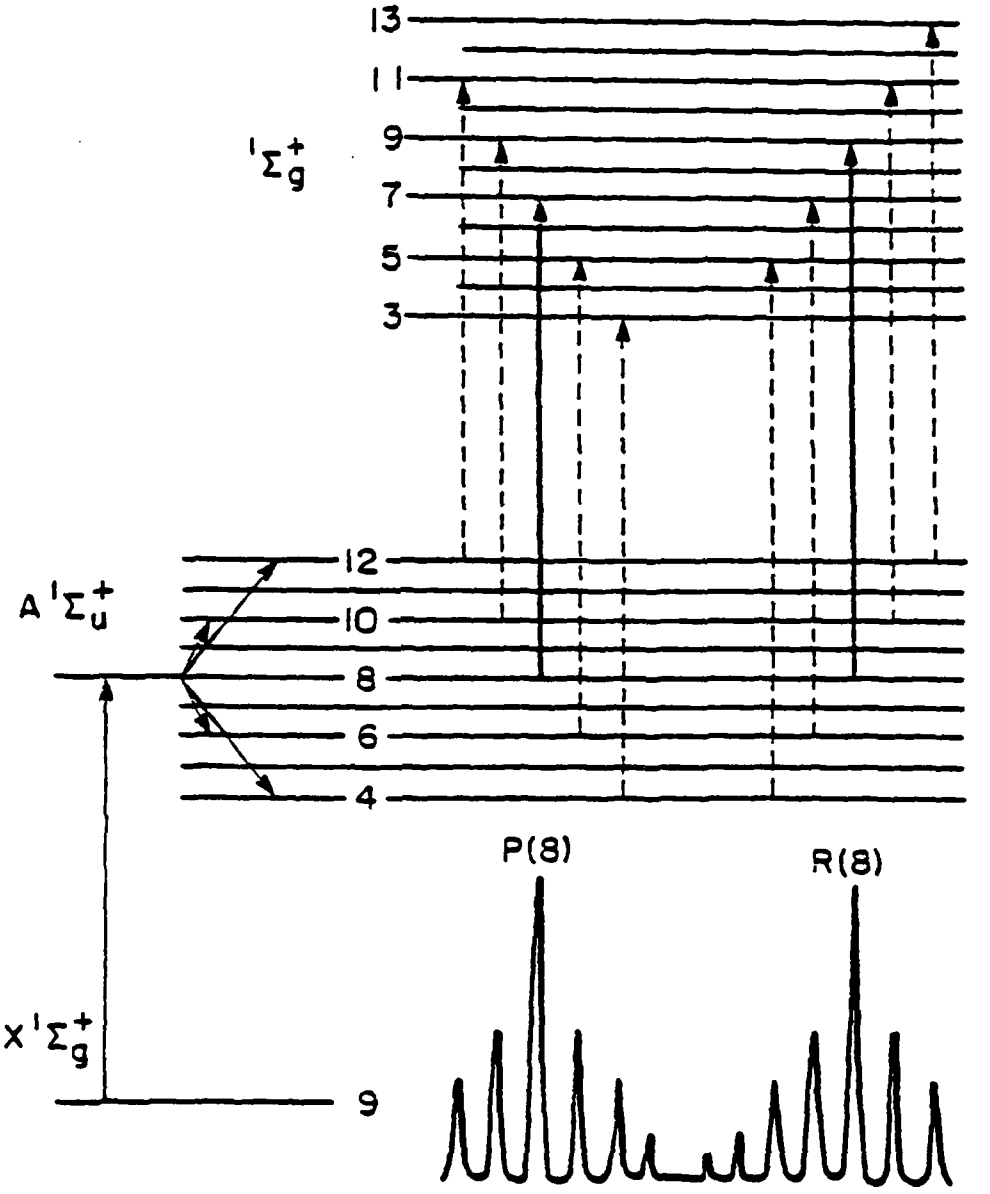

Figure 1. A simulated $^1\Sigma_g^+ \leftarrow A\,^1\Sigma_u^+ - X\,^1\Sigma_g^+$ OODR spectrum of Li_2. The rotational quantum number, J, is indicated for each energy level shown. The slanted arrows denote collisional relaxation. The solid and broken vertical arrows represent collision-independent and collision-dependent transitions, respectively. The spectral lines appear directly beneath the vertical arrows to which they correspond.

Hessel (20). The density of lines in these bands is sufficiently small that many nonoverlapped lines are available for use as pump transitions.

The rotational assignments of OODR lines are readily deduced from the assignment of the pump transition since the directly populated level of the $A^1\Sigma_u^+$ state is always the source of the strongest transitions in the OODR spectrum. These assignments can be verified independently by using combination differences involving the well-characterized (20) $A^1\Sigma_u^+$ state.

The assignments of quantum numbers to OODR transitions requires a knowledge of spectroscopic selection rules. A summary of the selection rules that are pertinent to the Li_2 molecule is given below (21):

1. Quantum number for the total angular momentum:

$$\Delta J=0,\pm1$$

2. Quantum number for the projection of the electronic angular momentum along the internuclear axis:

$$\Delta\Lambda=0,\pm1$$

3. Quantum number for the electron spin:

$$\Delta S=0$$

4. Electronic inversion symmetry of homonuclear diatomic molecules:

$$g \longleftrightarrow u$$

5. Electronic reflection symmetry:

$$+ \longleftrightarrow + \text{ and } - \longleftrightarrow -$$

6. Parity of the total eigenfunction:

$$+ \longleftrightarrow -$$

7. Nuclear exchange symmetry of homonuclear diatomic molecules:

$$s \longleftrightarrow s \text{ and } a \longleftrightarrow a$$

An illustration of how these rules apply to OODR transitions is given in figure 2.

The selection rules for nuclear exchange symmetry separate Li_2 into ortho and para forms. Interconversion of these two forms is forbidden even in nonradiative processes (21). Thus, rotational relaxation in the $A\,^1\Sigma_u^+$ state takes place in steps of $\Delta J=2$. The 5:3 population ratio that exists between the ortho and para forms of Li_2 plays an important role in the selection of pump transitions since a maximization of the number of pumped molecules is desirable.

The electronic selection rules restrict observations to $^1\Sigma_g^+$ and $^1\Pi_g$ states when the $A\,^1\Sigma_u^+$ state of Li_2 is pumped. This restriction is desirable in an initial investigation of Rydberg states since it lessens the likelihood of overlapping of bands from different electronic states. It is important to note that the $g \longleftrightarrow u$ selection rule restricts one-photon and two-photon excitations of Li_2 to mutually exclusive manifolds of electronic states.

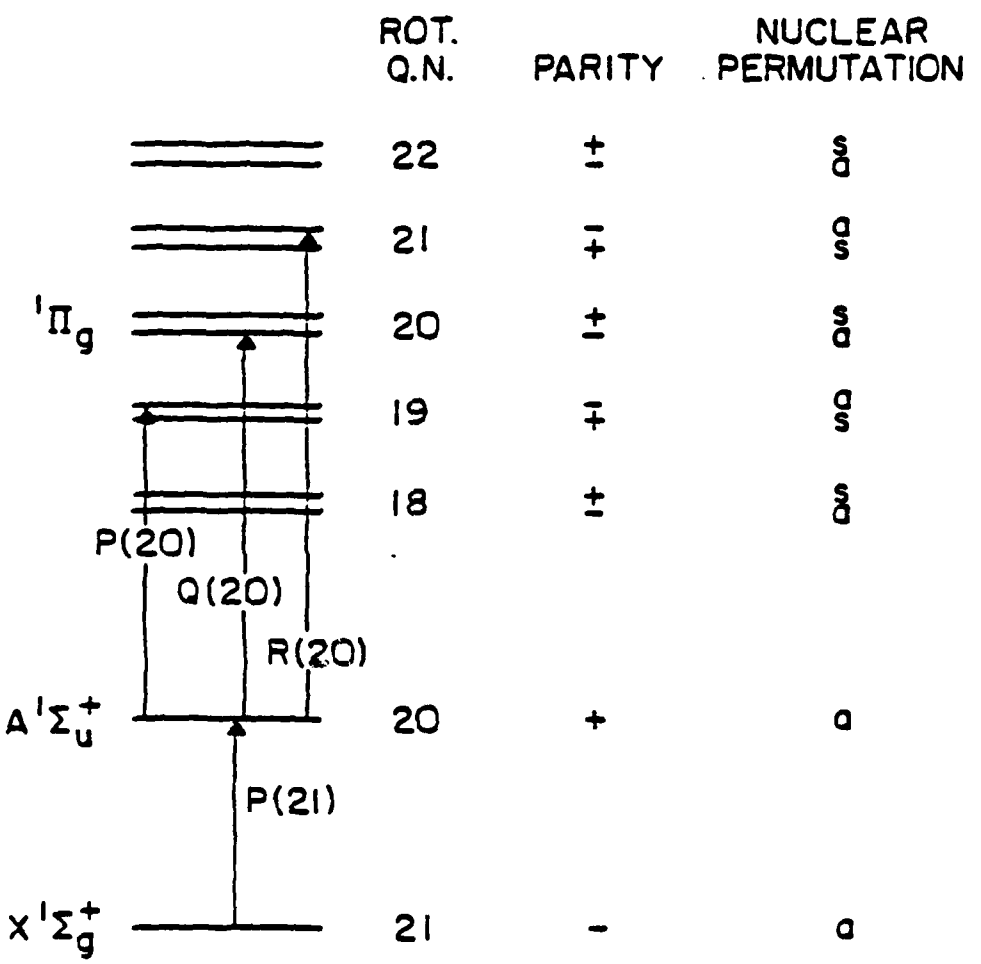

Figure 2. Illustration of selection rules pertaining to OODR excitations of Li_2. Only collision-independent lines are shown.

The electronic symmetries of the states at which OODR transitions terminate can be deduced from the number of branches per vibrational band. A $\Pi \leftarrow \Sigma$ transition is characterized by three branches per band (i.e., P, Q, and R) while a $\Sigma \leftrightarrow \Sigma$ transition has only two such branches (i.e., P and R). Since these were the only types of transitions allowed under the conditions used in the work reported here, it was trivial to assign electronic symmetries to the observed Rydberg states.

A representative OODR vibrational band, $7d\pi\,{}^1\Pi_g \leftarrow A\,{}^1\Sigma_u^+$ (0,0), is shown in figure 3. All other observed $n>6$ $nd\pi\,{}^1\Pi_g \leftarrow A\,{}^1\Sigma_u^+$ bands have a similar appearance to the one shown here but become progressively weaker in intensity as n increases. The three intense P, Q, and R transitions that arise from the directly populated rovibronic level of the intermediate $A\,{}^1\Sigma_u^+$ state are easily recognizable in this spectrum. A large number of rotational relaxation lines are also visible, particularly in the P branch. The bandhead of the nearby $7d\sigma\,{}^1\Sigma_g^+ \leftarrow A\,{}^1\Sigma_u^+$ (0,0) band can be seen on the short-wavelength end of this scan.

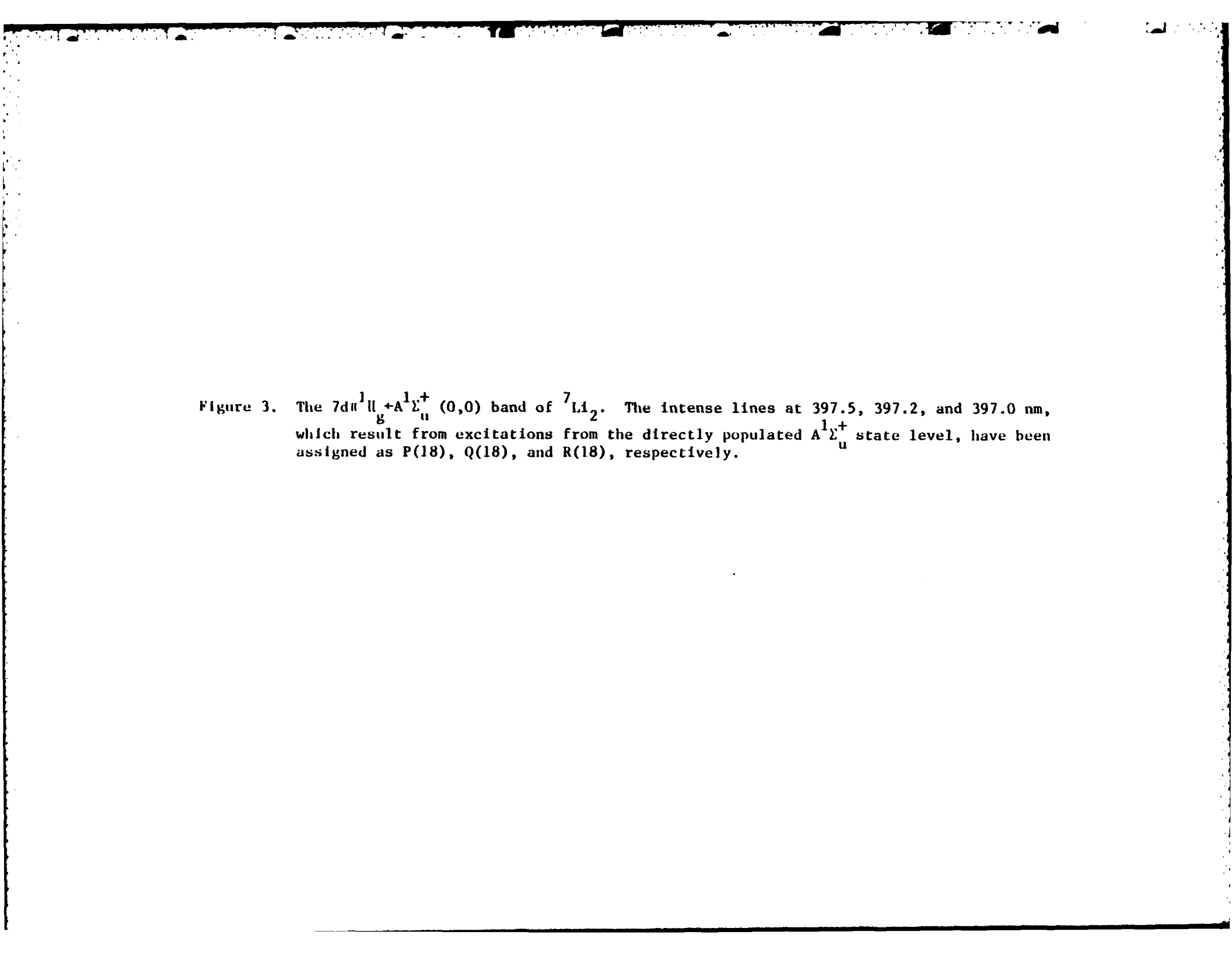

Figure 3. The $7d\pi\,^1\Pi_g \leftarrow A\,^1\Sigma_u^+$ (0,0) band of $^7Li_2$. The intense lines at 397.5, 397.2, and 397.0 nm, which result from excitations from the directly populated $A\,^1\Sigma_u^+$ state level, have been assigned as P(18), Q(18), and R(18), respectively.

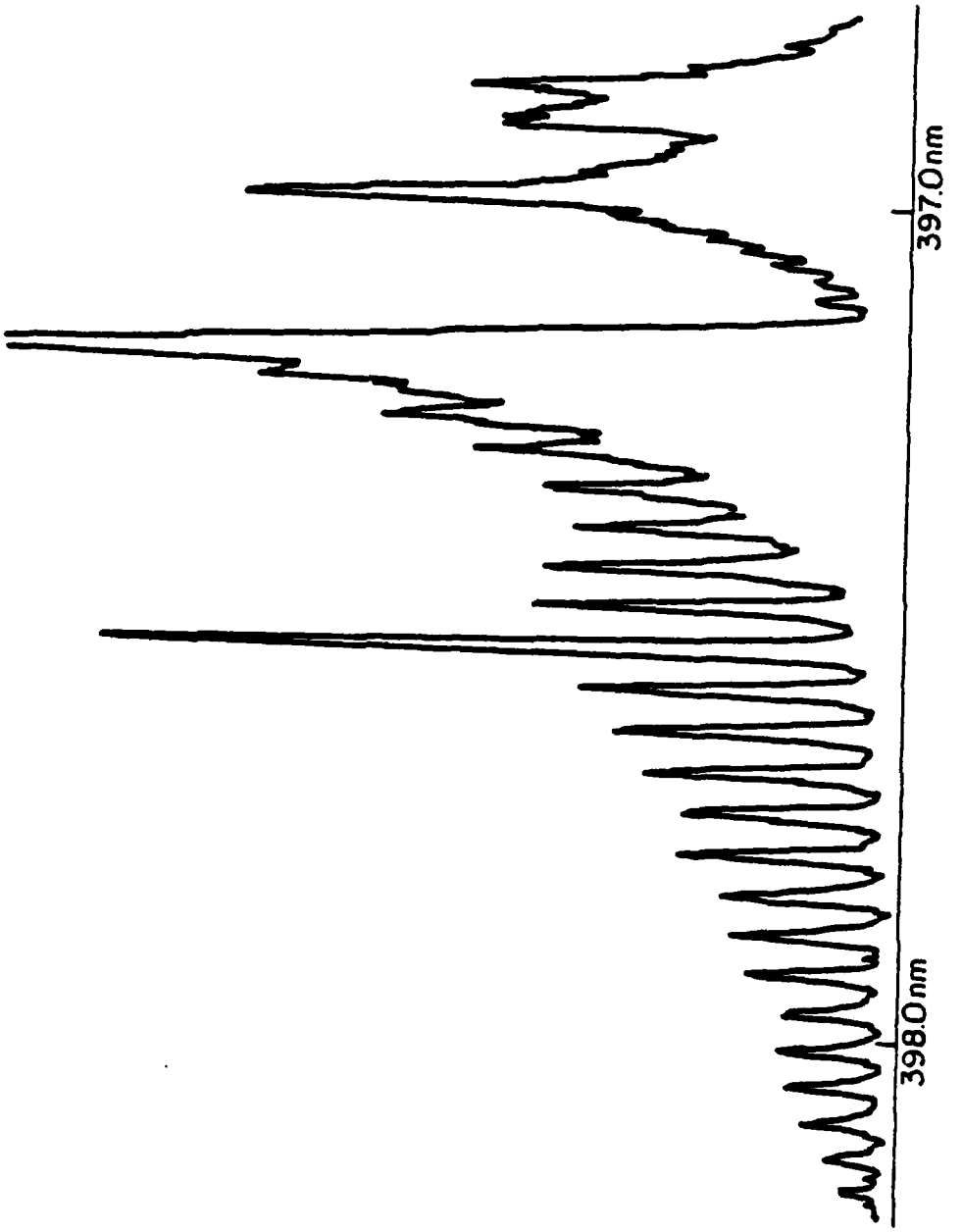
397.0nm
398.0nm

III. EXPERIMENTAL

A. Overview

The experimental arrangement that was used for the systematic study of the Rydberg states of $^7Li_2$ is nearly identical to one that has been described in detail by Kelly (6) and Veirs (7). Therefore, except for the newly-instituted computer data collection system, only an abbreviated description of the experimental apparatus will be presented here. Several modifications of the original arrangement were required for the $E^1\Sigma_g^+$ state investigation. These will be discussed after a review of the original setup is given.

B. The Nitrogen Laser System

The experimental arrangement that was used for the systematic study of the Rydberg states of $^7Li_2$ is shown in figure 4. OODR excitations were produced in $^7Li_2$ by overlapping the output beams of two tunable pulsed dye lasers in a cell containing $^7Li_2$ vapor and He buffer gas. The two dye lasers were pumped by the divided output beam of a Molectron UV-1000 nitrogen laser operating at 10 Hz and producing 700 kw at 337.1 nm. Both dye lasers were operated without etalons and had linewidths of 0.5 cm^{-1}. The output power of the pump dye laser was 75 μJ per pulse. The probe dye laser was operated with 60-300 μJ per pulse depending on the dyes that were used.

The sample cell consisted of a heat pipe oven to which was added several grams of lithium (99.99% ^7Li) and 30 torr of helium

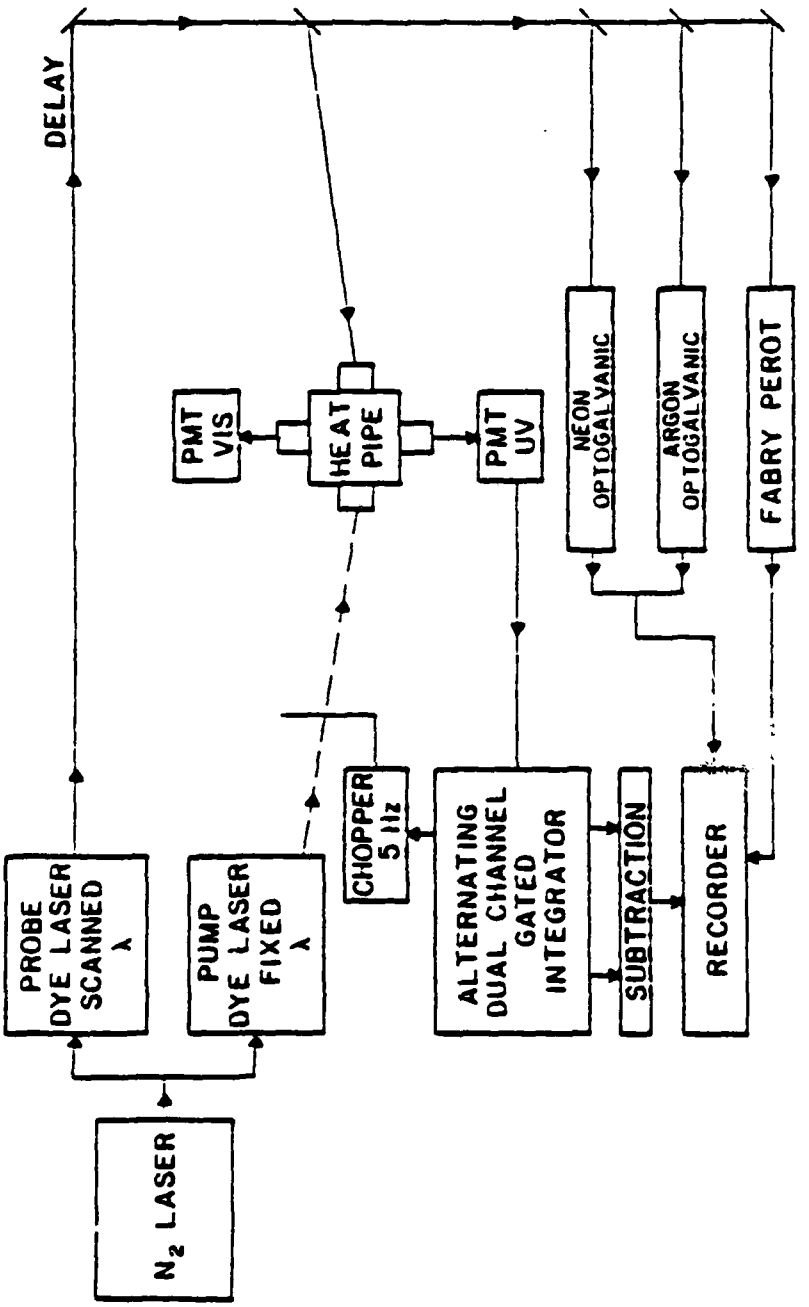

Figure 4. Block diagram of the nitrogen laser system.

at room temperature. An operating temperature of 650 °C was used for the study of Rydberg states up to n=6; 730 °C was used for higher states to compensate for the decrease in transition probability as n increases. At 650 °C, the partial pressures of the gaseous species in the heat pipe are estimated (22) to have been 90 torr He, 0.002 torr $^7Li_2$, and 0.2 torr Li. At 730 °C, the estimates are 100 torr He, 0.02 torr $^7Li_2$, and 0.7 torr Li.

The two dye laser output beams were arranged so that they intersected each other at the center of the heat pipe oven at nearly a 180° angle. A slight offset from 180° was needed to allow the probe beam to be directed into calibration devices after emerging from the heat pipe. The probe laser pulse was optically delayed by about 6 nsec with respect to the pump pulse by introducing an extra 2 m length into the optical path of the probe beam.

Excitation to Rydberg states was detected by monitoring the ultraviolet fluorescence from the heat pipe cell with a photomultiplier tube. Filters were used to discriminate against visible fluorescence. The ultraviolet emission was due, at least in part, to collisional transfer of energy from gerade to nearby ungerade states followed by single-photon transitions to the ground state (10).

The processing of the ultraviolet signals was complicated by the existence of undesired ultraviolet radiation resulting from successive excitations of $^7Li_2$ by two probe laser photons (23). This problem was circumvented by introducing a mechanical chopper and

a two-channel gated integrator into the experimental setup. OODR signals were extracted from the total ultraviolet emission by chopping the 10 Hz pump dye laser beam at 5 Hz, and subtracting the signal observed with the pump laser beam blocked from the signal observed with the pump beam unblocked.

Calibration of the probe laser wavelength was achieved by directing portions of the probe beam into neon and/or argon optogalvanic lamps (24) and a Fabry-Perot interferometer. The interferometer produced a ring pattern which expanded or contracted depending on whether the probe laser was scanning to smaller or larger wavelengths, respectively. A photodiode was placed near the middle of the projected pattern to monitor the movement of the fringes electronically. The interferometer spacing was adjusted so that one fringe traversed the photodiode for each 0.8 cm^{-1} change in frequency. This arrangement permitted accurate interpolation of wavelengths between successive neon and argon calibration lines. Spectral and calibration data were recorded on a four-pen chart recorder and, in digital form, on a cassette tape. The digital data were later transferred from the cassette tape to a minicomputer. The chart recorder was used solely as a back-up storage device. A detailed description of the computer data collection system is given below.

Aside from the addition of the data collection system, the only significant revision of the earlier experimental procedures was the introduction of a new dye mixture to the pump laser. It was found that the combination of the dyes LD700 and DCM

produces at least three times as much power throughout the range 680-780 nm than can be obtained with any previously reported (25) dye solution pumped by a nitrogen laser. The gain curve of this mixture can be peaked at any wavelength in the range 650-750 nm by adding varying amounts of LD700 to a solution containing 0.9 mg/ml DCM in 80% DMSO/20% ethanol. The behavior of the gain curve of this mixture as a function of the dye concentration ratio is illustrated in figure 5. The gain curve can be peaked at any point on the broken line curve shown in this figure.

Each OODR experiment was preceded by a search for an appropriate pump line. This search was begun by running a calibrated $A^1\Sigma_u^+ \leftarrow X^1\Sigma_g^+$ spectrum using only the pump dye laser. The lines in this spectrum were assigned by using the molecular constants and Franck-Condon factors of Kusch and Hessel (20). A transition was chosen for use as a pump line on the bases of its spectral intensity, its proximity to neighboring strong lines, and its $A^1\Sigma_u^+$ state vibrational quantum number. After a suitable line was found, the pump laser was tuned to the frequency of this line and left there while the probe laser was introduced and scanned.

C. The Computer Data Collection System

The function of the data collection system was to digitize analog d.c. voltage data, and store them on cassette tape for subsequent analysis on a Modcomp II/25 minicomputer. A block diagram of this system is given in figure 6. The interface between the laboratory equipment and the minicomputer was divided

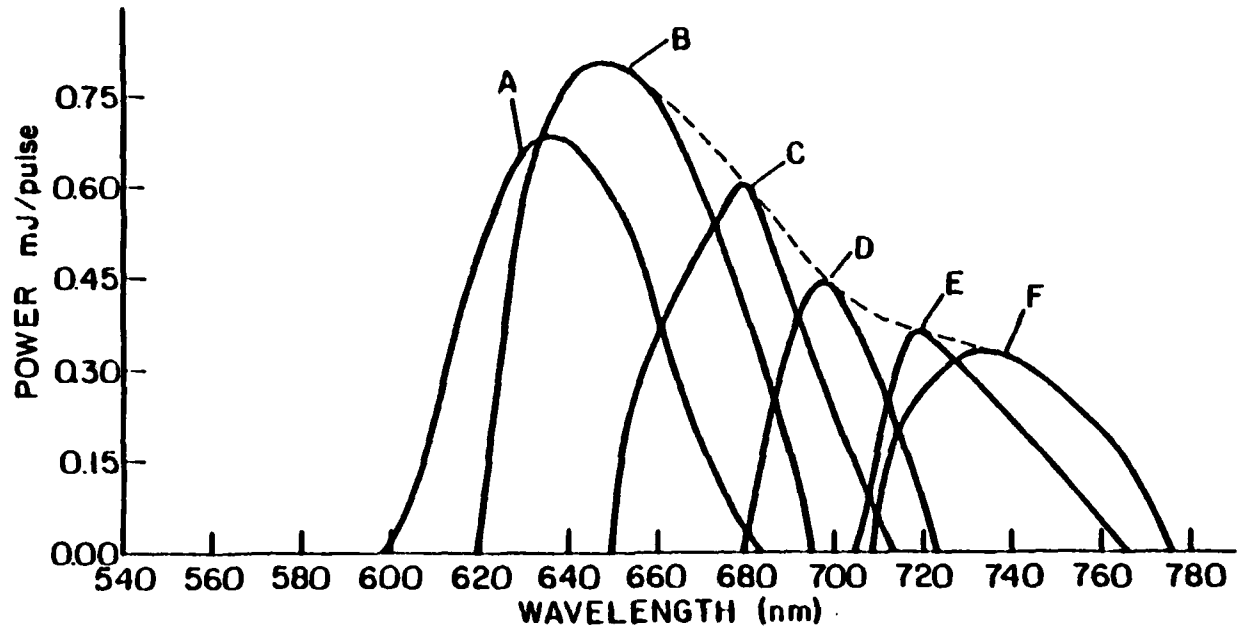

Figure 5. Gain curves for LD700+DCM laser dye mixtures pumped by a nitrogen laser. The DCM concentration is 0.9 mg/ml for all of the solutions tabulated below.

Gain Curve	Solvent	[LD700] Amount per ml
A	80% EtOH/20% DMSO	none
B	20% EtOH/80% DMSO	none
C	" " " "	1 drop of 5.0 mg/ml LD700
D	" " " "	6 drops " " " "
E	" " " "	1.0 mg
F	" " " "	1.0 mg

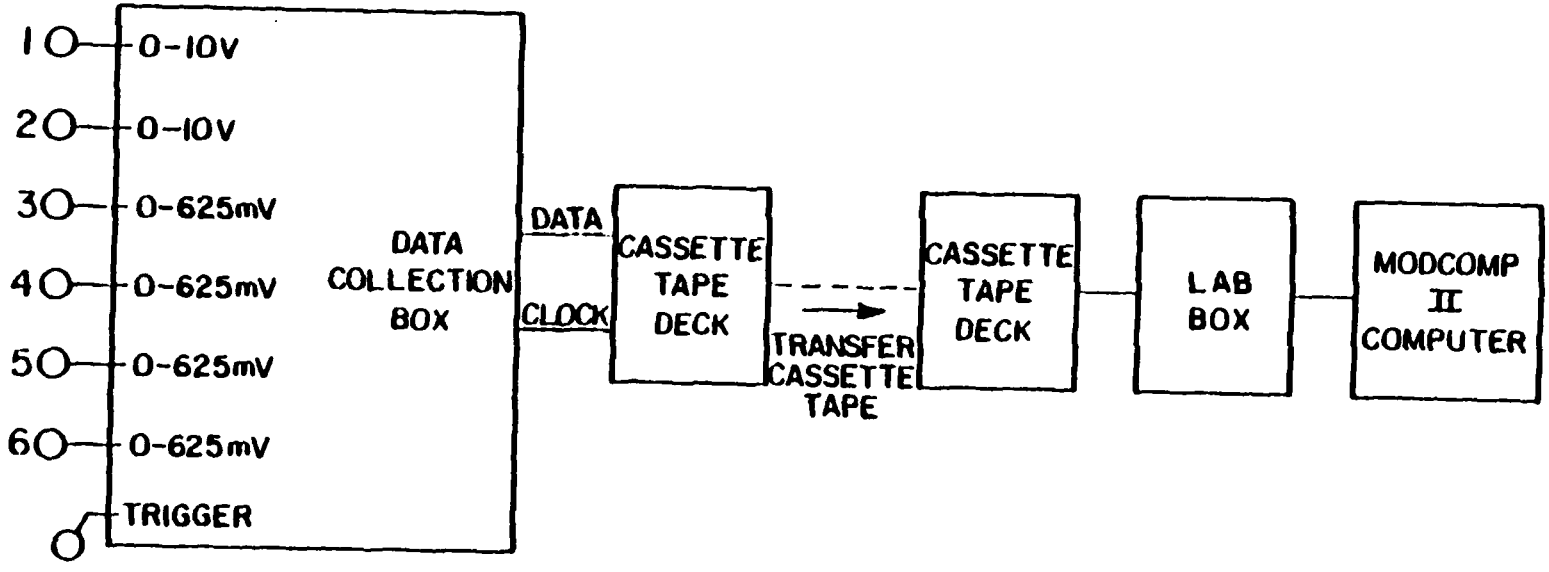

Figure 6. Block diagram of the digital data collection system.

into two separate sections: one in the laboratory and one at the site of the minicomputer. The former consisted of a data collection box and a cassette tape deck; the latter consisted of a second cassette tape deck and a device called a "lab box". Original software had to be developed to direct all of the data processing that was performed on the minicomputer.

The data collection box was triggered by sampling the probe laser pulses with a photodiode. These "clock" pulses were recorded along with the spectral data via a separate channel of the cassette tape deck. They were later used to control the input of data to the minicomputer during the second phase of the data collection process. Each time a trigger pulse was received by the data collection box, the voltages appearing at the inputs of the six available channels of this box were recorded. Each of these six-member sets of voltages was processed in the form of eight eight-bit words. Two words were allotted to each of the first two channels and one was allotted to each of the other four. Since words were occasionally lost during the transmission of data through the computer interface, the first four members of each eight-word set were labeled by fixing the first two bits of each of these words. This scheme enabled the data to be identified with the proper channels after they were read into the memory of the computer. A consequence of this labeling was that four of the sixteen bits assigned to each of the first two channels were unavailable for data. Thus, the resolution in the digitized spectral data was one part in 2^{12} for channels 1-2, and one part in 2^{8} for channels 3-6.

Voltages entering the data collection box were digitized by Teledyne Philbrick twelve-bit A/D converters. The outputs of these converters were changed from parallel to serial form and then routed through an audio oscillator. A cassette tape deck was used to record the resulting audio output. The data were processed continuously until either the dye laser wavelength scan was completed or the thirty-minute capacity of the cassette tape was used up.

The A/D converters were adjusted so that twelve bits could accommodate 0-10 volts of input. Thus, the input voltages ranges were 0-10 volts and 0-0.625 volts for channels 1-2 and 3-6, respectively. The smaller range was found to be adequate for the optogalvanic signals, while the larger range was required for the OODR and interferometer signals. In practice the OODR, interferometer, and optogalvanic signals were sent to channels one, two, and three, respectively. Channel 1 was later modified to accommodate -10 to +10 volts of input in order to allow for the negative baseline drifts that were frequently observed in the output of the gated integrator that was used to process the OODR signals. A voltage V entering the modified version of channel 1 was first reduced to V/2 by a voltage divider and then converted to 5-(V/2) by bipolar circuitry.

After the completion of an experiment, the data from the cassette tapes were read into an integer array in the memory of the minicomputer via a direct memory processor. The aforementioned "lab box" interface was used to convert the audio output of the

cassette tape deck to a form compatible with the computer. The binary tones from each cassette tape were converted to binary voltages and collected in an eight-bit register in the interface. Each time the register became full, the computer recorded the contents of the register in the form of an eight-bit word.

Due to computer memory limitations, data had to be periodically transferred from the above array to nine-track magnetic tape while other data were flowing into the array from the cassette tape. This operation was accomplished by means of two subroutines. The first subroutine suspended execution of the software for sufficient time to allow the first half of the array to fill, and then permitted the data in this half of the array to be transferred to nine-track magnetic tape. The second subroutine handled the second half of the array in basically the same manner. This process was repeated as many times as necessary by reusing the array for additional data.

As soon as the end of the cassette tape was reached, the computer read the stored data from the nine-track magnetic tape and attempted to determine which words, if any, had been garbled during transmission through the computer interface. Such data points could often be detected since they usually differed markedly from neighboring data. The computer replaced the spurious data with interpolated values and then wrote the corrected data set from each channel into a separate file of a magnetic disk. The rest of the data manipulation that was done on the minicomputer utilized this disk for both input and output.

The raw data had to be smoothed before peak positions could be read since, otherwise, the peak-reading algorithm would have been ineffective. The smoothing was accomplished by convoluting the raw data with a Gaussian function (26). This procedure consisted of multiplying each raw data point, R(t), by a normalized Gaussian, $f(t-t_o)$, and then summing the resulting functions to obtain smoothed data, S(t). Under these conditions, the area under the smoothed data is equal to the area under the raw data. In mathematical terms:

$$S(t_o) = \int_{-\infty}^{\infty} R(t) f(t-t_o) dt \tag{3}$$

$$\approx R(t_o) f(0) \Delta t + \sum_{i=1}^{N} [R(t_o+i\Delta t)+R(t_o-i\Delta t)] f(i\Delta t) \Delta t$$

where Δt is the data repetition period, and N is some finite integer value at which the above summation is truncated. The time constant, τ, of the Gaussian is related to the variance, σ^2, through the equation:

$$\tau = 2\sigma^2 \tag{4}$$

The above method is equivalent to the function performed by a time constant in an electrical circuit except that the latter corresponds to multiplying the input by a half-Gaussian. Although more elegant methods exist for smoothing data (27), the convolution procedure proved to be adequate for the pulsed OODR system.

In practice, the input data for the smoothing program had to be processed in piecemeal fashion because of computer memory

limitations. The smoothed data were stored on a magnetic disk and used subsequently as input for a peak-reading routine.

The peak-reading program located peak positions in terms of laser pulse numbers. Later, it converted the pulse numbers of the OODR and optogalvanic peaks to interferometer fringe numbers. Again, the input data had to be processed in portions because of computer memory limitations. The software directed the minicomputer to keep a running count of the number of consecutive increases in voltage that it encountered while reading the data, and to reset the counter to zero each time a decrease in voltage was detected. Whenever this counter exceeded a specified critical value, a peak-reading algorithm was implemented. This procedure enabled spectral peaks to be distinguished from random noise. The critical value of the counter was determined by the line width of the spectral peaks and the scan rate. The computer obtained a value for a peak location by averaging the pulse numbers of the points on each side of the peak which were at a specified fraction of the maximum intensity of that peak.

After the peak-reading process had been completed, the computer data processing was suspended until wavelengths had been assigned to all of the optogalvanic calibration lines, and a leastsquares fit of frequency vs. interferometer fringe number was performed on a calculator. This fit was used to generate OODR transition frequencies from the fringe numbers of the spectral lines. These frequencies were then stored permanently on a magnetic disk.

The last operation that was performed on the minicomputer consisted of recording the following information for each assigned OODR transition on nine-track magnetic tape: 1) the frequency; and 2) the rotational and vibrational quantum numbers of both the upper and lower electronic states. This tape served as a means of transferring spectral data to an IBM 370 computer. All subsequent data processing was performed as described previously (6,7).

A check of the reliability of the digital data collection and processing procedures described above was made by applying a digital analysis and a strip chart analysis to the same sample spectrum. The two methods were found to yield essentially the same spectral frequencies for identical spectral lines. The precision of the frequency measurements obtained by the newer method (0.2 cm^{-1}) is about the same as that reported (9) for the older.

D. Modifications of the Experimental Arrangement Made for the $E^1\Sigma_g^+$ State Investigation

The $E^1\Sigma_g^+$ state investigation reported in this work was preceded by a limited earlier study of this state (10). The earlier work, which was done using the nitrogen laser system described above, was inhibited by a lack of suitable infrared laser dyes. In order to circumvent this problem, several significant changes had to be made in the experimental arrangement. A block diagram of the revised system is given in figure 7. Acce s to the near infrared region was gained by sending the output of a dye laser through a pressurized (20 atm) Raman-shifting hydrogen cell (28). In this setup, the

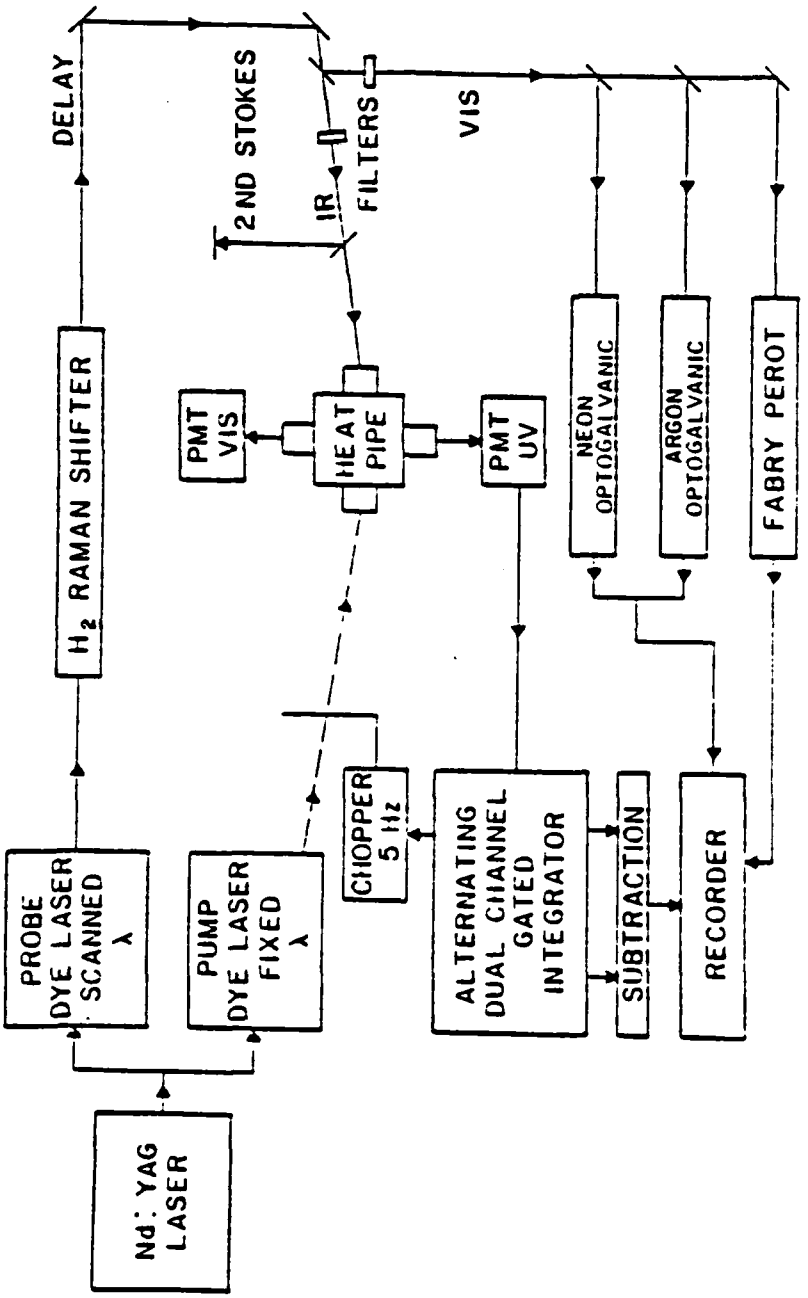

Figure 7. Block diagram of the Raman-shifting CODR apparatus.

nitrogen laser was replaced by a Quanta-Ray Nd:YAG laser in order to attain a dye laser power level sufficient to produce stimulated Raman emission in H_2. Since the latter was not then available at The Pennsylvania State University, the facilities of the Regional Laser Laboratory at the University of Pennsylvania were used. The frequency-doubled 10 Hz output of the Nd:YAG laser was 170 mJ per pulse at 532 nm, or about 25-fold larger than the maximum power output of a nitrogen laser. The output of the Nd:YAG laser was divided by a beamsplitter so that 90% of the power was directed to the probe dye laser and 10% to the pump dye laser.

Stimulated Raman emission occurred in the hydrogen cell at a threshold input power of about 50 mJ per pulse. Despite the high output power available from the Nd:YAG laser, only a few dyes are able to achieve this level in the setup that was used. Fortunately, Rhodamine 6G (Raman-shifted range 715-749 nm) and Rhodamine B (Raman-shifted range 747-773 nm) permitted full coverage of the wavelength range that was required for investigating the $E^1\Sigma_g^+$ state.

Vibrational Raman emission is produced by H_2 at multiples of 4155.20 cm^{-1} from the frequency of the exciting radiation as a result of the (1,0) Q(1) transition in the ground electronic state (2^0). Under the experimental conditions of the OODR study described here, lasing was observed at two Stokes and two anti-Stokes frequencies. Stimulated rotational Raman emission at the frequency of the $X^1\Sigma_g^+$ (0,0) S(1) transition of H_2 was also seen, but was much weaker than the vibrational emission.

The first vibrational Stokes frequency was used as the probe beam. Filters and dielectric mirrors were used to discriminate against all other radiation emanating from the Raman cell. The power available at the Raman-shifted probe frequency ranged up to 0.5 mJ per pulse. The linewidth of the Raman-shifted radiation was 0.2 cm^{-1}.

The probe dye laser consisted of an oscillator-amplifier combination, constructed according to the design of Littman (30). The basic difference between the Littman design and its predecessor, the Hänsch design (31), is that the former utilizes a grazing-incidence diffraction grating as a tuning element rather than a conventional diffraction grating. The newer design was devised to eliminate the need for an intracavity beam-expanding prism or telescope, and thereby simplify the procedure of laser alignment.

The pump dye laser was an oscillator-amplifier system containing an intracavity beam expander. This laser produced an output power of 0.5-1.2 mJ per pulse and a linewidth of 0.5 cm^{-1} when pumped with 10% (or 17 mJ per pulse) of the frequency-doubled output of the Nd:YAG laser.

Calibration was achieved by sampling the unshifted probe beam with neon and argon optogalvanic cells as well as a Fabry-Perot interferometer. The neon and argon calibration frequencies were later converted to Raman-shifted values using the known frequency (29) of the $X\,^1\Sigma_g^+$ (1,0) Q(1) transition of H_2 at 20 atm.

IV. ANALYSIS AND RESULTS

A. Time Constant Offset

The measured positions of the OODR lines had to be corrected for a small time constant offset that resulted from a difference between the electronic time constant used for the OODR signal (1.0 sec) and that used for the optogalvanic calibration spectrum (about 0.1 sec). An estimation of the magnitude of this offset can be obtained by convoluting a lineshape function with a smoothing function that is truncated so that only the section on one side of the symmetry axis is used. If both the lineshape function and the smoothing function are assumed to be Gaussians, then the electronically-smoothed lineshape is given by:

$$S(t_o)=\Delta t/\pi \left[\sum_{i=0}^{N} e^{-(\bar{t}-t_o+i\Delta t)^2} e^{-(i\Delta t)^2} \right] \qquad (5)$$

where the time constants of both Gaussians have been taken to be 1.0 sec, and $\bar{t}$ is the location of the maximum of the spectral line.

An evaluation of the above formula on a computer reveals that an electronic time constant of 1.0 sec delays the arrival of a spectral peak by about 0.5 sec. This result has been confirmed by convoluting experimental spectral data with a half-Gaussian, and by measuring the apparent change in the frequency of selected OODR lines when the direction of the frequency scan was reversed. In practice, the spectral frequency corrections that were

needed to compensate for electronic time constants ranged from 0.05 to 0.09 cm^{-1}.

B. $E^1\Sigma_g^+$ State Analysis and Discussion

Data for the $E^1\Sigma_g^+$ state were obtained by excitation of selected $A^1\Sigma_u^+ \leftarrow X^1\Sigma_g^+$ transitions followed by further excitations into the $E^1\Sigma_g^+$ state. A listing of all pump lines (32) that were used in the $E^1\Sigma_g^+$ state investigation is given in table 1. The vibrational numbering of the $E^1\Sigma_g^+$ state was tentatively assigned by assuming that the lowest observed vibrational level of this state is $v^*=0$. This numbering was later confirmed by comparing observed band intensities with calculated Franck-Condon factors. The vibrational quantum numbers of all observed bands are shown in figure 8.

The data consist of 681 assigned transitions from the $A^1\Sigma_u^+$ state to vibrational levels in the range $v^*=0$-12 of the $E^1\Sigma_g^+$ state. Transitions to what may be $v^*=13$ were observed but could not be assigned. The assigned data were fit by a linear leastsquares method with the conventional Dunham expansion (33):

$$\nu(v,J) = \sum_{n,k} Y_{nk}(v+1/2)^n[J(J+1)-\Lambda^2]^k \qquad (6)$$

where the symbols Y_{nk}, v, J, and Λ have their usual meanings. The measured wavelengths were converted to energies referred to the bottom of the $X^1\Sigma_g^+$ state using the $A^1\Sigma_u^+$ state constants of

Table 1. Pump lines ($A^1\Sigma_u^+ \leftarrow X^1\Sigma_g^+$) and probe laser scanning ranges used for the $E^1\Sigma_g^+$ state investigation.

Pump Line	λ (Å) Pump	Pump Freq[a] (cm^{-1})	Probe λ (Å) Range
(0,0) R(17)	7151	13985.122	7250-7640
(0,0) P(12)	7152	13981.632	7350-7390
(1,0) P(11)	7023	14238.503	7250-7660
(1,0) P(15)	7035	14215.336	7590-7660
(2,0) P(37)	7026	14232.240	7230-7700
(7,0) R(21)	6392	15644.152	7160-7730
(9,1) P(23)	6235	16037.87	7160-7730
(9,1) R(27)	6235	16037.99	7160-7730

[a]Reference 32.

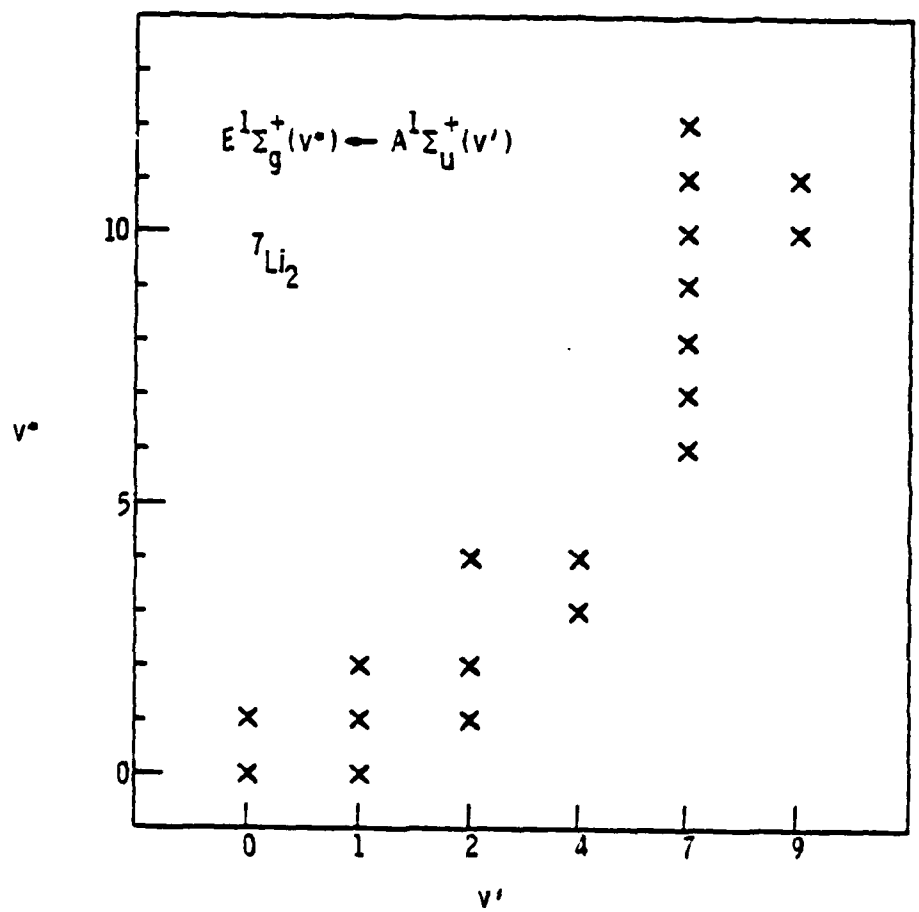

Figure 3. Observed $E^1\Sigma_g^+ - A^1\Sigma_u^+$ (v^*,v') bands of $^7Li_2$. The data for all of these bands were used to determine the Dunham coefficients listed in Table 2. The data for the $v'=0$ and $v'=1$ bands were additionally used to establish the v^* vibrational numbering. Observations were limited to the range 715-773 nm, and were incomplete within this range for $v'=4$.

Kusch and Hessel (20). A set of Dunham coefficients which describe the data is given in table 2. The $E^1\Sigma_g^+$ state energy levels that were used in this fit are shown in figure 9. The standard deviation of the fit (0.14 cm^{-1}) is consistent with the estimated accuracy of the measurements (0.2 cm^{-1}). The observed value of Y_{02} differs by only 0.5% from the value calculated from the relation:

$$Y_{02}=-4Y_{01}^3/Y_{10}^2 \tag{7}$$

which holds for most diatomic molecules (21).

The constants listed in table 2 were used to calculate a Rydberg-Klein-Rees (RKR) potential (34) using a computer program originally developed by Zare (35). The results are summarized in table 3 along with the values of:

$$G_v = \sum_{n=1} Y_{no}(v+1/2)^n \tag{8}$$

and

$$B_v = \sum_{n=0} Y_{n1}(v+1/2)^n \tag{9}$$

that were used to generate the potential.

The above RKR potential was used in conjunction with the previously published $A^1\Sigma_u^+$ state RKR potential (20) to calculate Franck-Condon factors (35) for transitions between the $A^1\Sigma_u^+$ and $E^1\Sigma_g^+$ states. The results for rotationless transitions are shown in table 4. The comparison of observed band intensities with

Table 2. The Dunham coefficients that describe the $E^1\Sigma_g^+$ state from v=0-12.

The quantities in parentheses are the exponents of 10 in the multiplying factor. All values are in cm^{-1} units.

n,k	Y_{nk}	Standard Error
T_e	2.7410214 (+4)	5.7 (-2)
1,0	2.4587675 (+2)	1.3 (-1)
2,0	-2.8266759 (0)	9.0 (-2)
3,0	-8.6365250 (-1)	2.5 (-2)
4,0	1.1339388 (-1)	3.6 (-3)
5,0	-5.4240404 (-3)	2.5 (-4)
6,0	7.3336943 (-5)	6.5 (-6)
0,1	5.0468926 (-1)	1.5 (-4)
1,1	-9.6442847 (-3)	3.0 (-4)
2,1	-3.5269089 (-4)	1.7 (-4)
3,1	-1.2639093 (-4)	3.2 (-5)
4,1	2.6168385 (-5)	2.5 (-6)
5,1	-1.2388547 (-6)	6.9 (-8)
0,2	-8.4613632 (-6)	8.2 (-8)
1,2	2.3363047 (-7)	1.5 (-7)
2,2	-5.6397248 (-7)	7.8 (-8)
3,2	1.1467136 (-7)	1.2 (-8)
4,2	-6.3522133 (-9)	5.4 (-10)

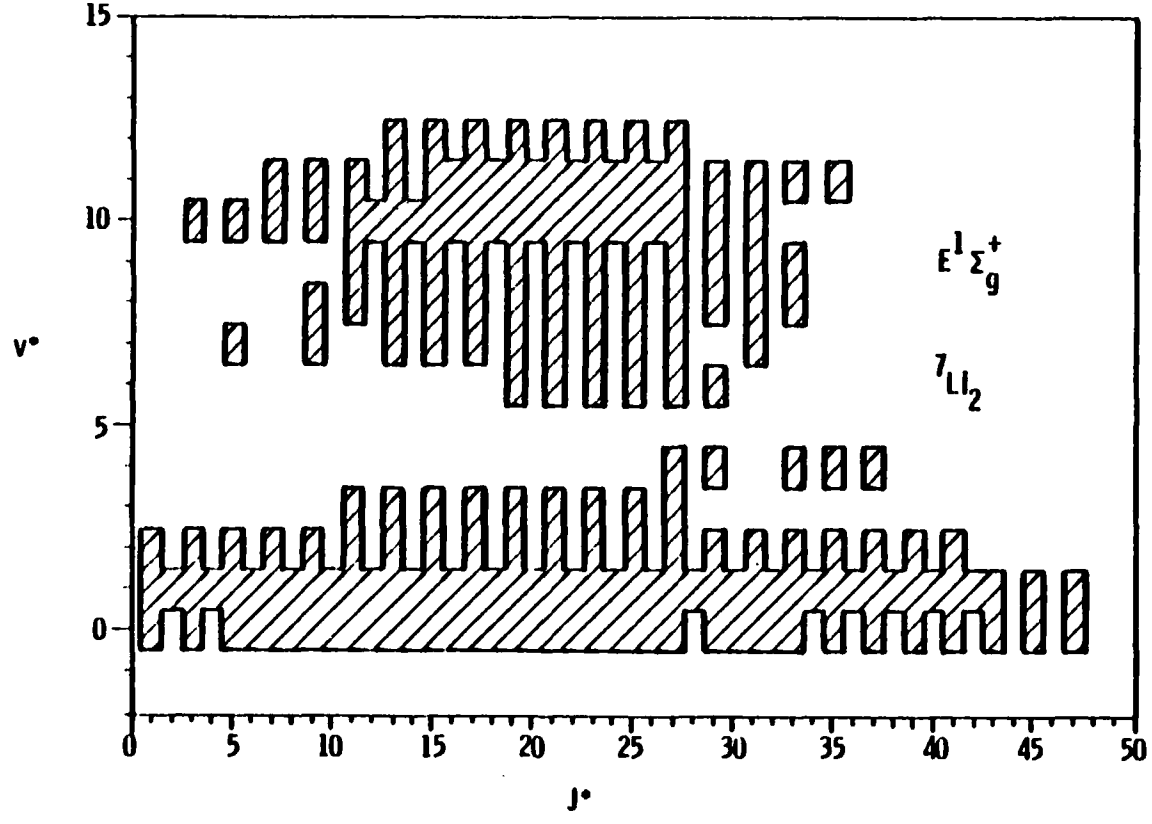

Figure 9. The $E^1\Sigma_g^+$ state energy levels used for the determination of Dunham coefficients.

Table 3. RKR data for the $E^1\Sigma_g^+$ state of $^7Li_2$ for J=0.

v	r(min) {Angstroms}	r(max) {Angstroms}	G_v $\{cm^{-1}\}$	B_v $\{cm^{-1}\}$
-1/2	3.086	3.086	0.00	0.5047
0	2.903	3.301	122.13	0.4998
1	2.787	3.487	360.07	0.4891
2	2.715	3.636	587.45	0.4773
3	2.660	3.775	803.21	0.4645
4	2.616	3.909	1007.60	0.4511
5	2.580	4.040	1201.62	0.4377
6	2.550	4.169	1386.60	0.4247
7	2.523	4.294	1563.84	0.4126
8	2.499	4.418	1734.25	0.4012
9	2.477	4.541	1898.06	0.3902
10	2.457	4.667	2054.61	0.3792
11	2.438	4.806	2202.18	0.3634
12	2.422	4.967	2337.85	0.3430

Table 4. Franck-Condon factors (x 1000) for the $E^1\Sigma_g^+ \leftarrow A^1\Sigma_u^+$ transitions of $^7Li_2$ for J'=J*=0.

v'/v*	0	1	2	3	4	5	6	7	8	9	10	11	12
0	996	3	1										
1	3	994	1	3									
2	1	1	990	2	6								
3		3	1	961	25	9	2						
4			8	15	874	93	4	5					
5				18	50	709	213		9	2			
6				1	38	101	476	355	19	5	5	1	
7					4	72	143	235	451	84		7	3
9					1	13	119	188	62	435	199	14	3
9						3	32	164	106		299	306	75
10							9	65	196	41	28	119	332
11							2	22	107	165	1	67	12
12								5	45	144	101	20	57
13								1	13	90	154	27	73
14									3	31	120	117	
15									1	9	61	144	52
16										2	23	101	130
17											7	50	130
18											2	19	80
19												6	35
20												2	11

calculated Franck-Condon factors was made using a separate table calculated for J'=J*=20 since most of the observed data were not near J*=0.

Two unusual features of the $E^1\Sigma_g^+$ state are revealed by the Birge-Sponer plot of figure 10. First, there is a bend in the curve near v=6. This is the reason for the unusually large number of vibrational constants that were required to fit the $E^1\Sigma_g^+$ state data. Second, the dissociation energy obtained from an extrapolation of this plot is only 322 cm^{-1} larger than the energy of the highest observed vibrational level (v*=12, J*=0). Since the energy of the lowest possible dissociation products, Li(2s)+Li(3s), is over 5000 cm^{-1} above v*=12, the upper part of the $E^1\Sigma_g^+$ state potential must differ radically from the Morse model. Indeed, recent theoretical calculations (36) predict the presence of a double minimum in the potential curve of this state. The close agreement between the theoretical and experimental potential curves for v*=0-12 of the $E^1\Sigma_g^+$ state substantiates this prediction. Potentials of this type have been observed previously in H_2 (37). The theoretical findings indicate that the second minimum is due to a configuration interaction involving the Li(+,-) ion pair potential.

The location of the Li(+,-) ion pair potential can be determined from the following equation:

$$E(Li^+ + Li^-) = E_i(Li) - E_a(Li) + D_e(Li_2\ X^1\Sigma_g^+) - 116{,}000/r(\mathring{A}) \qquad (10)$$

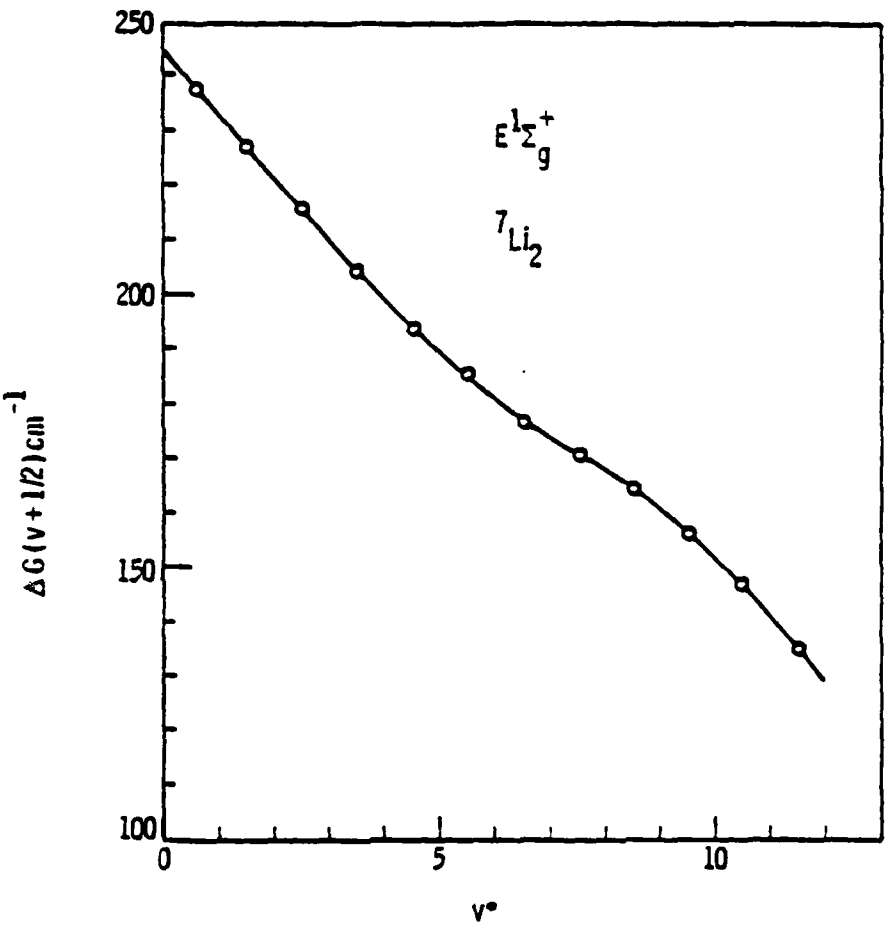

Figure 10. Birge-Sponer plot for the $E^1\Sigma_g^+$ state of $^7Li_2$.

where the first and second terms are the ionization potential and electron affinity of Li, respectively, the third term is the dissociation energy of the ground state of Li_2, and fourth term is the Coulomb potential. The energy is measured with respect to the base of the ground state potential well of Li_2 in cm^{-1} units. Using literature values (38-40) for the first three terms, one gets:

$$E(Li^+ + Li^-) = 43487 - 5001 + 8522 - 116{,}000/r(\mathring{A})$$

$$= 47008 - 116{,}000/r(\mathring{A})$$

This curve is plotted along with the $E^1\Sigma_g^+$ state potential in figure 11. A similar plot, which compares the experimental and theoretical potential curves and vibrational energies for the $E^1\Sigma_g^+$ state, has been given by Konowalow and Fish (36).

The interaction of the $E^1\Sigma_g^+$ state with the Li(+,-) ion pair potential is analagous to the well-known interaction of the $A^1\Sigma^+$ state of LiH with the corresponding ion pair potential of that molecule (41). Both the $E^1\Sigma_g^+$ state of Li_2 and the $A^1\Sigma^+$ state of LiH are nearly covalent at small internuclear distances; at larger r values, they become substantially ionic due to configuration mixing with a crossing ionic potential curve; finally, as $r \to \infty$, they revert to neutrality in order to dissociate to the proper atomic asymptotes.

The energy levels resulting from the above potential curves are also unusual. This is evidenced by the presence of anomalous maxima in the vibrational spacings (36,41) of the above states.

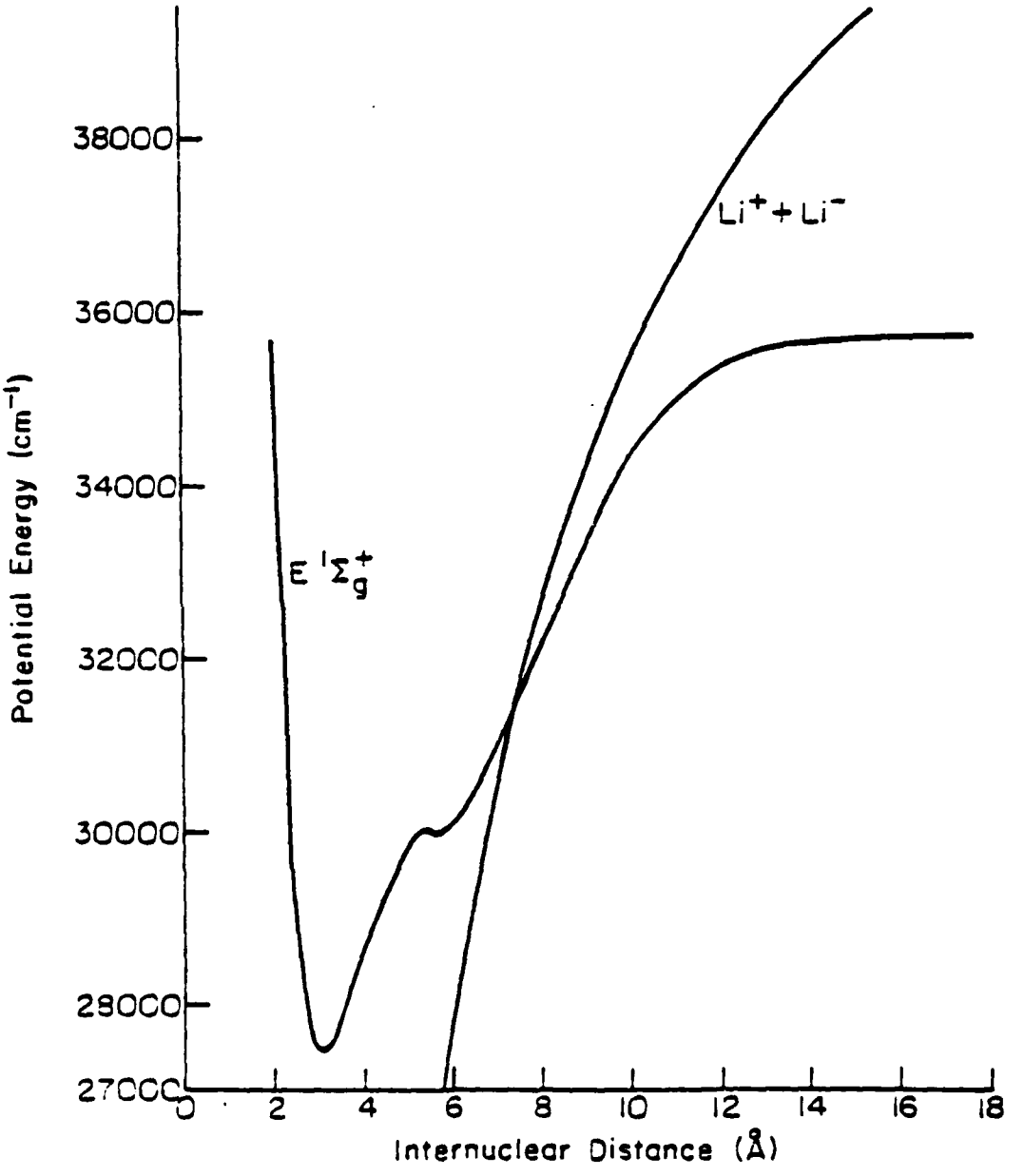

Figure 11. Potential curves for the mutually interacting $E^1\Sigma_g^+$ state and Li(+,-) ion pair. The lower 90% of the inner well of the $E^1\Sigma_g^+$ state is an experimental RKR potential. The remainder of the $E^1\Sigma_g^+$ state potential was obtained from theoretical calculations (36).

Such behavior is difficult to represent by a Dunham expansion. A satisfactory fit of the $E^1\Sigma_g^+$ state observations to Equation (6) was possible only because the ionic part of the curve was not sampled.

The RKR potential curves (9-11,14,20) for all states of $^7Li_2$ that were characterized prior to the systematic Rydberg series investigation are displayed in figure 12. Three of these states, $E^1\Sigma_g^+$, $F^1\Sigma_g^+$, and $G^1\Pi_g$, have been studied by means of OODR. The remainder have been examined using single-photon excitation methods.

C. Unassigned Vibrational Bands from the $E^1\Sigma_g^+$ State Experiment

There were four $\Sigma\leftrightarrow\Sigma$ bands observed in the $E^1\Sigma_g^+$ state experiment that cannot be fit with the Dunham coefficients listed in table 2. Data for these bands are presented in table 5. The identities of the $A^1\Sigma_u^+$ state vibrational levels associated with these bands have been confirmed by the method of combination differences. However, the apparent locations of the upper state energy levels of these bands do not closely approach those predicted (36,42) for the $E^1\Sigma_g^+$ state or any other electronic state that is expected to fall within the range of excitation energies that was used. A possible explanation for these observations is that large systematic errors may be present in the probe frequency data due to incomplete filtering of the output of the Raman-shifting cell.

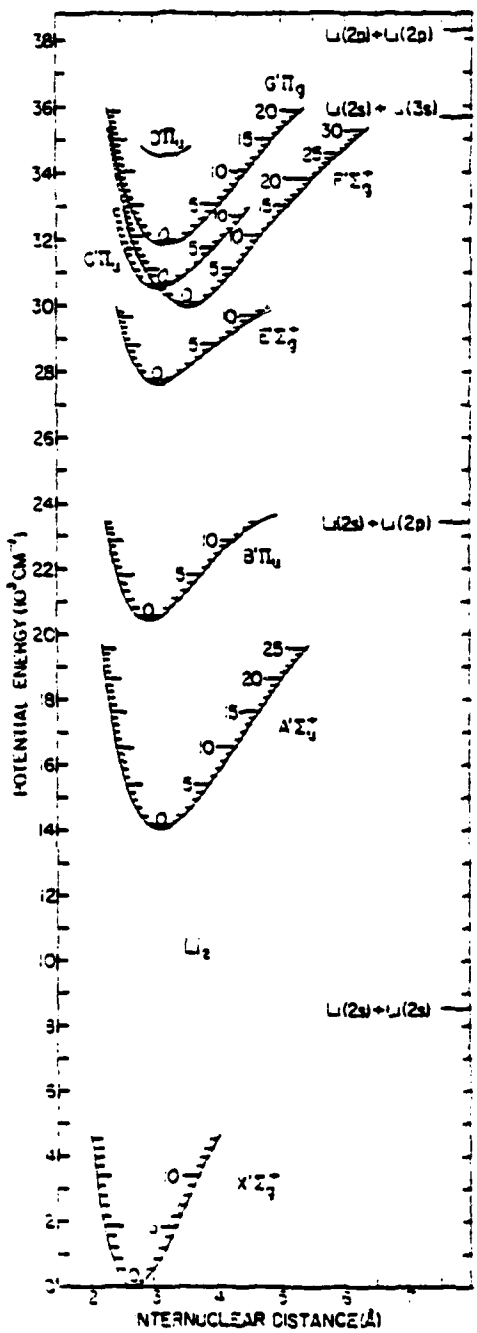

Figure 12. RKR curves for low-lying electronic states of $^{7}Li_{2}$.

Table 5. Molecular constants for the unassigned bands observed during the $E^1\Sigma_g^+$ state investigation.

Band Number	Number of Lines	B_v (cm^{-1})	D_v (cm^{-1})	$T_e + G_v$ (cm^{-1})
1	13	0.3564	8.4×10^{-6}	28477.66
2	14	0.3532	8.0×10^{-6}	28609.24
3	26	0.3237	5.1×10^{-6}	30139.48
4	25	0.3206	6.1×10^{-6}	30277.97

D. Analysis of the Rydberg States of $^7Li_2$

The three sets of gerade Rydberg states that have been identified in Li_2 consist of the lowest thirteen members (n=3-15) of an $nd\pi^1\Pi_g$ series and the lowest eight members (n=3-10) of an $nd\sigma^1\Sigma_g^+$ and an $ns\sigma^1\Sigma_g^+$ series. Only Rydberg states of $^1\Sigma_g^+$ and $^1\Pi_g$ symmetry were accessible since the second step of all of the OODR excitations originated at the $A^1\Sigma_u^+$ state. The T_e values of these states as well as those of all other previously observed states of Li_2 are shown schematically in figure 13. The latter include three gerade states investigated earlier in this laboratory: $E^1\Sigma_g^+$, $G^1\Pi_g$, and $F^1\Sigma_g^+$ (2,6-11). The $E^1\Sigma_g^+$ and $G^1\Pi_g$ states were determined to be the lowest members of the $ns\sigma^1\Sigma_g^+$ and $nd\pi^1\Pi_g$ Rydberg series, respectively. The $F^1\Sigma_g^+$ state correlates with the doubly excited Li(2p)+Li(2p) configuration.

The data consist of approximately 2800 transitions from the $A^1\Sigma_u^+$ state to 28 electronic states lying in the range 33000-42000 cm^{-1} above the base of the ground state potential well. Only levels v=0,1,2, and 4 of the intermediate $A^1\Sigma_u^+$ state were pumped since these were sufficient to establish vibrational numberings in the Rydberg states and to yield adequate data bases for the determination of low-order molecular constants. For each Rydberg state reported in this work, data have been obtained for at least v*=0,1, and 2. The highest observed vibrational level for any of these Rydberg states was v*=7. Most of the OODR transitions terminated on rotational levels within the range J*=0-40, although

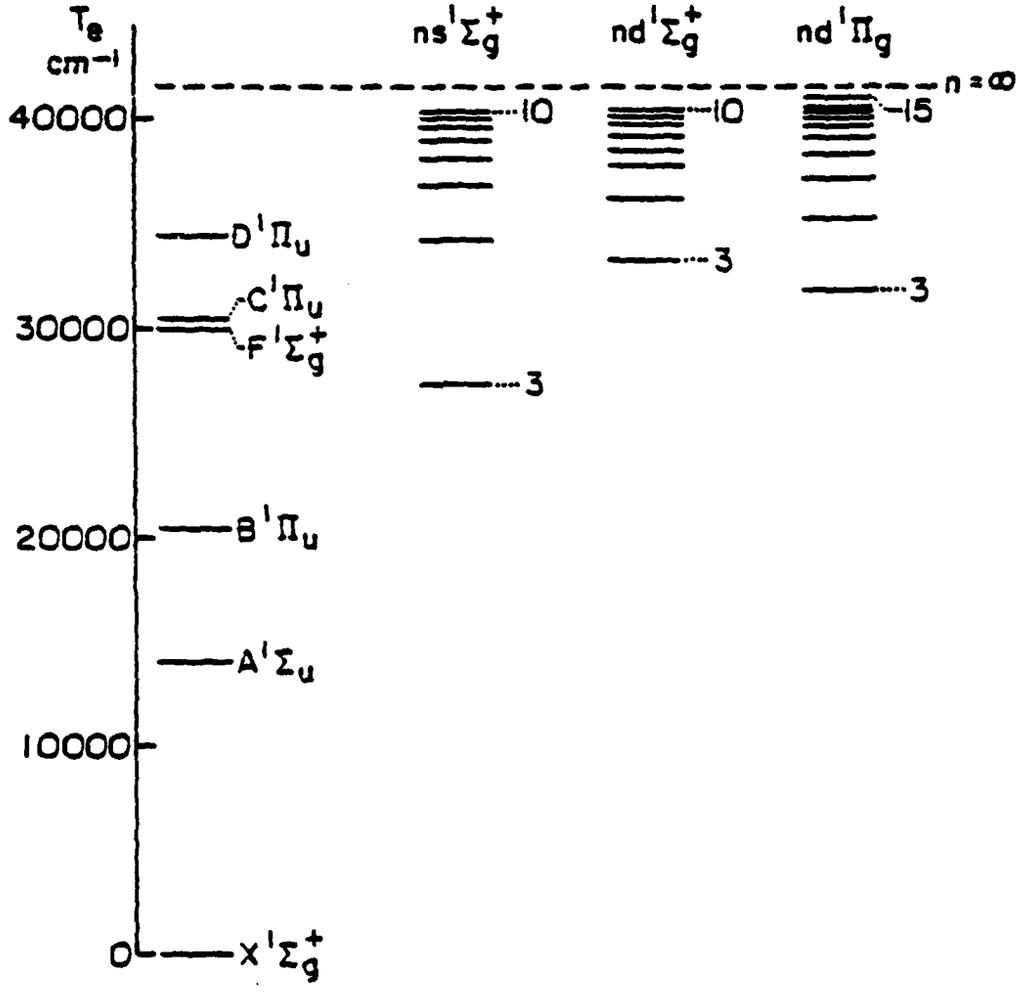

Figure 13. The electronic energies, T_e, of all experimentally observed states of $^7Li_2$. The three Rydberg series that are reported in this work are shown in columns 2-4 of this figure. All other observed states appear in column 1. The broken horizontal line denotes the calculated location of the ionization limit of $^7Li_2$.

levels up to J*=59 were observed in some instances. The wavelengths of the band origins of all $^1\Sigma_g^+ \leftarrow A^1\Sigma_u^+$ and $^1\Pi_g \leftarrow A^1\Sigma_u^+$ bands observed while pumping v'=0,1,and 2 of the $A^1\Sigma_u^+$ state are listed in table 6. The total energies of all J*=0 levels associated with the above bands are also given in this table.

A listing of all pump lines (32) used in the systematic study of the Rydberg states of $^7Li_2$ is given in table 7. Many of these lines were used solely to increase the data bases of the π^- components of the 7-11d$\pi^1\Pi_g$ states. Data for these components were difficult to obtain because the probe laser was unable to resolve lines in the Q branches of the observed 7-11d$\pi^1\Pi_g \leftarrow A^1\Sigma_u^+$ transitions.

The vibrational numbering was initially assigned to each state by assuming that the lowest observed level is v*=0. In all cases, the lowest observed vibrational level seen while pumping v'=1,2, or 4 in the $A^1\Sigma_u^+$ state was no lower than the lowest level seen from v'=0. Franck-Condon factors were derived from the Dunham coefficients for states n=4-11 of the nd$\pi^1\Pi_g$ series, n=3-6 of the ns$\sigma^1\Sigma_g^+$ series, and n=3-5 of the nd$\sigma^1\Sigma_g^+$ series. In all cases, the initial assignments were confirmed by comparisons of the Franck-Condon factors with the observed relative band intensities. Several high-lying observed members of the nd$\pi^1\Pi_g^+$, ns$\sigma^1\Sigma_g^+$, and nd$\sigma^1\Sigma_g^+$ series could not be used in this analysis because of the substantial influence of $^1\Sigma_g^+ \leftrightarrow {}^1\pi_g^+$ lambda-doubling perturbations on the rotational constants of these states. However, since Franck-

Table 6a. Rydberg state band origins (33,500-38,500 cm^{-1}). Tabulations of: 1) the observed probe laser wavelength (Å) of each band origin observed while pumping v'=0, 1, and 2 of the $A^1\Sigma_u^+$ state of $^7Li_2$ and probing the range 5300-3700 Å; and 2) the potential energies (cm^{-1}) of the upper state J*=0 levels associated with the above band origins.

The potential energy is measured with respect to the potential minimum of the $X^1\Sigma_g^+$ state of $^7Li_2$. The range of potential energy covered by this table is 33,000-38,500 cm^{-1}.

nl	Λ	v*	Potential Energy of the Upper State J*=0 Level	Observed λ (Å) of the Band Origin v'=0	v'=1	v'=2
3d	0	0	33445	5194	5262	
3d	0	1	33688	5129	5196	5264
3d	0	2	33926	5067	5132	5199
3d	0	3	34160		5072	5136
3d	0	4	34390			5076
4s	0	0	34428	4941	5004	
4s	0	1	34693	4877	4938	5000
4s	0	2	34951	4817	4876	4936
4s	0	3	35202		4817	4875
4d	1	0	35475	4698	4754	
4d	1	1	35699	4649	4704	4760
4d	1	2	35920		4656	4711
4d	1	3	36135		4610	4663
4d	1	4	36346			4618
4d	0	0	36416	4499		
4d	0	1	36672	4448	4498	
4d	0	2	36920		4449	4499
5s	0	0	36957	4392	4441	4491
4d	0	3	37157			4450
5s	0	1	37200		4394	4443
5d	1	0	37376	4313	4360	
4d	0	4	37376			4404
5s	0	2	37438		4348	4396
5d	1	1	37610	4270	4316	4363
5d	1	2	37841		4274	4320
5d	0	0	37968	4205	4250	
5d	1	3	38069			4277
5d	0	1	38152	4173	4217	
6s	0	0	38254	4155	4199	
5d	0	2	38361		4181	4225
6s	0	1	38498		4157	

Table 6b. Rydberg state band origins (38,500-40,500 cm^{-1}). Tabulations of: 1) the observed probe laser wavelength (Å) of each band origin observed while pumping v'=0, 1, and 2 of the $A^1\Sigma_u^+$ state of $^7Li_2$ and probing the range 5300-3700 Å; and 2) the potential energies (cm^{-1}) of the upper state J*=0 levels associated with the above band origins.

The range of potential energy covered by this table is 38,500-40,500 cm^{-1}.

nl	Λ	v*	Potential Energy of the Upper State J*=0 Level	Observed λ (Å) of the Band Origin v'=0	v'=1	v'=2
5d	0	3	38579			4186
6d	1	0	38585	4099		
6d	0	0	38695	4081		
6s	0	2	38733			4159
6d	1	1	38831	4058	4100	
6d	0	1	38941	4040	4082	4124
6d	1	2	39074		4060	4101
7s	0	0	39137	4008	4049	
6d	0	2	39184		4042	
6d	1	3	39314			4061
7d	1	0	39376	3970		
7s	0	1	39394		4007	
7d	0	0	39408	3965		
6d	0	3	39425			4043
7d	1	1	39628		3970	4010
7s	0	2	39647			4007
7d	0	1	39665		3964	4004
8s	0	0	39755	3911	3950	
7d	1	2	39877			3970
8d	1	0	39908	3888		
7d	0	2	39918			3964
8d	0	0	39929	3885		
8s	0	1	40015		3910	
8d	1	1	40162		3888	3926
9s	0	0	40175	3848	3886	
8d	0	1	40187		3884	
8s	0	2	40271			3909
9d	1	0	40272	3834		
9d	0	0	40295	3830		
8d	1	2	40414			3887
9s	0	1	40434		3847	3884
8d	0	2	40441			3883
10s	0	0	40470	3805		

Table 6c. Rydberg state band origins (40,500 cm^{-1} and above). Tabulations of: 1) the observed probe laser wavelength (Å) of each band origin observed while pumping v'=0, 1, and 2 of the $A^1\Sigma_u^+$ state of $^7Li_2$ and probing the range 5300-3700 Å; and 2) the potential energies (cm^{-1}) of the upper state J*=0 levels associated with the above band origins.

The range of potential energy covered by this table is 40,500 cm^{-1} up to the maximum observed value.

nl	Λ	v*	Potential Energy of the Upper State J*=0 Level	Observed λ (Å) of the Band Origin v'=0	v'=1	v'=2
9d	1	1	40530		3833	3870
10d	1	0	40546	3794		
9d	0	1	40553		3830	
10d	0	0	40558	3792		
9s	0	2	40690			3846
10s	0	1	40730		3804	
11d	1	0	40737	3767		
9d	1	2	40783			3832
10d	1	1	40805		3793	
9d	0	2	40809			3829
10d	0	1	40817		3791	
12d	1	0	40890	3745		
10s	0	2	40986			3803
11d	1	1	40996		3766	
13d	1	0	41007	3729		
10d	1	2	41060			3792
10d	0	2	41073			3790
14d	1	0	41099	3716		
12d	1	1	41149		3744	
15d	1	0	41174	3706		
11d	1	2	41251			3765
13d	1	1	41267		3728	
14d	1	1	41358		3715	
12d	1	2	41405			3743
15d	1	1	41433		3705	
13d	1	2	41524			3727
14d	1	2	41614			3714
15d	1	2	41688			3704

Table 7. Pump lines ($A^1\Sigma_u^+ \leftarrow X^1\Sigma_g^+$) and probe laser scanning ranges used for the systematic investigation of the Rydberg states of $^7Li_2$.

Pump Line	λ (Å) Pump	Pump Freq[a] (cm^{-1})	Probe λ (Å) Range
(0,0) R(17)	7151	13985.122	5300-3700
(0,0) R(15)	7145	13994.597	4000-3725
(0,0) P(5)	7138	14010.420	4000-3720
(1,0) R(39)	7125	14035.614	4075-3900
(1,0) P(17)	7041	14201.645	4150-3800
(1,0) R(21)	7037	14211.589	4200-3760
(1,0) R(19)	7030	14224.296	4000-3700
(1,0) P(13)	7029	14227.621	3900-3760
(1,0) P(11)	7023	14238.503	5300-3725
(2,0) R(45)	7047	14190.997	4000-3750
(2,0) P(37)	7026	14232.240	5400-3800
(2,0) P(23)	6945	14398.746	4055-3770
(2,0) P(21)	6936	14417.026	4460-3700
(2,0) P(9)	6898	14496.767	4055-3740
(4,0) P(29)	6750	14815.933	5235-4100

[a]Reference 32.

Condon factors for transitions originating from the $A^1\Sigma_u^+$ state are expected to become nearly independent of n and Λ at large n, the factors derived for the high-lying $^1\Pi_g^-$ components ought to apply to the nearby $^1\Pi_g^+$ components and $^1\Sigma_g^+$ states as well. The experimental observations qualitatively confirm this expectation.

The measured wavelengths were converted to energies referred to the bottom of the $X^1\Sigma_g^+$ state potential using the $A^1\Sigma_u^+$ state constants of Kusch and Hessel (20). The assigned data for each electronic state were fitted by a linear least squares procedure with the conventional Dunham expansion (Equation 6). For the P and R branches of the $^1\Pi_g$ states, the term q[J(J+1)-1] was appended to Equation (6) in order to describe lambda-doubling interactions. The quantity q in this term is the lambda-doubling constant. The Dunham coefficients obtained from the above fits are presented in Table 8. Digits beyond the determined standard deviations are given for each coefficient to compensate for the effects of statistical correlations. Dunham coefficients were not calculated for the observed n=12-15 states of the $nd\pi^1\Pi_g$ series because of limited data. The term values and limited vibrational constants for these four states are given later in Table 10. The standard deviations of the Dunham fits and extents of the corresponding data bases are indicated in Table 9.

The statistical analyses of the 7-11$d\pi^1\Pi_g$ states were hampered by the aforementioned scarcity of Π^- data for these states. It was found that the rotational constants for the 7-11$d\pi^1\Pi_g^-$ components

Table 8a. Dunham coefficients (cm^{-1} units) for the Rydberg $nd\pi\,^1\Pi_g$ states. Standard deviations are given in parentheses. For n=7-11, the Π^- and Π^+ components were fitted separately. The Y_{02} values listed for the $10d\pi\,^1\Pi_g^-$ and $11d\pi\,^1\Pi_g^-$ components were estimated using equation (7), and then incorporated into the Dunham fits.

n	T_e	Y_{10}	Y_{20}	
4	35360.761 (0.05)	228.9824 (0.06)	-2.12979 (0.02)	
5	37257.700 (0.05)	237.3867 (0.04)	-1.60874 (0.007)	
6	38460.909 (0.05)	249.2891 (0.05)	-1.56509 (0.008)	
7-	39249.495 (0.3)	253.8988 (0.6)	-1.18132 (0.2)	
7+	39248.478 (0.07)	255.0904 (0.09)	-1.50679 (0.03)	
8-	39779.262 (0.2)	257.3414 (0.4)	-1.32537 (0.1)	
8+	39779.301 (0.1)	257.7284 (0.1)	-1.46659 (0.04)	
9-	40150.674 (0.01)	253.8808 (0.01)	-0.44708 (0.004)	
9+	40142.275 (0.3)	261.1221 (0.2)	-1.96116 (0.07)	
10-	40415.804 (0.5)	263.7765 (0.8)	-1.36528 (0.3)	
10+	40414.932 (0.3)	261.3922 (0.3)	-1.44148 (0.1)	
11-	40609.962 (0.2)	259.1735 (0.3)	-1.25676 (0.09)	
11+	40606.600 (0.2)	261.7270 (0.2)	-1.56765 (0.05)	

n	$Y_{30}\times10^2$	Y_{01}	$Y_{11}\times10^3$	$\alpha\times10^3$
4	-2.6759 (0.2)	0.4744853 (0.00008)	-7.36177 (0.01)	0.8315 (0.03)
5		0.4794069 (0.0001)	-5.38328 (0.02)	1.9305 (0.04)
6		0.4859699 (0.00009)	-5.27802 (0.02)	
7-		0.4912869 (0.0006	-5.34246 (0.3)	
7+		0.4727549 (0.0002)	-4.90869 (0.02)	
8-		0.4949026 (0.0004)	-4.70064 (0.2)	
8+		0.4663607 (0.0005)	-4.39667 (0.04)	
9-		0.4950088 (0.00002)	-3.96518 (0.01)	
9+		0.4834892 (0.0005)	-3.79613 (0.09)	
10-		0.4960389 (0.001)	-7.08892 (0.9)	
10+		0.4556259 (0.001)	-4.89457 (0.2)	
11-		0.4963454 (0.0005)	-3.91218 (0.3)	
11+		0.4811837 (0.0005)	-4.14780 (0.2)	

n	$Y_{02}\times10^6$	$Y_{03}\times10^9$	$Y_{04}\times10^{12}$
4	-7.86359 (0.04)		
5	-7.33819 (0.04)		
6	-6.52103 (0.05)		
7-	-6.77949 (0.3)		
7+	4.33594 (0.3)	-3.27750 (0.1)	0.40065 (0.02)
8-	-6.87597 (0.3)		
8+	13.98919 (0.9)	-7.40925 (0.6)	1.03667 (0.1)
9-	-6.31729 (0.007)		
9+	-1.63552 (0.5)	-0.85494 (0.2)	
10-	-7.1		
10+	36.50169 (2)	-15.65633 (1)	
11-	-7.1		
11+	3.03638 (0.4)		

Table 8b. Dunham coefficients (cm^{-1} units) for the Rydberg $ns\sigma^1\Sigma_g^+$ states. Standard deviations are given in parentheses.

n	T_e	Y_{10}	Y_{20}
4	34293.643 (0.07)	270.7360 (0.09)	-2.92366 (0.04)
5	36832.622 (0.04)	249.4297 (0.07)	-2.93425 (0.02)
6	38129.130 (0.1)	251.7842 (0.2)	-4.08597 (0.07)
7	39007.312 (0.1)	260.5552 (0.2)	-1.91811 (0.05)
8	39624.361 (0.05)	262.5268 (0.06)	-1.62886 (0.02)
9	40044.034 (0.2)	262.0960 (0.2)	-1.49164 (0.06)
10	40339.509 (0.09)	262.6953 (0.1)	-1.61811 (0.08)

n	$Y_{30}\times10^2$	Y_{01}	$Y_{11}\times10^3$
4	-8.1534 (0.4)	0.4796918 (0.0001)	-6.27868 (0.06)
5		0.4897651 (0.00008)	-10.00585 (0.04)
6		0.4856933 (0.0005)	-9.88352 (0.3)
7		0.4958304 (0.0002)	-4.44020 (0.06)
8		0.4915980 (0.00006)	-5.33864 (0.02)
9		0.4908477 (0.0005)	-4.40224 (0.2)
10		0.4808107 (0.0006)	-6.84330 (0.5)

n	$Y_{21}\times10^4$	$Y_{02}\times10^6$	$Y_{03}\times10^9$
4	-2.83031 (0.1)	-6.1618 (0.04)	
5		-7.6376 (0.03)	
6		-8.6932 (0.4)	
7		-8.2105 (0.2)	0.26038 (0.04)
8		-6.6164 (0.02)	
9		-10.8119 (0.7)	2.55303 (0.3)
10		-1.1051 (0.7)	

n	$Y_{04}\times10^{12}$
4	
5	
6	
7	
8	
9	-0.415160 (0.05)
10	

Table 8c. Dunham coefficients (cm^{-1} units) for the Rydberg $nd\sigma^1\Sigma_g^+$ states. Standard deviations are given in parentheses.

n	T_e	Y_{10}	Y_{20}
3	33320.180 (0.04)	248.6108 (0.06)	-3.07061 (0.03)
4	36284.875 (0.07)	263.2002 (0.1)	-3.65664 (0.03)
5	37890.096 (0.1)	145.6560 (0.3)	23.02141 (0.1)
6	38571.788 (0.1)	247.5540 (0.09)	-1.05137 (0.02)
7	39277.230 (0.3)	261.5741 (0.5)	-2.04438 (0.2)
8	39798.738 (0.2)	261.0142 (0.2)	-1.63425 (0.06)
9	40163.871 (0.2)	262.2483 (0.2)	-1.74167 (0.05)
10	40426.921 (0.3)	261.9442 (0.3)	-1.41824 (0.1)

n	$Y_{30}\times10^2$	$Y_{40}\times10^2$	Y_{01}
3	18.3739 (0.5)	-1.12034 (0.03)	0.4653795 (0.00007)
4			0.4935457 (0.0001)
5	-239.3077 (2)		0.4760104 (0.0002)
6			0.4972418 (0.0005)
7			0.5121084 (0.0006)
8			0.5285922 (0.0006
9			0.5342577 (0.0008)
10			0.5459900 (0.001)

n	$Y_{11}\times10^3$	$Y_{21}\times10^4$	$Y_{31}\times10^5$
3	-2.85777 (0.04)	0.04659 (0.1)	-2.84601 (0.1)
4	-5.43616 (0.1)	-6.03726 (0.4)	
5	-10.42365 (0.3)	16.76032 (0.6)	
6	-4.41331 (0.2)		
7	-4.39225 (0.2)		
8	-5.79298 (0.1)		
9	-6.17789 (0.1)		
10	-5.54291 (0.3)		

n	$Y_{02}\times10^6$	$Y_{12}\times10^6$	$Y_{03}\times10^9$
3	-6.5530 (0.06)	-0.18182 (0.007)	0.09922 (0.02)
4	-7.2513 (0.04)		
5	-10.9856 (0.1)	2.07768 (0.08)	
6	-9.0409 (0.6)	1.06952 (0.[illegible])	-0.74908 (0.09)
7	-10.0650 (0.5)		0.44018 (0.1)
8	-18.1594 (0.7)		2.12325 (0.2)
9	-22.6178 (1)		3.71539 (0.4)
10	-33.4130 (2)		

Table 8d. Dunham coefficients (cm^{-1} units) for an observed $^1\Pi_g$ state of $^7Li_2$ having an unidentified atomic correlation.

Constant	Value (St. Dev.)
T_e	38849.420 (0.07)
Y_{10}	260.4173 (0.09)
Y_{20}	-1.64461 (0.03)
Y_{01}	0.5042050 (0.00009)
$Y_{02} \times 10^6$	-7.42273 (0.03)
$Y_{11} \times 10^3$	-6.16985 (0.03)

Table 9. Statistical data for the Rydberg states of diatomic lithium.

$ns\sigma^1\Sigma_g^+$ series

n	Maximum v	Maximum J	St. Dev. of Fit (cm^{-1})	Number of Lines Fit
4	5	45	0.20	271
5	3	49	0.12	145
6	2	31	0.14	35
7	2	59	0.27	136
8	2	49	0.08	73
9	2	57	0.21	78
10	2	25	0.06	17

$nd\sigma^1\Sigma_g^+$ series

n	Maximum v	Maximum J	St. Dev. of Fit (cm^{-1})	Number of Lines Fit
3	7	51	0.08	393
4	4	45	0.13	161
5	3	43	0.15	132
6	3	49	0.20	111
7	2	53	0.37	52
8	2	45	0.19	44
9	2	39	0.15	35
10	2	25	0.24	26

$nd\pi^1\Sigma_g$ series

n	Maximum v	Maximum J	St. Dev. of Fit (cm^{-1})	Number of Lines Fit
4	6	45	0.17	246
5	5	49	0.17	162
6	4	45	0.12	99
7-	2	46	0.21	8
7+	2	59	0.13	102
8-	2	46	0.15	8
8+	2	49	0.18	83
9-	2	40	0.00	2
9+	2	47	0.28	35
10-	2	22	0.29	6
10+	2	35	0.34	55
11-	2	22	0.10	6
11+	2	31	0.18	51

are very sensitive to statistical correlations within the sets of constants that were obtained from combined fits of Π^- and Π^+ data. Therefore, the Π^- and Π^+ levels were analyzed separately. In two cases ($10\text{-}11d\pi\,^1\Pi_g$), it was necessary to use an assumed value for the centrifugal distortion constant, Y_{02}, based on Equation (7) in order to circumvent the problem of limited Π^- data.

When comparing Dunham coefficients of electronic states within the same Rydberg series, it is desirable to use the same set of coefficients for fitting each state and to restrict the data bases to roughly the same range of v and J since the Dunham coefficients are sensitive to these parameters. However, this procedure was used only sparingly in the analysis described here since only a few of the observed Rydberg states are useful for deriving the properties of the ground state of Li_2^+. For the remaining Rydberg states, the advantage of having constants that fit all of the observed levels outweighs the desirability of using the same coefficients for all members of the series. The vibrational analyses of all $n\geq 7$ Rydberg states were restricted to two constants Y_{10} and Y_{20} and three vibrational levels ($v^*=0\text{-}2$). The Π^- components of the $7\text{-}11d\pi\,^1\Pi_g$ states were additionally restricted to three rotational constants (Y_{01}, Y_{02}, and Y_{11}) but lambda-doubling interactions of the type $^1\Sigma_g^+ \leftrightarrow {}^1\Pi_g^+$ render restrictions in the rotational constants pointless for all other observed high-lying Rydberg states. The correlations between the rotational and vibrational constants

in each Dunham fit are sufficiently small that restrictions did not have to be applied to the two subsets of constants simultaneously.

A summary of the most significant information contained in the above listings of Dunham coefficients is presented in Table 10. This listing includes several parameters that are not explicitly given in Table 8. The lambda-doubling constants that are presented in Table 10 for the 7-11d$\pi^1\Pi_g$ states have been computed from the relation

$$q=B_e(nd\pi^+)-B_e(nd\pi^-) \qquad (11)$$

The constants listed for members n=12-15 of the nd$\pi^1\Pi_g$ series had to be determined indirectly since the observations for each of these states consist of only one rotational level for each of the v*=0-2 vibrational levels. These values were calculated using the asymptotic values of the rotational constants obtained as described later.

The Dunham coefficients of Table 8 were used to calculate RKR potential curves for all states for which lambda-doubling interactions appeared to be negligible. These potentials are presented in Table 11 along with the associated G_v and B_v values. Each of these RKR curves was then used to calculate Franck-Condon factors for J'=J*=0 transitions originating from the $A^1\Sigma_u^+$ state. These factors are listed in Table 12.

Principal quantum numbers were assigned to each member of a particular Rydberg series by comparing the successive molecular potential well separations with energy differences between

Table 10a. Selected molecular constants for the $nd\pi^1\Pi_g$ Rydberg states of $^7Li_2$. All of the constants listed for the $7\text{-}15d\pi^1\Pi_g$ states were derived exclusively from Π^- data except for the lambda-doubling constant, q. All units are cm^{-1} except where indicated differently.

$nd\pi^1\Pi_g$ series								
n	T_o	T_e	ω_e	$\omega_e x_e$	B_e	α_e	r_e(Å)	q
3	31807.6	31868.4	229.3	1.6	0.469	0.0055	3.20	0.001
4	35299.7	35360.8	229.0	2.1	0.474	0.0074	3.18	0.001
5	37201.0	37257.7	237.4	1.6	0.479	0.0060	3.17	0.002
6	38410.1	38460.9	249.3	1.6	0.486	0.0053	3.14	0.000
7	39201.1	39249.5	253.9	1.2	0.491	0.0053	3.13	-0.019
8	39732.5	39779.3	257.3	1.3	0.495	0.0047	3.12	-0.029
9	40102.5	40150.7	253.9	0.4	0.495	0.0040	3.12	-0.012
10	40372.1	40415.8	263.8	1.9	0.496	0.0071	3.11	-0.040
11	40564.2	40610.0	259.2	1.3	0.496	0.0039	3.11	-0.015
12	40715.0	40759.3	262.4	1.7				
13	40832.4	40876.7	262.2	1.3				
14	40924.2	40968.6	262.1	1.6				
15	40998.6	41042.3	263.8	2.2				

Table 10b. Selected molecular constants for the $nd\sigma\,^1\Sigma_g^+$ and $ns\sigma\,^1\Sigma_g^+$ Rydberg states of $^7Li_2$. All units are cm^{-1} except where indicated differently.

$ns\sigma\,^1\Sigma_g^+$ series

n	T_o	T_e	ω_e	$\omega_e x_e$	B_e	α_e	r_e(Å)
3	27357.2	27410.2	245.9	2.8	0.505	0.0096	3.09
4	34253.2	34293.6	270.7	2.9	0.480	0.0063	3.17
5	36781.6	36832.6	249.4	2.9	0.490	0.0100	3.13
6	38079.0	38129.1	251.8	4.1	0.486	0.0099	3.15
7	38962.1	39007.3	260.6	1.9	0.496	0.0044	*
8	39580.2	39624.4	262.5	1.6	0.492	0.0053	*
9	39999.7	40044.0	262.1	1.5	0.491	0.0044	*
10	40295.4	40339.5	262.7	1.6	0.481	0.0068	*

$nd\sigma\,^1\Sigma_g^+$ series

n	T_o	T_e	ω_e	$\omega_e x_e$	B_e	α_e	r_e(Å)
3	33268.9	33321.1	246.8	2.1	0.465	0.0018	3.22
4	36240.5	36284.9	263.2	3.7	0.494	0.0054	3.12
5	37793.4	37890.1	145.7	-23.0	0.476	0.0104	3.18
6	38520.3	38571.8	247.6	1.1	0.497	0.0044	*
7	39232.5	39277.2	261.6	2.0	0.512	0.0044	*
8	39753.8	39798.7	261.0	1.6	0.529	0.0058	*
9	40119.5	40163.9	262.2	1.7	0.534	0.0062	*
10	40382.5	40426.9	261.9	1.4	0.546	0.0055	*

*r_e is not given because B_e is substantially perturbed by lambda-doubling interactions.

Table 11a. RKR data for the $ns\sigma\,^1\Sigma_g^+$ and $nd\sigma\,^1\Sigma_g^+$ Rydberg states of $^7Li_2$.

nl	v	r(min) {Angstroms}	r(max) {Angstroms}	G_v $\{cm^{-1}\}$	B_v $\{cm^{-1}\}$
3d	-1/2	3.2134	3.2134	0.00	0.4654
	0	3.0252	3.4204	123.56	0.4639
	1	2.8966	3.5873	366.57	0.4610
	2	2.8123	3.7113	604.77	0.4579
	3	2.7469	3.8184	838.72	0.4542
	4	2.6928	3.9166	1068.72	0.4500
	5	2.6470	4.0098	1294.79	0.4451
	6	2.6075	4.1005	1516.70	0.4392
	7	2.5731	4.1910	1733.93	0.4322
4s	-1/2	3.1651	3.1651	0.00	0.4797
	0	2.9885	3.3671	134.63	0.4765
	1	2.8733	3.5355	399.25	0.4696
	2	2.8005	3.6646	657.29	0.4622
	3	2.7452	3.7797	908.27	0.4542
	4	2.7002	3.8884	1151.68	0.4457
	5	2.6623	3.9942	1387.04	0.4366
4d	-1/2	3.1204	3.1204	0.00	0.4935
	0	2.9401	3.3245	130.69	0.4907
	1	2.8212	3.4950	386.57	0.4840
	2	2.7464	3.6269	635.15	0.4762
5s	-1/2	3.1324	3.1324	0.00	0.4898
	0	2.9521	3.3466	123.98	0.4848
	1	2.8386	3.5288	367.54	0.4749
	2	2.7688	3.6690	605.24	0.4648
5d	-1/2	3.1774	3.1774	0.00	0.4760
	0	2.9550	3.4399	78.28	0.4712
	1	2.8407	3.6174	262.21	0.4641
	2	2.7726	3.7329	470.63	0.4604
	3	2.7119	3.8298	689.21	0.4601
6s	-1/2	3.1455	3.1455	0.00	0.4857
	0	2.9657	3.3591	124.97	0.4808
	1	2.8513	3.5423	368.48	0.4709
	2	2.7798	3.6847	603.92	0.4610

Table 11b. RKR data for the $nd\pi\,^1\Pi_g$ Rydberg states of $^7Li_2$.

nl	v	r(min) Angstroms	r(max) Angstroms	G_{v_1} cm^{-1}	B_{v_1} cm^{-1}
4d	-1/2	3.1825	3.1825	0.00	0.4745
	0	2.9917	3.4030	113.96	0.4723
	1	2.8683	3.5867	339.59	0.4634
	2	2.7906	3.7259	566.73	0.4561
	3	2.7312	3.8479	774.20	0.4487
	4	2.6824	3.9606	984.85	0.4414
	5	2.6407	4.0678	1190.52	0.4340
	6	2.6038	4.1716	1391.05	0.4266
5d	-1/2	3.1661	3.1661	0.00	0.4794
	0	2.9773	3.3809	118.29	0.4764
	1	2.8539	3.5569	362.46	0.4704
	2	2.7755	3.6884	583.41	0.4644
	3	2.7157	3.8021	811.15	0.4585
	4	2.6665	3.9058	1035.60	0.4525
	5	2.6246	4.0029	1256.96	0.4465
6d	-1/2	3.1446	3.1446	0.00	0.4863
	0	2.9596	3.3533	124.25	0.4833
	1	2.8376	3.5232	370.41	0.4791
	2	2.7596	3.6495	613.44	0.4728
	3	2.6997	3.7583	853.34	0.4675
	4	2.6502	3.8572	1090.11	0.4622
7d	-1/2	3.1184	3.1184	0.00	0.4942
	0	2.9350	3.3242	127.14	0.4917
	1	2.8134	3.4909	379.17	0.4869
	2	2.7366	3.6145	628.21	0.4820
8d	-1/2	3.1172	3.1172	0.00	0.4945
	0	2.9343	3.3214	128.49	0.4923
	1	2.8124	3.4862	383.27	0.4880
	2	2.7338	3.6079	635.13	0.4836
9d	-1/2	3.1211	3.1211	0.00	0.4933
	0	2.9386	3.3234	130.11	0.4914
	1	2.8155	3.4865	387.29	0.4877
	2	2.7363	3.6072	640.48	0.4839
10d	-1/2	3.1224	3.1224	0.00	0.4929
	0	2.9413	3.3256	130.43	0.4905
	1	2.8211	3.4900	389.00	0.4857
	2	2.7431	3.6118	644.52	0.4809
11d	-1/2	3.1251	3.1251	0.00	0.4920
	0	2.9433	3.3276	130.49	0.4900
	1	2.8217	3.4906	389.09	0.4859
	2	2.7431	3.6111	644.53	0.4817

Table 12a. Franck-Condon factors (x 1000) for $ns\sigma\,^1\Sigma_g^+ \leftarrow A\,^1\Sigma_u^+$ transitions of $^7Li_2$ ($J'=J''=0$).

4s

v'/v''	0	1	2	3	4	5
0	954	40	5	1		
1	46	863	75	13	3	1
2		97	765	106	23	6
3			155	657	136	34
4				223	536	165

5s

v'/v''	0	1	2
0	987	13	
1	12	946	39
2		40	920
3			97
4			2

6s

v'/v''	0	1	2
0	974	25	1
1	26	906	64
2		69	796
3		1	133
4			5

Table 12b. Franck-Condon factors (x 1000) for $nd\sigma\,^1\Sigma_g^+ \leftarrow A\,^1\Sigma_u^+$ transitions of $^7Li_2$ ($J'=J^*=0$).

3d

v'/v*	0	1	2	3	4	5	6	7
0	873	114	11	1				
1	122	671	178	26	2			
2	4	204	531	214	41	5		
3		10	262	427	235	56	9	1
4			17	306	344	248	69	13

4d

v'/v*	0	1	2
0	998	2	
1	2	992	5
2		6	979
3			15
4			

5d

v'/v*	0	1	2	3
0	914	84		1
1	66	760	172	1
2	19	121	614	235
3	1	33	171	498
4		2	40	213

Table 12c. Franck-Condon factors (x 1000) for 4-6d$\pi^1\Pi_g \leftarrow A^1\Sigma_u^+$ transitions of $^7Li_2$ ($J'=J^*=0$).

4d

v'/v*	0	1	2	3	4	5	6
0	925	72	3				
1	71	771	147	10			
2	3	144	609	219	23	1	
3		12	213	447	280	44	4
4		1	27	270	296	324	74

5d

v'/v*	0	1	2	3	4	5
0	956	43	1			
1	43	866	87	4		
2	1	88	773	130	3	
3		3	132	678	172	15
4			7	176	581	240

6d

v'/v*	0	1	2	3	4
0	983	17			
1	17	949	33	1	
2		34	916	48	2
3			51	882	63
4				69	844

Table 12d. Franck-Condon factors (x 1000) for 7-11d$\pi^1\Pi_g \leftarrow A^1\Sigma_u^+$ transitions of $^7Li_2$ ($J'=J^*=0$).

7d

v'/v*	0	1	2
0	999	1	
1	1	997	2
2		2	994

8d

v'/v*	0	1	2
0	999	1	
1	1	998	1
2		1	997

9d

v'/v*	0	1	2
0	999	1	
1	1	997	1
2		1	996

10d

v'/v*	0	1	2
0	998	2	
1	2	994	3
2		4	994

11d

v'/v*	0	1	2
0	997	3	
1	3	993	4
2		4	989

successive Li atomic levels (38,43). This comparison is based on the assumption that the molecular dissociation energies of the high-lying Rydberg states are not significantly influenced by a distant Rydberg electron (16). It was found that corresponding atomic and molecular separations agree to within a few percent for n>6 in all three observed Rydberg series. These separations are shown in Table 13. The convention used for assigning n values to the molecular electronic states was the hydrogenic model.

For the $ns\sigma\,^1\Sigma_g^+$ Rydberg series, the procedure used for assigning n also fixes the azimuthal quantum number, ℓ, since the energy spacings of the atomic s levels of Li are easily distinguishable from those of any other set of atomic Rydberg levels. However, this procedure is unable to distinguish between different $\ell\neq 0$ series. Therefore, the remaining assignments could be made only by resorting to the argument that the strongest molecular transitions are expected to be those that correspond to allowed atomic transitions (16). Since the second step of all of the OODR excitations originated at the $A\,^1\Sigma_u^+$ state, which dissociates to Li(2s) + Li(2p), and since the $\ell=0$ series was separately identified, it was concluded that $\ell=2$ for both of the series that were not directly assignable.

Listings of the diatomic molecular states that arise from various combinations of atomic lithium states are presented in Table 14. All of the observed $^1\Sigma_g^+$ states were assigned to the Li(2s) + Li(ns) or Li(2s) + Li(nd) Rydberg series asymptotes or to the doubly excited Li(2p) + Li(2p) configuration. The

Table 13. Comparison of corresponding atomic and molecular energy spacings in the Rydberg states of lithium. All values are in cm^{-1} units.

nd series

n pair	ΔT_o ($nd\sigma^1\Sigma_g^+$)	ΔT_o ($nd\pi^1\Pi_g$)	ΔE (atomic)
3-4	2972	3492	5340
4-5	1553	1901	2472
5-6	727	1209	1342
6-7	712	791	809
7-8	521	531	525
8-9	366	370	360
9-10	263	270	258
10-11		192	189
11-12		151	147
12-13		117	113
13-14		92	89
14-15		74	72

ns series

n pair	ΔT_o ($ns\sigma^1\Sigma_g^+$)	ΔE (atomic)
3-4	6896	7806
4-5	2528	3287
5-6	1297	1688
6-7	883	980
7-8	618	619
8-9	419	416
9-10	296	295

Table 14. Singlet electronic states of Li_2 resulting from various combinations of Li atoms.

Combination of Unlike Atoms	g	u
[a] Li(ns) + Li(n's)	$^1\Sigma_g^+$	$^1\Sigma_u^+$
Li(ns) + Li(np)	$^1\Sigma_g^+$, $^1\Pi_g$	$^1\Sigma_u^+$, $^1\Pi_u$
Li(ns) + Li(nd)	$^1\Sigma_g^+$, $^1\Pi_g$, $^1\Delta_g$	$^1\Sigma_u^+$, $^1\Pi_u$, $^1\Delta_u$

[a] $n \neq n'$

Combination of Like Atoms	g	u
Li(2s) + Li(2s)	$^1\Sigma_g^+$	none
Li(2p) + Li(2p)	$^1\Sigma_g^+(2)$, $^1\Pi_g$	$^1\Sigma_u^-$, $^1\Pi_u$

identifications of the $E^1\Sigma_g^+$ and $F^1\Sigma_g^+$ state dissociation products have been confirmed by ab initio calculations (36,42). The $^1\Pi_g$ state correlations are also straightforward except in two cases. First, none of the observed states can be identified with the doubly excited Li(2p) + Li(2p) asymptote. Quantum mechanical calculations (42) indicate that the molecular constants of this state differ markedly from those of any of the observed states. The second irregularity in the $^1\Pi_g$ state observations is the presence of a $^1\Pi_g$ state located about halfway between the $6d\pi\,^1\Pi_g$ and $7d\pi\,^1\Pi_g$ states. This state probably correlates with a doubly excited atomic configuration. It does not appear to be a member of a Li(2s) + Li(nℓ) Rydberg series as no other series members were observed. The most probable correlation is Li(2p) + Li(3s), which would give D_o=11,646 cm^{-1}. The Dunham coefficients, RKR potential, and Franck-Condon factors that were derived for this state are presented in Table 15. There are no signs of any perturbations that might be causing this state to be observable solely on account of configuration mixing.

One of the electronic states that was identified as a Rydberg state in the above analysis was characterized prior to the experiments described in this work (9). This state, $G^1\Pi_g$, has been found to correlate with the Li(2s) + Li(3d) asymptote. This assignment differs from an earlier Li(2p) + Li(2p) assignment (9) which was made on the basis of much more limited information than is now available. It is interesting to note that the $G^1\Pi_g$ state may actually dissociate to the lower-lying Li(2p) + Li(2p)

Table 15. Summary of results derived for an observed $^1\Pi_g$ state of $^7Li_2$ having an unidentified atomic correlation.

Dunham coefficients (cm^{-1})

Constant	Value (St. Dev.)
T_e	38849.420 (0.27)
Y_{10}	260.4173 (0.09)
Y_{20}	-1.64461 (0.03)
Y_{01}	0.5042050 (0.0000?)
$Y_{02} \times 10^6$	-7.42273 (0.33)
$Y_{11} \times 10^3$	-6.16985 (0.33)

RKR Data

v	r(min) (Angstroms)	r(max) (Angstroms)	$G_{v+\frac{1}{2}}$ (cm^{-1})
-1/2	3.0872	3.0872	0.0
0	2.9069	3.2922	129.80
1	2.7890	3.4598	386.93
2	2.7141	3.5849	640.76

Franck-Condon factors (x 1000) for transitions originating from the $A^1\Sigma_u^+$ state.

v'/v"	0	1	2
0	995	5	
1	5	985	10
2		9	990

configuration in accordance with the non-crossing rule. This is because the state that formally belongs to the Li(2p) + Li(2p) configuration is predicted (42) to lie above the observed location of the $G^1\Pi_g$ state.

The electronic energies of several of the upper members of each Rydberg series were fit with the molecular Rydberg equation:

$$T_o(n)=T_o(\infty)-R(n-\delta)^{-2} \qquad (12)$$

where n is the principal quantum number, δ is the quantum defect, and R is the Rydberg constant (109733 cm^{-1} for $^7Li_2$).

The quantum defect is a measure of the non-Coulombic contribution to the electric field experienced by a Rydberg electron. This quantity increases as ℓ decreases since the probability of finding an electron in the non-Coulombic core region increases with decreasing ℓ. For a given ℓ value, the quantum defect is expected to approach a constant as n increases since the shape of the inner part of a Rydberg state wave function is approximately independent of n at large n (44). The optimum value for the ionization potential, $T_o(\infty)$, is therefore determined by choosing trial values of this quantity until a plot of δ vs. $T_o(\infty)-T_o(n)$ exhibits a plateau at large n.

The $nd\pi^1\Pi_g$ series provides the most reliable estimation of the ionization potential of Li_2 since the observations extend to a considerably higher n value in this series than in the two $^1\Sigma_g^+$ series. The extrapolation of the term energies of the $nd\pi^1\Pi_g^-$ components by the method described above yields $T_o(\infty)=41496\pm4$ cm^{-1}.

No rotational correction of this value is required since the virtual v=0, J=0 levels of the $^1\Pi_g^-$ components correlate with the v=0, N=0 level of the $X^2\Sigma_g^+$ state of Li_2^+ (21). A plot of δ vs. $T_o(\infty)-T_o(n)$ for $T_o(\infty)$=41496 cm^{-1} is shown in figure 14 for the $nd\pi^1\Pi_g$ series. A listing of the δ values associated with this figure is presented in Table 16 along with similar listings obtained using several other trial values of $T_o(\infty)$. A comparison of the above $T_o(\infty)$ value with corresponding values obtained from photoionization (45-47), electron impact ionization (48,49) ab initio calculations (50) and an earlier Rydberg extrapolation (51) is given in Table 17.

The values of $T_o(\infty)$ obtained from the $ns\sigma^1\Sigma_g^+$ and $nd\sigma^1\Sigma_g^+$ series data are consistent with the value stated above but are not as precise. Both series give a well-defined lower limit of $T_o(\infty)$=41490 cm^{-1}. However, in both cases, the upper limit (approximately 41510 cm^{-1}) can only be crudely estimated since it is impossible to determine whether or not δ reaches a plateau for n<11 in this series. Listings of δ values obtained for the $nd\sigma^1\Sigma_g^+$ and $ns\sigma^1\Sigma_g^+$ states are presented in Table 18 for several trial values of $T_o(\infty)$. For $T_o(\infty)$=41496 cm^{-1}, the limiting quantum defects for the $nd\pi^1\Pi_g$, $nd\sigma^1\Sigma_g^+$, and $ns\sigma^1\Sigma_g^+$ series are 0.15, 0.07, and 0.44, respectively.

In addition to deriving values for $T_o(\infty)$ and δ, the Rydberg equation can be used to determine which of the observed electronic states can be regarded as pure Rydberg states. If the Ritz equation $\delta=\alpha+\beta/n^2$ is assumed (52), where α and β are adjustable constants, then the $T_o(n)$ values of members n=7-9 and 11-15 of the $nd\pi^1\Pi_g$ series and members n=7-10 of the $ns\sigma^1\Sigma_g^+$ and $nd\sigma^1\Sigma_g^+$

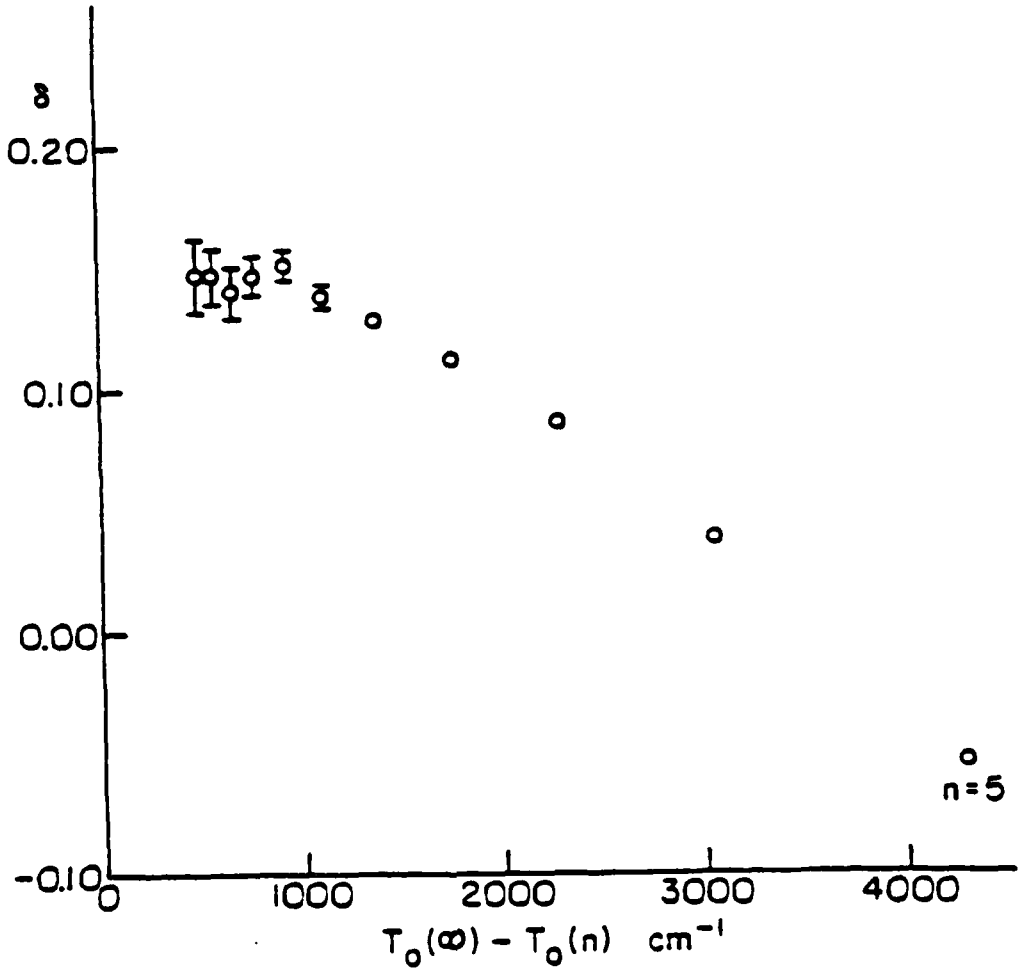

Figure 14. The quantum defects, δ, of the $nd\pi\,^1\Pi_g$ Rydberg states of $^7Li_2$. The δ values were calculated from the Rydberg equation for $T_0(\infty)$=41496 cm^{-1}. The asymptotic behavior exhibited by δ in this plot indicates that the ionization potential is at its optimum value with respect to the observed spectral data.

Table 16. Determination of $T_o(\infty)$ from $nd\pi^1\Pi_g$ Rydberg series data.

The objective is to find a value of $T_o(\infty)$ that causes the calculated value of the quantum defect, δ, to reach a plateau at large n. This table gives quantum defects for several trial values of $T_o(\infty)$. The $T_o(\infty)$ values are specified in the headings in cm^{-1} units. The uncertainties listed for $T_o(\infty)$=41496 cm^{-1} apply to all five columns of δ values. The bottom section of this table shows the results of a statistical determination of which trial value of $T_o(\infty)$ is the best value.

n	δ (41492)	δ (41494)	δ (41496)	δ (41498)	δ (41500)
5	-0.057	-0.056	-0.055	-0.054	-0.052
6	0.033	0.035	0.037	0.039	0.041
7	0.080	0.083	0.086	0.089	0.092
8	0.103	0.107	0.112±0.002	0.116	0.121
9	0.115	0.122	0.128±0.003	0.134	0.141
10[a]	-----	-----	-----	-----	-----
11	0.127	0.139	0.151±0.006	0.162	0.174
12	0.119	0.134	0.149±0.008	0.165	0.180
13	0.105	0.125	0.144±0.010	0.164	0.183
14	0.103	0.127	0.151±0.012	0.176	0.200
15	0.093	0.123	0.153±0.015	0.182	0.212

[a]This state is homogeneously perturbed.

Trial $T_o(\infty)$ Value (cm^{-1})	[b]Weighted Average of δ Values (n=11-15)	Standard Deviation of δ
41492	0.113	0.010
41494	0.131	0.006
41496	0.149	0.003
41498	0.169	0.007
41500	0.186	0.013

[b]The weighting factors are based on the uncertainties in the quantum defects.

Results:

Limit of δ = 0.15

$T_o(\infty)$ = 41498±2 cm^{-1}

Table 17. Comparison of selected experimental and theoretical values for the ionization potential of Li_2 (cm^{-1} units).

Source	To(∞)	Reference
OODR	41496 ± 4	present work
Ab initio	41630 ± 200	50
OODR ionization in a molecular beam	41475 ± 8	45
OODR with two argon ion lasers	41730 ± 100	47
Electron impact ionization	39200 ± 800 39800 ± 800	49 48
Photoionization	41500 ± 800	46
$B^1\Pi_u$, $C^1\Pi_u$, $D^1\Pi_u$ series extrapolation	40250	51

Table 18. Determination of $T_o(\infty)$ for the $ns\sigma\,^1\Sigma_g^+$ and $nd\sigma\,^1\Sigma_g^+$ Rydberg series of $^7Li_2$.

For an explanation of this table, see Table 16.

$ns\sigma\,^1\Sigma_g^+$ series

n	δ (41485)	δ (41490)	δ (41496)	δ (41500)	δ (41510)
6	0.324	0.328	0.333	0.336	0.345
7	0.405	0.411	0.419	0.424	0.437
8	0.410	0.420	0.432±0.002	0.440	0.459
9	0.405	0.419	0.436±0.003	0.448	0.476
10	0.395	0.415	0.439±0.004	0.455	0.495

$nd\sigma\,^1\Sigma_g^+$ series

n	δ (41485)	δ (41490)	δ (41496)	δ (41500)	δ (41510)
6	-0.084	-0.079	-0.073	-0.069	-0.058
7	0.020	0.028	0.037±0.002	0.043	0.059
8	0.038	0.050	0.064±0.002	0.073	0.095
9	0.035	0.052	0.071±0.003	0.084	0.116
10	0.023	0.046	0.073±0.004	0.090	0.134

series can be fit with the Rydberg equation to within 1 cm^{-1}. The $T_o(n)$ value for the $10d\pi\,^1\Pi_g$ state cannot be fit accurately because of a homogeneous perturbation.

Six of the states for which Dunham coefficients are listed in Table 8 contain a substantial number of energy levels that cannot be fit satisfactorily with Equation (6). These consist of members n=9-11 of the $nd\pi\,^1\Pi_g$ series, n=4-5 of the $nd\sigma\,^1\Sigma_g^+$ series, and n=5 of the $ns\sigma\,^1\Sigma_g^+$ series. Each of these states is discussed below.

The irregularities in the $9d\pi\,^1\Pi_g$ and $10d\pi\,^1\Pi_g$ data can be attributed to homogeneous perturbations of the v+1 vibrational levels of the $9d\pi\,^1\Pi_g$ state by the v levels of the $10d\pi\,^1\Pi_g$ state. These interactions can be described in terms of a model that was developed by Herzberg and Jungen to account for observed vibrational and rotational perturbations in Rydberg states of H_2 (53). This model predicts strong homogeneous perturbations between closely lying pairs of $\Delta v=1$ vibrational levels belonging to a common Rydberg series. The $\Delta v=1$ perturbations have been formulated in terms of $d\delta/dr$, where r is the internuclear distance, and an explicit expression has been obtained which can be applied to $\Delta v=1$ interactions in any diatomic Rydberg series. The relative magnitudes of the observed $9d\pi\,^1\Pi_g$ $(v+1)\leftrightarrow 10d\pi\,^1\Pi_g$ (v) perturbations in Li_2 were found to be in good agreement with the above model.

The homogeneous displacements of the $9d\pi\,^1\Pi_g$ and $10d\pi\,^1\Pi_g$ vibrational levels were measured by fitting data from adjacent

unperturbed Rydberg states with a Taylor-expanded form of the Rydberg-Ritz formula:

$$T(n)=T(\infty)-Rn^{-2}+c_3n^{-3}+c_5n^{-5} \qquad (13)$$

where c_3 and c_5 are adjustable constants, and T(n) is the sum of the electronic and vibrational energies of the nth Rydberg state. The downward displacements of the $9d\pi\,^1\Pi_g$ (v+1;J=0) levels (matched by the upward displacements of the $10d\pi\,^1\Pi_g$ (v;J=0) levels) are 4.4 cm^{-1}, 6.3 cm^{-1}, and 7.1 cm^{-1}, for v=0,1, and 2, respectively. The interaction matrix element, H, can be determined for each of the interacting vibrational levels by means of the following relation, which is well known from perturbation theory (21):

$$H=\sqrt{\varepsilon(\varepsilon+\Delta E_o)} \qquad (14)$$

where ΔE_o is the separation of the unperturbed pair of vibrational levels and ε is the magnitude of the displacement of either level from its unperturbed location. The H values corresponding to the above perturbations are 7.7, 10.8, and 13.3 cm^{-1}, respectively.

The rotational constants, B_e and α_e, of the $9d\pi\,^1\Pi_g^-$ component were deperturbed by applying two assumptions: 1) the v=0 level of the $9d\pi\,^1\Pi_g$ state is unperturbed since there is no $10d\pi\,^1\Pi_g$ vibrational level nearby; and 2) the α_e value for the $9d\pi\,^1\Pi_g$ state is approximately the same as the α_e values of nearby unperturbed Rydberg states. The B_v values for the $10d\pi\,^1\Pi_g^-$ component were deperturbed by assuming equal and opposite repulsions occur between the $9d\pi\,^1\Pi_g$ (v+1) and

$10d\pi\,^1\Pi_g$ (v) levels. The results of the above procedures are presented in Table 19.

Additional homogeneous perturbations are likely to be present in most of the n>10 states of the $nd\pi\,^1\Pi_g$ series but only those in the $11d\pi\,^1\Pi_g$ state were found to be significantly larger than the precision of measurement. An attempt to deperturb the $11d\pi\,^1\Pi_g$ state was abandoned when it became clear that a large number of possible perturbing states would have to be considered in the calculations.

The most unusual state that was observed was the $5d\sigma\,^1\Sigma_g^+$ state. The vibrational spacings in this state are expected to start at about 250 cm^{-1} and then slowly decrease. However, the first three observed vibrational spacings are 184 cm^{-1}, 208 cm^{-1}, and 219 cm^{-1}, respectively. This behavior suggests a repulsion of the lower vibrational levels of the $5d\sigma\,^1\Sigma_g^+$ state by an unidentified $^1\Sigma_g^+$ state lying at lower energy. Indeed, a fit of the neighboring $nd\sigma\,^1\Sigma_g^+$ states to a Rydberg formula indicates that the bottom of the potential well of the $5d\sigma\,^1\Sigma_g^+$ state is displaced upward by about 300 cm^{-1}. Despite the unusual vibrational structure presented by this state, there is good agreement between observed relative band intensities and calculated Franck-Condon factors.

Other unusual states include $4d\sigma\,^1\Sigma_g^+$ and $5s\sigma\,^1\Sigma_g^+$. The B_v values of each of these states decrease at a normal rate over the first few vibrational levels but then drop sharply at v=3 in the $5s\sigma\,^1\Sigma_g^+$ state and at v=4 in the $4d\sigma\,^1\Sigma_g^+$ state. Since such behavior cannot be represented accurately by a Dunham expansion, only

Table 19. Deperturbed molecular constants for the Π^- components of the $9d\pi\,^1\Pi_g$ and $10d\pi\,^1\Pi_g$ states.

n	T_o (cm^{-1})	T_e (cm^{-1})	ω_e (cm^{-1})	$\omega_e x_e$ (cm^{-1})	B_e (cm^{-1})	α_e (cm^{-1})	r_e(Å)	δ
10	40367.7	40412.2	261.9	1.7	0.497	0.0052	3.11	0.14
9	40102.5	40147.6	260.8	1.7	0.496	0.0052	3.12	0.13

the lowest few vibrational levels of the above two states were fitted with Equation (6).

A noteworthy feature of the upper Rydberg states of Li_2 is the prominent role that is played by heterogeneous perturbations. Lambda-doubling, which is an interaction between rotational and electronic motion, is the most commonly observed perturbation of this type. Lambda-doubling can occur between any pair of electronic states with $\Delta\Lambda = \pm 1$ and $\Delta S = \Delta\Sigma = 0$ but manifests itself most prominently in the removal of the double degeneracy of pi state rotational levels. Figure 15 illustrates the splitting produced in a $^1\Pi_g$ state as a result of lambda-doubling interactions. In this case, the perturbed energy levels can be represented in terms of two effective rotational constants, one describing the Π^+ component (also called "c" levels) of the pi state and one describing the Π^- component (also called "d" levels).

The effect of lambda-doubling on the structure of an OODR band is illustrated in figure 3. The intense P-Q-R triplet of this band does not have the nearly equal P-Q and Q-R energy spacings that characterize an unperturbed pi band. Instead, the P and R lines are displaced to lower energies as a result of $^1\pi_g^+ \longleftrightarrow {}^1\sigma_g^+$ lambda-doubling perturbations.

Lambda-doubling becomes important in the $nd\pi\,^1\Pi_g$ series at $n=7$. This observation is consistent with the fact that the spacings between corresponding members of the $nd\sigma\,^1\Sigma_g^+$ and $nd\pi\,^1\Pi_g$ series are much larger for $n<7$ than for $n\geq 7$. Furthermore, the observed

AD-A121 487 RYDBERG STATES OF 7LI(2) BY PULSED OPTICAL DOUBLE RESONANCE SPECT.. (U) PENNSYLVANIA STATE UNIV UNIVERSITY PARK APPLIED RESEARCH LAB.. T L TIPTON

UNCLASSIFIED 12 AUG 82 ARL/PSU/TM-82-181 F/G 20/6 NL

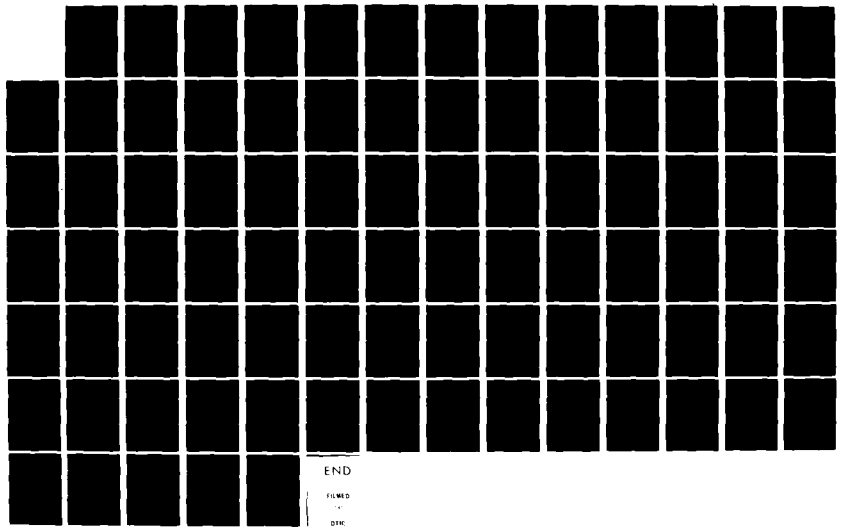

END

FILMED

DTIC

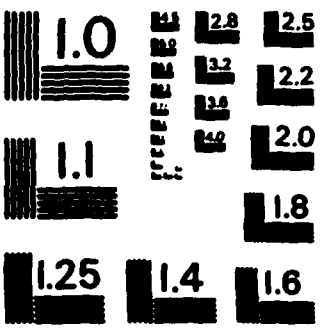

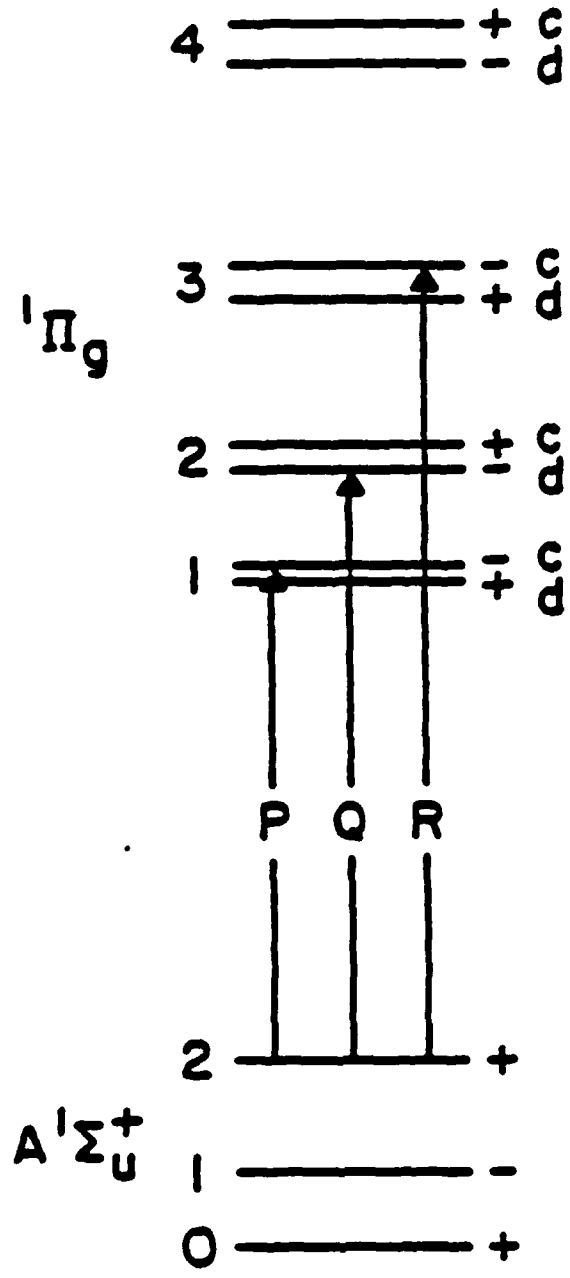

Figure 15. Illustration of lambda-doubling in a $^1\Pi_g$ state. The c and d components interact with $^1\Sigma_g^+$ and $^1\Sigma_g^-$ states, respectively. Here, the c levels are depicted as lying higher in energy than the corresponding d levels, but the opposite is also possible.

behavior of the rotational constant, B_v, in each of these two series is consistent with the fact that the $nd\sigma\,^1\Sigma_g^+$ states lie higher in energy than the corresponding $nd\pi\,^1\Pi_g$ states. However, the B_v values for these states cannot be deperturbed simply by treating each nd complex as an isolated entity. The failure of conventional methods to handle similar perturbation problems in H_2 and He_2 has led to the development of multichannel quantum defect theory (54). However, such a procedure is not essential in the present analysis since the rotational constants of the ground state of Li_2^+ can be determined through examination of the Π^- components of the $nd\pi\,^1\Pi_g$ Rydberg states.

Accurate estimates of the vibrational constants of the ground state of Li_2^+ can be readily obtained from the observed molecular Rydberg states since these constants reach their asymptotic values within the range of experimentally observed states. This is illustrated in figure 16 by plots (16) of ω_e vs. $1/n^2$ for the three observed Rydberg series (the quantity $1/n^2$ was chosen since the electronic energies of the Rydberg states are approximately functions of $1/n^2$). The result of averaging the eleven ω_e values that lie near the asymptotes of these plots is ω_e=262.2±1.5 cm^{-1}. The average $\omega_e x_e$ value derived from these same states is $\omega_e x_e$=1.7±0.5 cm^{-1}. These values are in agreement with ab initio calculations (50). An alternate method of obtaining the foregoing results is to extrapolate the rotationless term energies of v*=0,1, and 2 of the $nd\pi\,^1\Pi_g$ states of Li_2 and use the

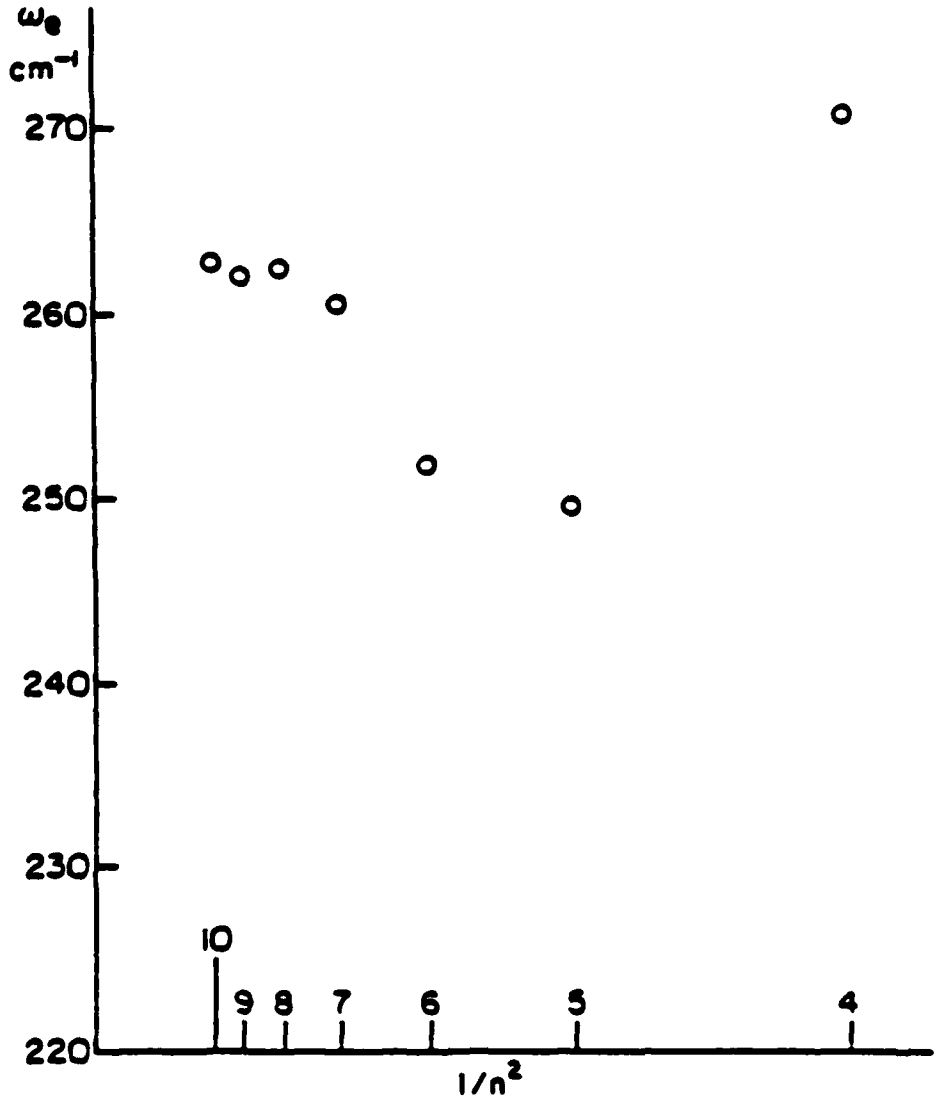

Figure 16a. The vibrational constant, ω_e, as a function of $1/n^2$ for the $nsc^{1}\Sigma_g^+$ Rydberg series of $^7Li_2$.

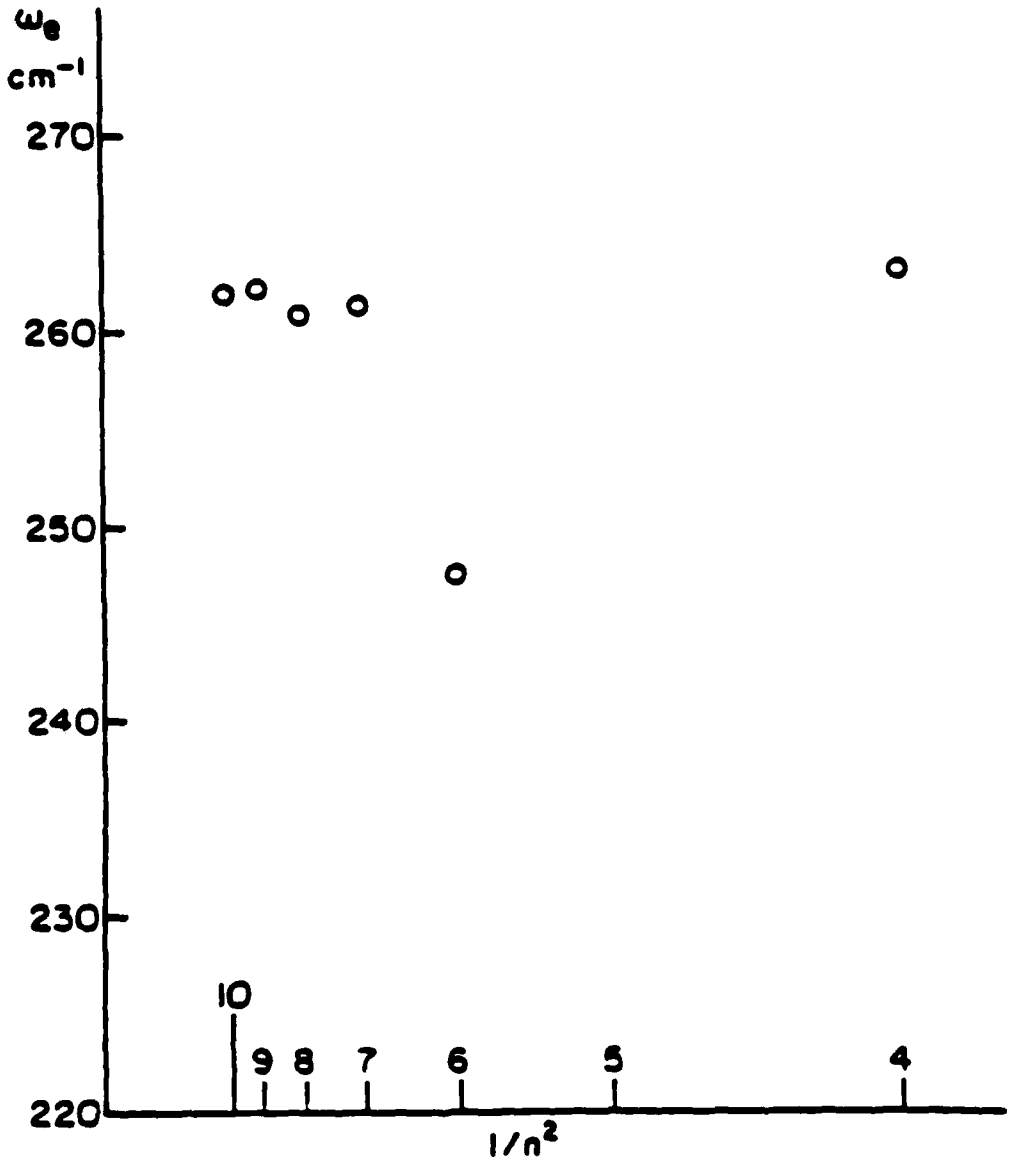

Figure 16b. The vibrational constant, ω_e, as a function of $1/n^2$ for the $nd\sigma\,^1\Sigma_g^+$ Rydberg series of $^7Li_2$.

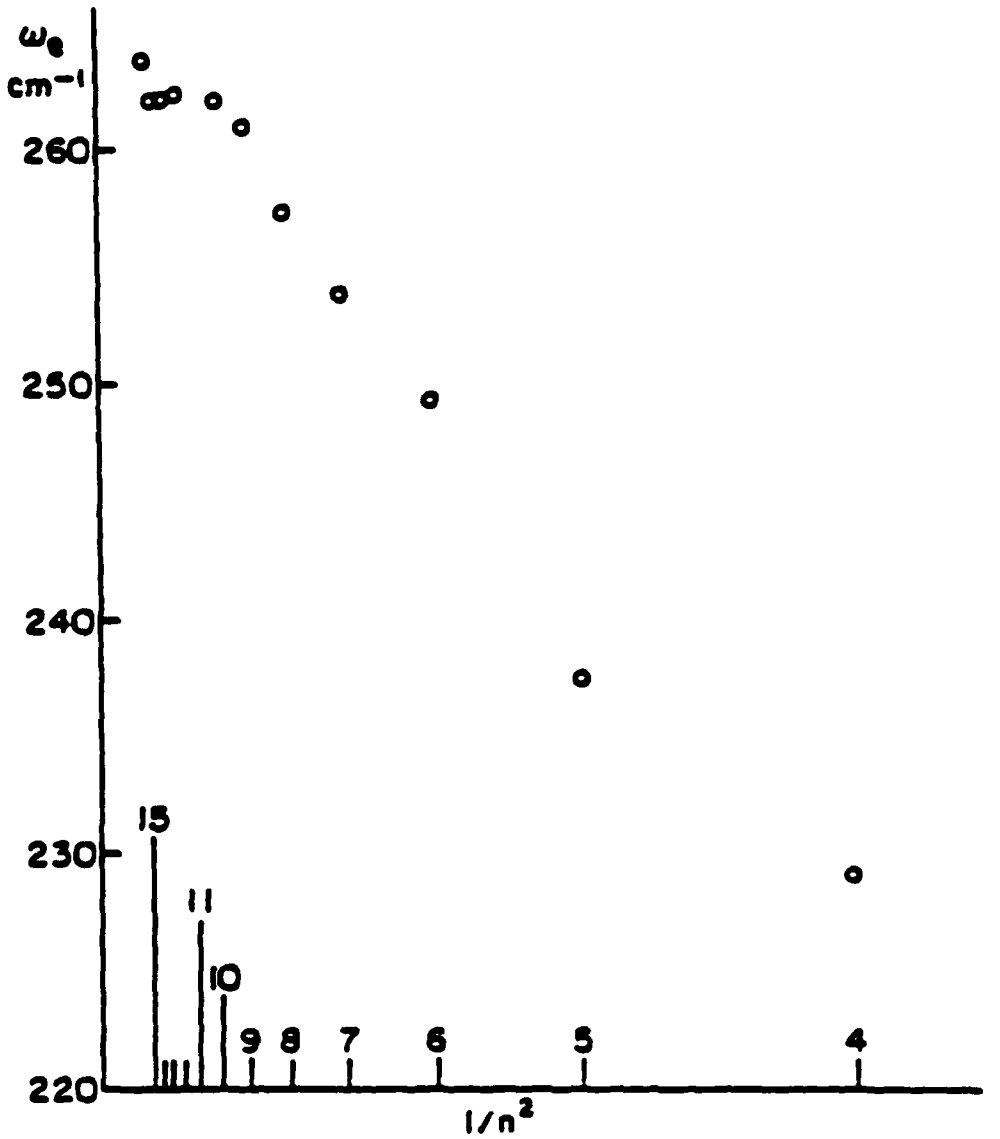

Figure 16c. The vibrational constant, ω_e, as a function of $1/n^2$ for the $nd\pi\,{}^1\Pi_g$ Rydberg series of $^7Li_2$.

three series limits to calculate ω_e and $\omega_e x_e$. The constants derived in this manner are in agreement with the values stated above but are less precise. The term energies used to perform these extrapolations are presented in Table 20. The series limits of the $v^+=1$ and 2 levels were deduced from the values listed in Table 21 in the same manner as was done earlier for $v^+=0$.

The extrapolations of the rotational constants are less reliable because of lambda-doubling perturbations. However, the Π^- components of the $nd\pi\,^1\Pi_g$ Rydberg series are likely to be free of such interactions since the lowest-lying $^1\Sigma_g^-$ state correlates with Li(2p) + Li(3d), a configuration that lies more than 13,000 cm^{-1} above the highest vibrational level for which rotational constants have been obtained. Perturbations involving $^1\Delta_g^-$ states are also possible but are likely to be negligible since a plot of B_e vs. $1/n^2$ for the $nd\pi\,^1\Pi_g$ series exhibits no significant irregularities. Additional evidence for the absence of large lambda-doubling perturbations in the $^1\Pi_g^-$ components is that equation (7) is accurate to within twelve percent for all $^1\Pi_g^-$ components for which data are available. On the other hand, this relation is inaccurate by as much as several hundred percent when applied to states for which substantial lambda-doubling interactions are known to be present.

The B_e values for the Π^- components of the $nd\pi\,^1\Pi_g$ states are summarized in Table 13, and plotted in figure 17. The asymptotic B_e value was obtained by adding one-half of the average α_e value to the average B_o value of members n=8-11 of the

Table 20. Rydberg equation data (cm^{-1} units) for the $nd\pi\,^1\Pi_g$ series.

n	$T_e(n)$	$T_o(n)$	$T_1(n)$	$T_2(n)$
3	31868.4	31807.6	32033.7	32256.5
4	35360.9	35299.7	35524.3	35744.5
5	37257.7	37201.0	37435.1	37666.1
6	38460.9	38410.1	38656.3	38899.3
7	39248.6	39200.7	39452.7	39701.7
8	39779.0	39732.5	39987.3	40239.1
9[a]	40142.3	40101.8	40358.6	40607.8
10[a]	40415.6	40371.0	40629.5	40885.0
11[b]	40606.6	40563.7	40820.7	41074.4
12	40759.6	40718.6	40972.6	41227.2
13	40876.8	40832.0	41090.8	41347.5
14	40968.9	40923.8	41181.9	41437.2
15	41042.6	40999.2	41256.7	41511.5

[a]The v=1 levels of the $9d\pi\,^1\Pi_g$ state homogeneously perturbed the v levels of the $10d\pi\,^1\Pi_g$ state. Therefore, the v=0 level of the $9d\pi\,^1\Pi_g$ state had to be fit separately from the v=1 and 2. All constants listed for the $9d\pi\,^1\Pi_g$ and $10d\pi\,^1\Pi_g$ states are perturbed except for $T_o(n)$ of the $9d\pi\,^1\Pi_g$ state.

[b]The least squares fit does not predict the observed low J levels of the $11d\pi\,^1\Pi_g$ state accurately. The values listed for $T_o(n)$ and $T_2(n)$ were obtained by fitting low J data only.

Table 21. Determination of excited vibrational energies of the ground state of $^7Li_2^+$ from $nd\pi\,^1\Pi_g$ Rydberg series data.

Determination of $T_e(^2\Sigma_g^+)+G_v$			Determination of $T_e(^2\Sigma_g^+)+G_v$		
v	(81795)		v	(82011)	
5	-0.380		5	-0.324	
6	0.389		6	0.361	
7	0.396		7	0.407	
8	0.121±0.332		8	0.133±0.332	
9[a]	———		9[b]	———	
10[a]	———		10[b]	———	
11	0.162±0.136		11	0.176±0.136	
12	0.157±0.304		12	0.163±0.304	
13	0.186±0.319		13	0.180±0.319	
14	0.164±0.312		14	0.171±0.312	
15	0.140±0.319		15	0.178±0.319	

[a]Consecutively perturbed

[b]Consecutively perturbed

Trial Value of $T_e(^2\Sigma_g^+)+G_v$ (cm^{-1})	Av. B Value	St. Dev. of B	Trial Value of $T_e(^2\Sigma_g^+)+G_v$ (cm^{-1})	Av. B Value	St. Dev. of B
81795	0.122	0.319	82027	0.153	0.319
81794	0.189	0.308	82010	0.190	0.314
81795	0.158	0.320	82011	0.166	0.326
81796	0.168	0.307	82012	0.173	0.295
81799	0.196	0.293	82019	0.221	0.319

Results:

Limit of $T_e(^2\Sigma_g^+)+G_v$ = 81795.16 ± 0.16 cm^{-1}

Results:

Limit of $T_e(^2\Sigma_g^+)+G_v$ = 82011.16 ± 0.16 cm^{-1}

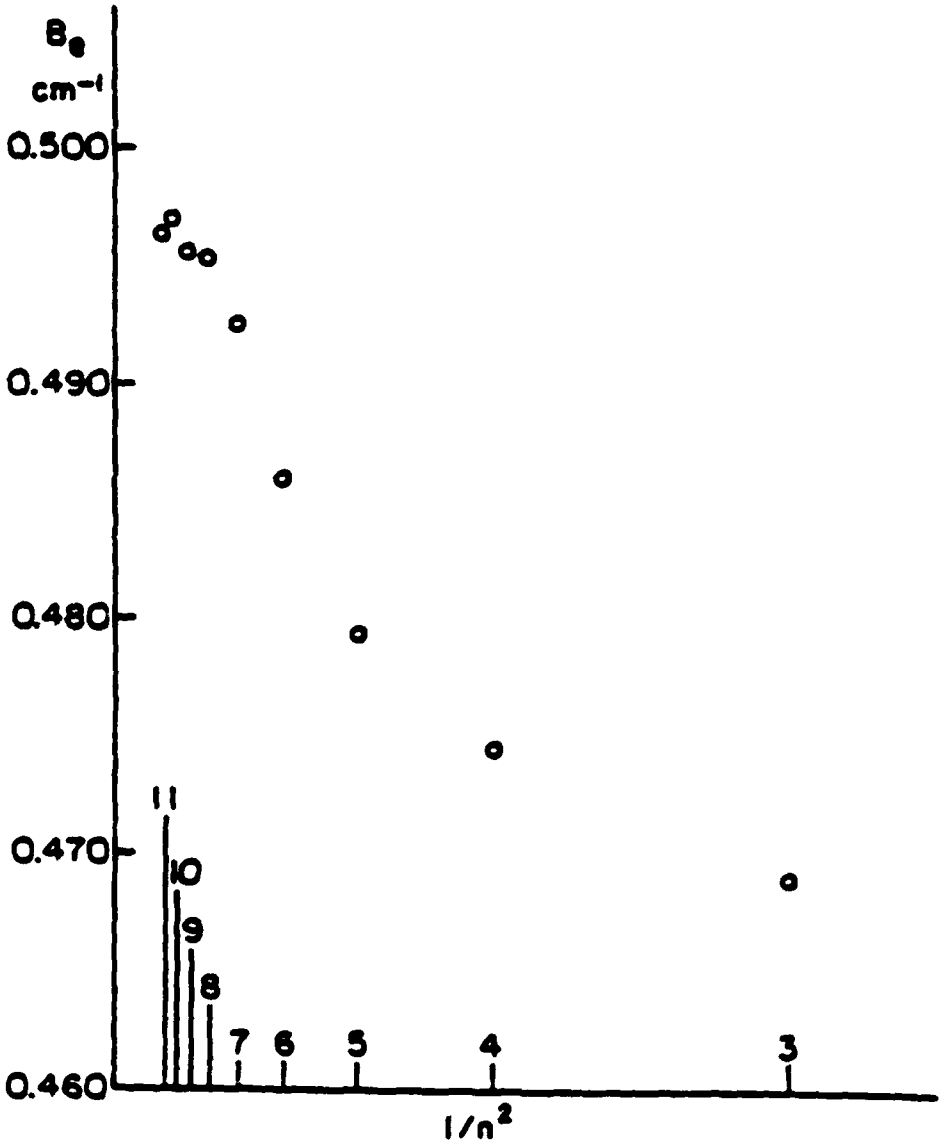

Figure 17. The rotational constant, B_e, as a function of $1/n^2$ for the Γ^- components of the $nd\pi\,^1\Pi_g$ Rydberg series of $^7Li_2$.

$nd\pi\,^1\Pi_g$ series. This procedure took advantage of the fact that the v=0 levels are the least perturbed levels in the $nd\pi\,^1\Pi_g$ states. The asymptotic value of α_e was obtained by averaging the values of all of the pure Rydberg states since this constant does not exhibit any discernable dependence on n, Λ, or on the amount of lambda-doubling. The results obtained from the above procedures are: B_e=0.496±0.002 cm^{-1} and α_e=(5.2±1.9)x10^{-3} cm^{-1}. A summary of the estimated constants of the ground state of $^7Li_2^+$ is given in Table 22.

The dissociation energies of the Rydberg states of Li_2 can be readily determined by using the T_e values listed in Table 9 along with the value (40) of D_e=8521.5±4 cm^{-1} for the ground state of Li_2. These D_e values are listed in Table 23 and plotted vs. $1/n^3$ in figure 18 for each of the observed Rydberg series. The variation of D_e with $1/n^3$ becomes approximately linear at large n, as expected. The sign of the linear slope is given by the sign of the difference between the limiting molecular and atomic quantum defects. The sign of the slope at low n values is positive or negative depending on whether the Rydberg electron is bonding or antibonding, respectively. All of the plots in figure 18 correspond to the latter. Using $T_0(\infty)$=41496 cm^{-1} and correcting for the difference in the zero point vibrational energies of the ground states of Li_2 and Li_2^+, the dissociation energy D_e=10469±6 cm^{-1} is obtained for the ground state of Li_2^+. This is within the error limits of D_e=10320±200 cm^{-1} obtained from the best available ab initio calculations (30). However, a recent value of $D_0(Li_2^+$

Table 22. Summary of results derived from the observed Rydberg states of $^7Li_2$.

$T_0(^1\Sigma_g^+) = 41496.3\ cm^{-1}$

$D_e(Li_2^+\ X^2\Sigma_g^+) = 10869.6\ cm^{-1}$

Estimated molecular constants for $^7Li_2^+\ X^2\Sigma_g^+$:

Constant	Value (cm^{-1})	95% Confidence Limit (cm^{-1})	Number of Values Averaged
ω_e	262.2	1.5	[a] 11
$\omega_e x_e$	1.7	0.5	[a] 11
B_e	0.496	0.002	[b] 8
$\alpha_e \times 10^3$	5.2	1.9	[c] 11

[a] The values given for ω_e and $\omega_e x_e$ are derived from data of the 8-10sc$^1\Sigma_g^+$, 7-10dc$^1\Sigma_g^+$, and 12-15d-$^1\Pi_g$ states.

[b] The B_e values of the 8-11d-$^1\Pi_g$ states were used.

[c] The α_e values of the 7-10sc$^1\Sigma_g^+$, 7-10dc$^1\Sigma_g^+$, and 7,8-11d-$^1\Pi_g$ states were used.

Table 23. Dissociation energies (cm^{-1}) for the observed Rydberg states of Li_2.

n	D_e ($ns\sigma^1\Sigma_g^+$)	D_e ($nd\pi^1\Pi_g$)	De ($nd\sigma^1\Sigma_g^+$)
3	8317	7937	6484
4	9240	9784	8860
5	9989	10359	9727
6	10381	10498	10387
7	10483	10519	10491
8	10485	10514	10494
9	10481	10505	10489
10	10480	10499	10484
11		10490	
12		10488	
13		10483	
14		10480	
15		10479	

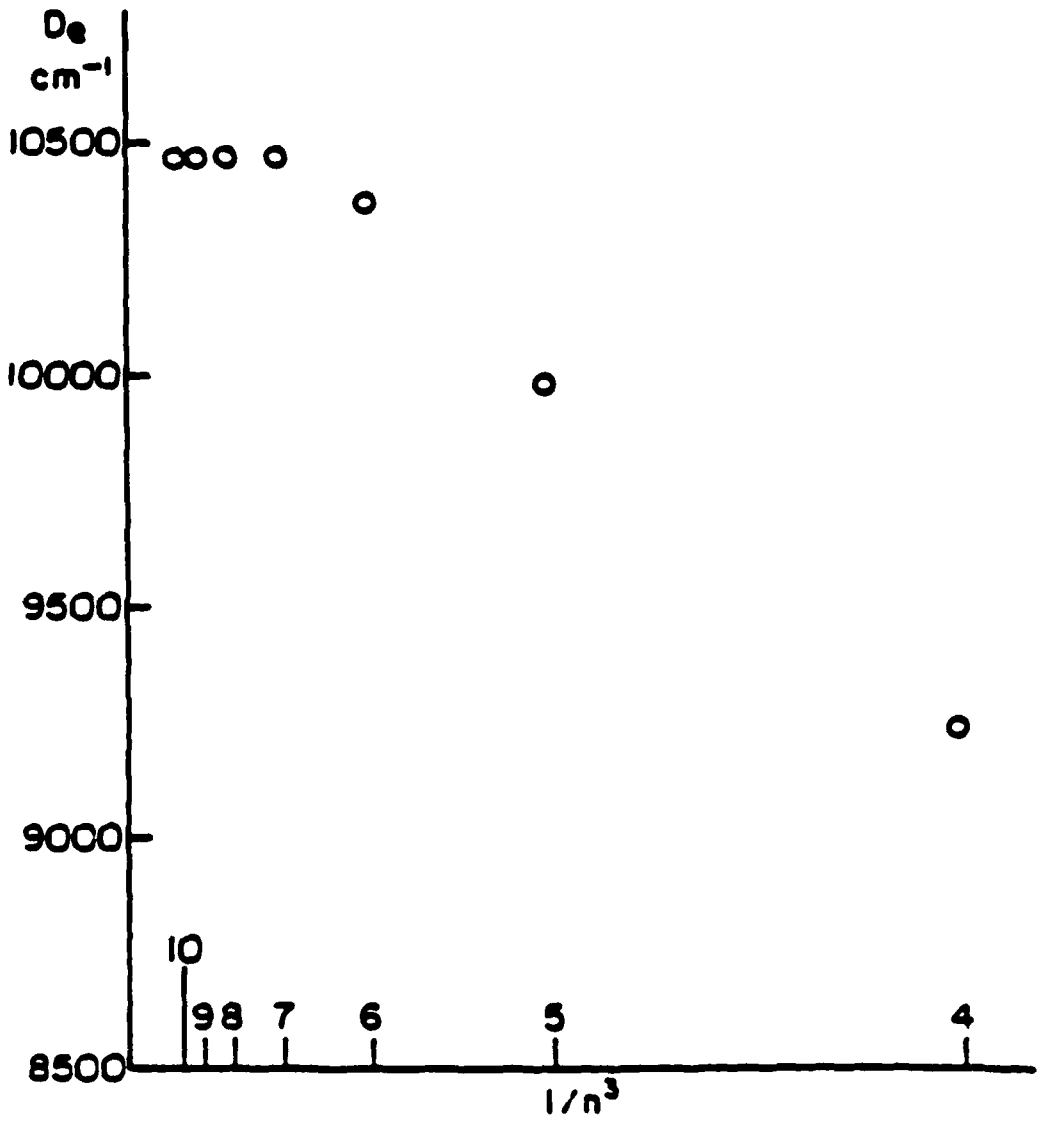

Figure 18a. The dissociation energy, D_e, as a function of $1/n^3$ for the $nsc^{1}\Sigma_g^+$ Rydberg series of $^7Li_2$.

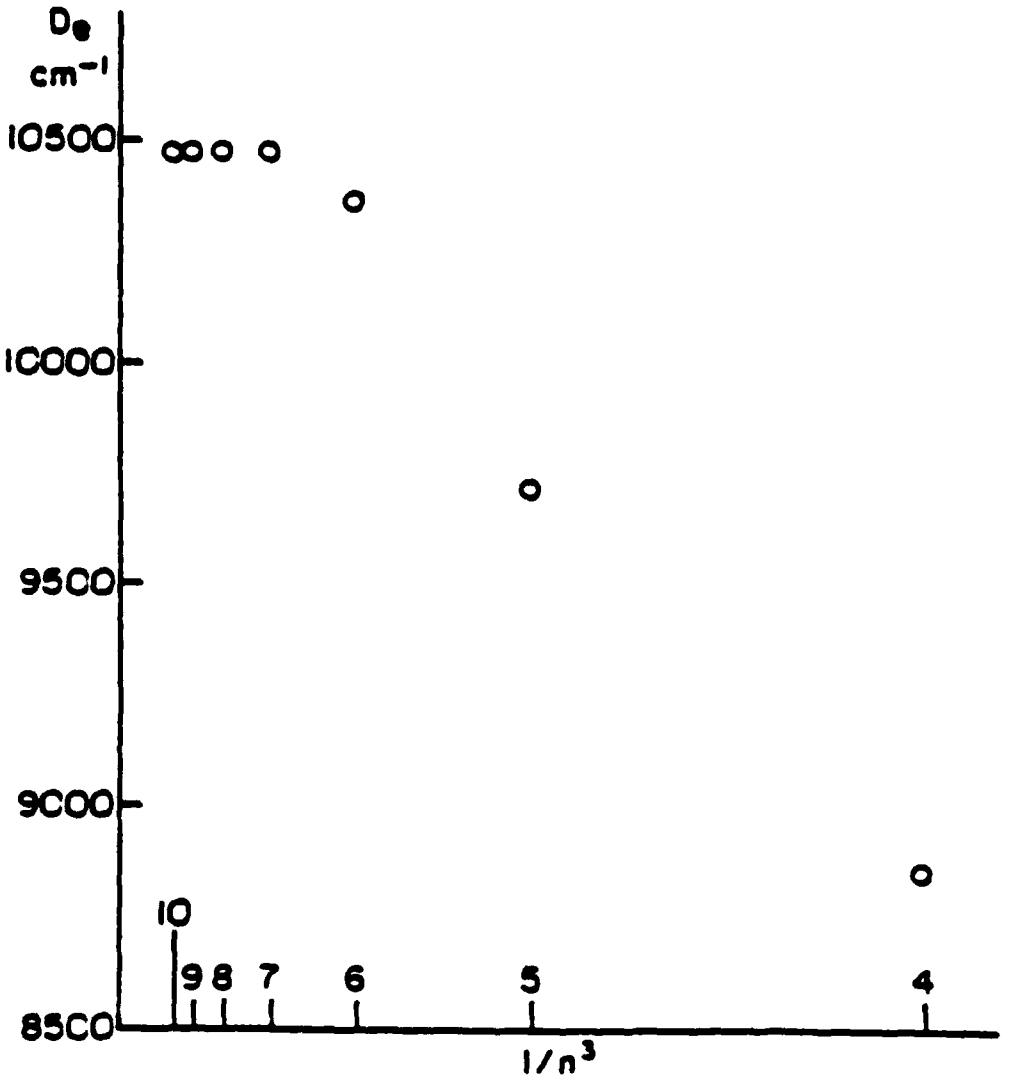

Figure 19b. The dissociation energy D_e, as a function of $1/n^3$ for the $nd\sigma\,^1\Sigma_g^+$ Rydberg series of $^7Li_2$.

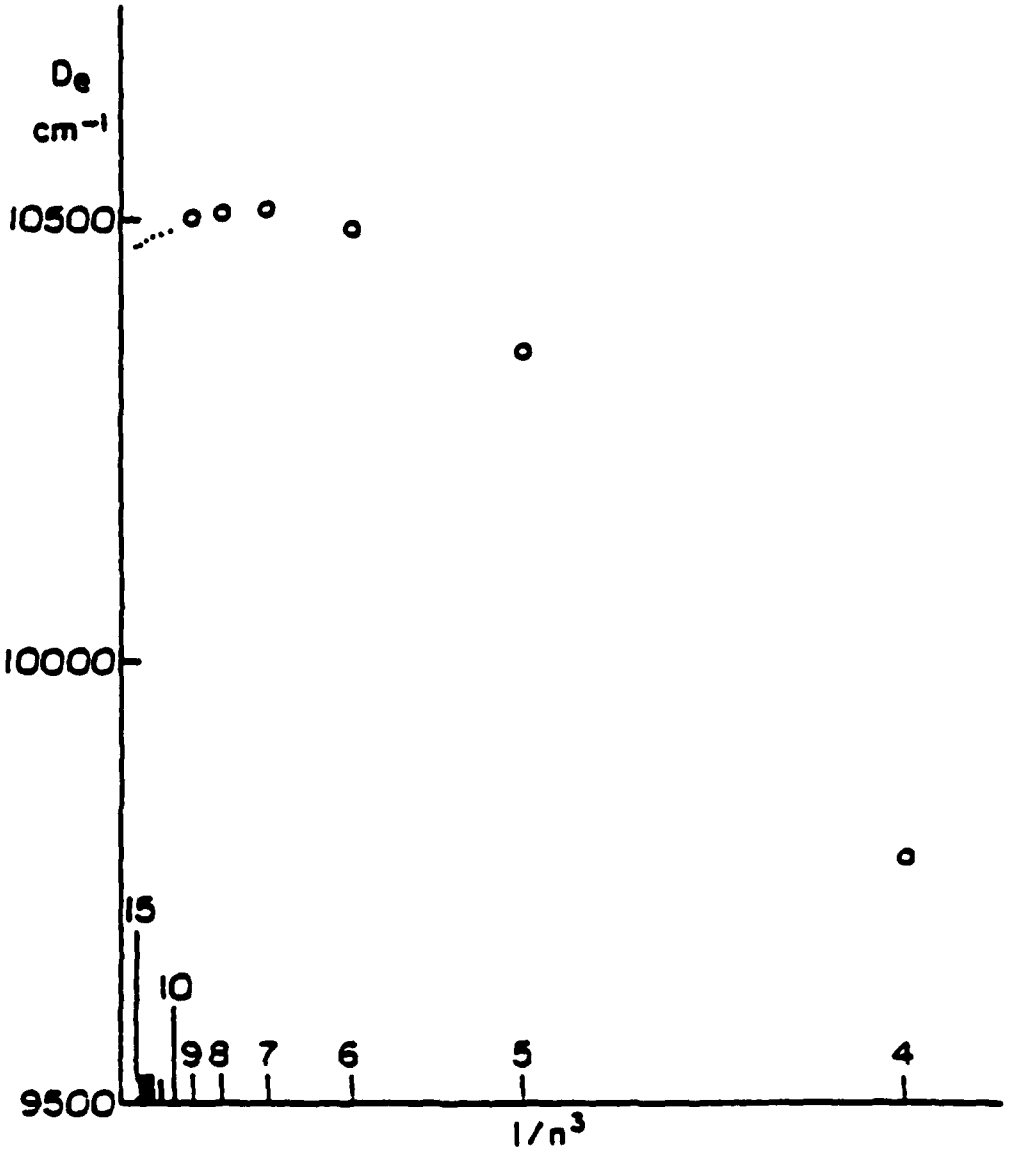

Figure 18c. The dissociation energy D_e, as a function of $1/n^3$ for the $nd\sigma\ ^1\Pi_g$ Rydberg series of $^7Li_2$.

$X^2\Sigma_g^+)=D_e+G(v=0)=10359\pm9$ cm^{-1} obtained by autoionization in a molecular beam (45) disagrees slightly with the present value of $D_o=10338\pm6$ cm^{-1}. The source of this discrepancy has not yet been identified.

Some of the bands in the upper $^1\Sigma_g^+$ states of Li_2 exhibit intensity anomalies similar to those reported in the Rydberg states of other diatomic molecules (55). The most conspicuous of these occur in the n>4 $ns\sigma\,^1\Sigma_g^+ \leftarrow A^1\Sigma_u^+$ bands. Most of the P branches of these bands are much weaker than the corresponding R branches, especially at large J values. In some instances, the P branch is completely missing. The qualitative behavior of these perturbations is indicative of a mixing of $^1\Sigma_g^+$ and $^1\Pi_g$ states (5). For similar perturbations observed in other diatomic molecules, it is generally found that a weakening of the P branch usually occurs for the lower energy transition to one of two mutually perturbing $\Delta\Lambda=\pm1$ states (55). This pattern suggests that the intensity anomalies found in the $ns\sigma\,^1\Sigma_g^+ \leftarrow A^1\Sigma_u^+$ bands may be due to $ns\sigma\,^1\Sigma_g^+ \leftarrow\!\rightarrow nd\pi\,^1\Pi_g$ interactions. However, there are no corresponding P/R intensity asymmetries in the $nd\pi\,^1\Pi_g \leftarrow A^1\Sigma_u^+$ bands although both the P and the R branches are much less intense than the Q branch. In view of this complication, no further attempt was made to interpret the above anomalies.

The lithium dimer is the second diatomic molecule for which a systematic study of Rydberg states has been performed by OODR. Results for the first such molecule, Na_2, have been obtained by

polarization-labeling spectroscopy (16,17), and by two-step autoionization in a supersonic molecular beam (18,19). The $^1\Sigma_g^+$ and $^1\Pi_g$ Rydberg series reported here correspond to those observed in a Na_2 (16-18) but an attempt has not yet been made to locate the corresponding $^1\Delta_g$ series (16-19). It is interesting to note that, in analogy to the Li_2 observations, the lowest doubly excited state is reported to be missing from the polarization-labeled spectrum of Na_2 (16).

Previous work on $^7Li_2$ by single-photon excitation methods has failed to produce a reliable identification of any Rydberg series. Although it has been suggested (51) that the $B^1\Pi_u$, $C^1\Pi_u$, and $D^1\Pi_u$ states of Li_2 are members of the $np\pi^1\Pi_u$ series, it now appears likely (56) that the $C^1\Pi_u$ state correlates with Li(2s) + Li(3d) or Li(2p) + Li(2p). In any event, the experimentally determined molecular constants for these states do not give accurate extrapolations to asymptotic values.

E. Experimental vs. Theoretical Molecular Constants of $^7Li_2^+$

An immediate comparison of the above experimental results for Li_2^+ with the best theoretical calculations is not possible since the latter are in the form of potential energy data. The most convenient way to obtain such a comparison is to use the method of Dunham (33) to convert the theoretical potential energy data to Dunham coefficients. This method is briefly summarized below.

The effective potential function of a vibrating molecule may be expressed in the form:

$$V(r)=a_o[\xi^2+a_1\xi^3+a_2\xi^4+\ldots] \qquad (15)$$

where $\xi=(r-r_e)/r_e$ and the a_i values are constants that are determined by a leastsquares fit of V(r) vs. ξ. Dunham has described (33) how to invert Equation (15) to obtain energy levels in terms of a power series in vibrational and rotational quantum numbers. The latter has been presented earlier as Equation (6). Each of the coefficients of this series (i.e., the so-called Dunham coefficients) can be expressed in terms of B_e, ω_e, and the a_i values; where B_e and ω_e are given by:

$$B_e=h/8\pi^2\mu r_e^2 c \qquad (16)$$

$$\omega_e=2\sqrt{B_e a_o} \qquad (17)$$

the latter equation is obtained from the harmonic oscillator part of V(r). Two of Dunham's formulas of interest in the present work are:

$$Y_{20}=-\omega_e x_e=(3B_e/2)(a_2-5a_1^2/4) \qquad (18)$$

$$Y_{11}=-\alpha_e=(6B_e^2/\omega_e)(1+a_1) \qquad (19)$$

A number of terms have been dropped from the original expressions because they were found to be negligible for Li_2.

The above formulas were tested on a number of RKR potentials of Li_2 to determine what degree of accuracy could be expected for the Li_2^+ computations that are presented below. The results of these tests are given in Table 24. These examples suggest that Dunham's method will yield accurate molecular constants when applied to any potential curve that resembles a Morse potential. The large error in the $\omega_e x_e$ value for the $E^1\Sigma_g^+$ state can be attributed to the peculiar shape of the $E^1\Sigma_g^+$ state potential well. The accuracy of all other listed values is sufficient for the present application.

The Li_2^+ calculations of Konowalow and Rosenkrantz (50) as well as those of Muller and Jungen (57) were selected for Dunham analyses because these are among the best such calculations available. The results of these analyses are presented in Table 25 along with the corresponding experimental quantities. The results of Konowalow and Rosenkrantz are found to nearly coincide with the present findings while those of Muller and Jungen are in fair agreement. The concurrence between the experimental results and the calculations of Konowalow and Rosenkrantz is strong evidence that both are accurate since Konowalow and Rosenkrantz have produced similar calculations for the neutral lithium dimer which have been found to be accurate to within a few percent. An interesting feature of these results is that Li_2^+ has a weaker force constant

Table 24. Derivation of Dunham coefficients from RKR potential curves for several test cases.

The following is a summary of results obtained by using a linear least squares procedure to fit previously published (9,11,20) RKR data with Equation (15). The column entitled "Percent Error" gives a comparison between the derived value of a given molecular constant (i.e. the value obtained by applying Dunham's inversion method to an RKR potential) and the original value of this constant obtained from energy level measurements.

State	Constant	Percent Error	St. Dev. of Fit (cm^{-1})	Maximum G_v (cm^{-1}) Fitted	Degree of Fit
$X\,^1\Sigma_g^+$	ω_e	0.0	0.07	2173	6
	$\omega_e x_e$	1.9			
	α_e	0.1			
$A\,^1\Sigma_u^+$	ω_e	0.0	0.28	5332	7
	$\omega_e x_e$	-0.1			
	α_e	0.9			
$B\,^1\Sigma_g^+$	ω_e	-0.3	4.30	1898	6
	$\omega_e x_e$	59.0			
	α_e	5.8			
$G\,^1\Pi_g$	ω_e	-0.1	0.37	2614	6
	$\omega_e x_e$	-5.3			
	α_e	0.9			

Table 25. Comparison of experimental and theoretical molecular constants for the $X^2\Sigma_g^+$ state of $^7Li_2^+$. All units are cm^{-1}.

Constant	OODR	Ab Initio[a]	Frozen Core[b]
ω_e	262.2±1.5	261.5	258.5
$\omega_e x_e$	1.7±0.5	1.6	1.8
B_e	0.496±0.002	0.491	0.480
α_e	0.0052±0.0017	0.0053	0.0042
D_e	10469±6	10320±200	10160

[a]Reference 50.

[b]Reference 57.

and longer bond length than Li_2 even though the molecular ion has a greater bond strength than the neutral molecule.

V. SUMMARY

The application of the OODR technique to the systematic study of three Rydberg series of $^7Li_2$ has been described. A detailed discussion of this technique has been given, and the advantages of OODR over conventional spectroscopic methods have been outlined.

Two experimental apparatuses were described: a nitrogen laser system and a Nd:YAG laser system. The latter included a Raman-shifting hydrogen cell which was used to extend the tuning range of the probe laser beam into the near infrared region. A computer data acquisition system, common to both of the above setups, was outlined in detail.

Dunham coefficients that describe at least the range $v^+=0-2$ were obtained for twenty-nine excited gerade states of $^7Li_2$. One of these states (a $^1\Pi_g$ state) apparently dissociates to a doubly excited atomic configuration while the others were identified as members of the $ns\sigma\,^1\Sigma_g^+$, $nd\sigma\,^1\Sigma_g^+$, and $nd\pi\,^1\Pi_g$ Rydberg series. The Dunham coefficients obtained for these states were later used to calculate RKR potentials and Franck-Condon factors. Arguments were presented to justify all of the stated assignments of quantum numbers to the observed energy levels, particularly the vibrational, principal, and azimuthal quantum numbers.

The $E\,^1\Sigma_g^+$ state was discussed at length because of its unusual properties and the disproportionately extensive data base that was obtained for it. The experimentally-derived molecular constants of this state are in accordance with theoretical calculations but no

attempt has yet been made to characterize the predicted second minimum in the potential curve using OODR.

A number of perturbations have been discussed, most notably the lambda-doubling interactions in the high-lying Rydberg states, and the homogeneous interactions between nearby pairs of $9d\pi\,^1\Pi_g$ and $10d\pi\,^1\Pi_g$ vibrational levels. A deperturbation procedure has been successfully applied to the latter.

An accurate ionization potential for Li_2 has been obtained by fitting the term energies of the Π^- components of the $nd\pi\,^1\Pi_g$ Rydberg series with the Rydberg equation. The less accurate extrapolations of the $nd\sigma\,^1\Sigma_g^+$ and $ns\sigma\,^1\Sigma_g^+$ term energies confirm the limit obtained for the $nd\pi\,^1\Pi_g$ series.

Several low-order Dunham coefficients have been derived for the $X^2\Sigma_g^+$ state of $^7Li_2^+$ by extrapolating the corresponding coefficients of the above Rydberg series. These results are the first experimentally determined molecular constants for Li_2^+, and are found to be in good agreement with the best available theoretical values.

VI. FUTURE WORK

An important unresolved question that has arisen from this work is whether the $^1\Pi_g^- \leftrightarrow {}^1\Delta_g^-$ lambda-doubling interactions in the upper Rydberg states of Li_2 are small enough to be ignored. The presence of large perturbations of this type would affect the rotational constants of the $nd\pi\,{}^1\Pi_g^-$ components and thereby invalidate the B_e value that has been determined for Li_2^+ in this work. This issue could be resolved by performing an OODR experiment in which the intermediate state is $B^1\Pi_u$. This scheme ought to enable the $nd\delta\,{}^1\Delta_g$ Rydberg series to be observed and thereby permit a determination of the magnitudes of $nd\pi\,{}^1\Pi_g \leftrightarrow nd\delta\,{}^1\Delta_g$ interactions.

Another subject for future investigation is the experimental characterization of the upper part of the $E^1\Sigma_g^+$ state potential curve. OODR excitations to high vibrational levels of the $E^1\Sigma_g^+$ state can probably be produced by pumping into a v>10 vibrational level of the $A^1\Sigma_u^+$ state. However, recent theoretical calculations (36) reveal that most of the experimentally accessible $E^1\Sigma_g^+ \text{-} A^1\Sigma_u^+$ transitions of this type lie beyond the long wavelength limits of all available laser dyes that can be used in the nitrogen laser system. The best way to circumvent this problem would be to conduct a preliminary search for some high-lying $E^1\Sigma_g^+$ state levels with the nitrogen laser system, and then switch to the less tractable Raman-shifting arrangement if this initial study is productive.

Still another topic that merits further study is the characterization of electronic states in the triplet manifold of Li_2. The only information that is presently available for triplet states of Li_2 is that obtained by ab initio calculations. An investigation of the triplet manifold by OODR awaits the discovery of a singlet-triplet perturbation in either the intermediate or upper level of an OODR excitation. In the former case, triplet states could be examined using the same experimental procedures as described in this work. In the latter case, triplet-triplet transitions would likely be observed in the dispersed ultraviolet fluorescence. An attempt to effect the latter process by exciting perturbed $F^1\Sigma_g^+$ state levels with c.w. lasers has already been made, but without success. Thus, a new method for accessing the triplet states has been proposed which is based on the former process. This method consists of scanning the probe laser and monitoring a particular atomic Li line that is expected to result from the relaxation of certain unbound triplet states (e.g. monitoring the 610.4 nm Li line would permit the observation of repulsive triplet states that correlate with the Li(2s) + Li(3d) asymptote). Even if this scheme fails to yield observations of triplet states, it may permit an investigation of unbound singlet states.

No attempt is planned to extend the investigation of the three observed gerade Rydberg series of $^7Li_2$ to higher energies since such a study would likely duplicate the autoionization

work of Eisel and Demtröder that is in progress (45). It is expected that a detailed analysis of the autoionization spectra will explain the discrepancy between the ionization potential for Li_2 obtained in this work and that found by Eisel and Demtröder in a preliminary analysis (45).

REFERENCES

1. K. P. Huber and G. Herzberg, Molecular Spectra and Molecular Structure, (Van Nostrand Reinhold, New York, 1979), Vol. IV.

2. R. A. Bernheim, L. P. Gold, P. B. Kelly, C. Kittrell, and D. K. Veirs, Phys. Rev. Lett. 43, 123 (1979).

3. R. G. Bray and R. M. Hochstrasser, Molecular Physics 31, 1199 (1976).

4. R. Zito, Jr., and A. E. Schraeder, Appl. Opt., 2, 1323 (1963).

5. R. A. Gottscho, J. B. Koffend, R. W. Field, and J. R. Lombardi, J. Chem. Phys. 68, 4410 (1978).

6. P. B. Kelly, "A Spectroscopic Study of the $F^1\Sigma_g^+$ State of Li_2 by Pulsed Optical-Optical Double Resonance," Dissertation, The Pennsylvania State University, 1981, University Park, Pennsylvania.

7. D. K. Viers, "A Spectroscopic Study of the $G^1\pi_g$ State of Li_2 by Pulsed Optical-Optical Double Resonance," Dissertation, The Pennsylvania State University, 1981, University Park, Pennsylvania.

8. R. A. Bernheim, L. P. Gold, P. B. Kelly, C. Kittrell, and D. K. Veirs, Chem. Phys. Lett. 70, 104 (1980).

9. R. A. Bernheim, L. P. Gold, P. B. Kelly, T. Tipton, and D. K. Veirs, J. Chem. Phys. 74, 2749 (1981).

10. R. A. Bernheim, L. P. Gold, P. B. Kelly, C. Tomczyk, and D. K. Veirs, J. Chem. Phys. 74, 3249 (1981).

11. R. A. Bernheim, L. P. Gold, P. B. Kelly, T. Tipton, and D. K. Veirs, J. Chem. Phys. 76, 57 (1982).

12. R. A. Bernheim, L. P. Gold, and T. Tipton, Chem. Phys. Lett., to be published.

13. R. A. Bernheim, L. P. Gold, and T. Tipton, in press.

14. M. M. Hessel and C. R. Vidal, J. Chem. Phys. 70, 4439 (1979).

15. H. A. Boorse and L. Motz, ed., The World of the Atom, (Basic Books, New York, 1966), p. 363.

16. N. W. Carlson, A. J. Taylor, and A. L. Schawlow, Phys. Rev. A 24, 822 (1981).

17. N. W. Carlson, A. J. Taylor, and A. L. Schawlow, Phys. Rev. Lett. 45, 18 (1980).

18. S. Martin, J. Chevaleyre, S. Valignat, J. P. Perrot, M. Broyet, B. Cabaud, and A. Hoareau, Chem. Phys. Lett. 87, 235 (1982).

19. S. Leutwyler, T. Heinis, M. Jungen, H. P. Harri, and E. Schumacher, J. Chem. Phys. 76, 4290 (1982).

20. P. Kusch and M. M. Hessel, J. Chem. Phys. 67, 586 (1977).

21. G. Herzberg, Molecular Spectra and Molecular Structure, (van Nostrand, Princeton, N.J., 1950), Second Edition, Vol. I.

22. D. R. Stull and H. Prophet, JANAF Thermochemical Tables, 2nd Edition (U. S. Government Printing Office, Washington, D.C., 1971).

23. J. G. Balz, R. A. Bernheim, L. P. Gold, P. B. Kelly, and D. K. Veirs, J. Chem. Phys. 75, 5226 (1981).

24. D. S. King, P. K. Schenck, K. C. Smyth, and J. C. Travis, Appl. Opt. 16, 2617 (1977).

25. Exciton Laser Dyes, Exciton Chemical Company, Dayton, Ohio.

26. E. Hecht and A. Zajac, Optics, (Addison-Wesley, Reading Mass., 1976).

27. P. D. Willson and T. H. Edwards, Appl. Spectrosc. Rev. 12, 1 (1976).

28. M. Bierry, R. Frey, and F. Pradere, Rev. Sci. Instrum. 48, 733 (1977).

29. P. J. Brannon, C. H. Church, C. W. Peters, J. Mol. Spectrosc. 27, 44 (1968).

30. M. G. Littman and H. J. Metcalf, Appl. Opt. 17, 2224 (1978).

31. T. W. Hänsch, Appl. Opt. 11, 895 (1972).

32. D. K. Hsu, "The Absorption Spectra of the A-X and C-X Transitions of the Lithium Molecules," Dissertation, Fordham University, 1974, University Microfilms, Ann Arbor, Michigan.

33. J. L. Dunham, Phys. Rev. 41, 721 (1932).

34. A. L. G. Rees, Proc. Phys. Soc. 59, 998 (1947).

35. W. Demtröder, M. McClintock, and R. N. Zare, J. Chem. Phys. 51, 5495 (1969).

36. D. D. Konowalow and J. L. Fish, J. Chem. Phys. 76, 4571 (1982).

37. W. Kolos and L. Wolniewicz, J. Chem. Phys. 50, 3228 (1969).

38. C. E. Moore, Atomic Energy Levels, NBS Circular 467 (1949).

39. T. A. Patterson, H. Hotop, A. Kasdan, D. W. Norcross, and W. C. Lineberger, Phys. Rev. Lett. 32, 189 (1974).

40. K. K. Verma, M. E. Koch, and W. C. Stwalley, in press.

41. W. C. Stwalley, W. T. Zemke, K. R. Way, K. C. Li, T.R. Proctor, J. Chem. Phys. 66, 5412 (1977).

42. J. L. Fish and D. D. Konowalow, private communication.

43. N. Anderson, W. S. Bickel, G. W. Carriveau, K. Jensen, and E. Veje, Physica Scripta 4, 113 (1971).

44. W. R. Hindmarsh, Atomic Spectra, (Pergamon Press, London, 1967).

45. D. Eisel and W. Demtröder, Chem. Phys. Lett. 88, 481 (1982).

46. P. J. Foster, R. E. Leckenby, and E. J. Robbins, J. Phys. B 2, 478 (1969).

47. B. P. Mathur, E. W. Rothe, G. P. Reck, and A. J. Lightman, Chem. Phys. Lett. 56, 336 (1978).

48. A. M. Emel'yanov, V. A. Peredvigina, and L. N. Goroknov, High Temp. (USSR) 9, 164 (1971).

49. C. H. Wu, J. Chem. Phys. 65, 3181 (1976).

50. D. D. Konowalow and M. E. Rosenkrantz, Chem. Phys. Lett. 61, 489 (1979).

51. R. F. Barrow, N. Travis, and C. V. Wright, Nature 187, 141 (1960).

52. H. G. Kuhn, Atomic Spectra, (Academic Press, New York, 1969).

53. G. Herzberg and Ch. Jungen, J. Mol. Spectrosc. 41, 425 (1972).

54. U. Fano, Phys. Rev. A 2, 353 (1970).

55. Ch. Jungen, J. Chem. Phys. 53, 4168 (1970).

56. M. Allegrini, A. Kopystynska, and L. Moi, J. Chem. Phys. 71, 2324 (1979).

57. Müller and Jungen, Chem. Phys. Lett. 40, 199 (1976).

APPENDIX I. Assigned spectral lines for the Rydberg states of $^7Li_2$. The following is a listing of all OODR spectral lines observed while pumping the v'=0,1,2, and 4 levels of the $A^1\Sigma_u^+$ state of $^7Li_2$ and scanning the range 530-370 nm with a probe dye laser. A separate table is given for each $^1\Sigma_g^+$ and $^1\Pi_g$ upper electronic state that was observed. The tabulated frequencies are those of the probe laser, and the quantum numbers refer to transitions from the $A^1\Sigma_u^+$ state to the high-lying electronic states. The column entitled "DEV" specifies the difference between each observed frequency, "OBS FREQ," and the corresponding frequency calculated from Dunham coefficients. Listings of all observed transitions that were not used in the final Dunham fits are presented on the last three pages. Data for the Π^- and Π^+ components of each 7-11dπ $^1\Pi_g$ state are listed separately since they were fitted with separate sets of Dunham coefficients.

3d sigma

BAND	TOT LINE	OBS FREQ (CM-1)	DEV	*	BAND	TOT LINE	OBS FREQ (CM-1)	DEV
(0,0)	P(12)	19232.30	0.16	*	(0,1)	P(38)	13994.47	-0.10
(0,0)	P(14)	19229.94	0.08	*	(0,1)	P(40)	13920.02	0.03
(0,0)	P(16)	19225.16	0.11	*	(0,1)	P(42)	13915.39	-0.02
(0,0)	P(18)	19221.27	0.14	*	(0,1)	R(42)	13900.27	-0.03
(0,0)	P(20)	19217.05	0.07	*	(1,0)	P(6)	19484.16	-0.01
(0,0)	P(22)	19212.64	0.03	*	(1,0)	P(8)	19481.41	0.00
(0,0)	P(24)	19208.09	0.06	*	(1,0)	P(10)	19478.25	0.04
(0,0)	R(24)	19252.67	-0.05	*	(1,0)	P(12)	19474.92	0.07
(0,0)	P(26)	19203.25	0.01	*	(1,0)	P(14)	19471.37	0.04
(0,0)	R(26)	19251.59	0.15	*	(1,0)	P(16)	19467.45	0.10
(0,0)	P(28)	19198.26	0.01	*	(1,0)	P(18)	19463.30	0.08
(0,0)	R(28)	19249.95	0.02	*	(1,0)	P(20)	19458.92	0.09
(0,0)	P(30)	19193.02	-0.04	*	(1,0)	P(22)	19454.29	0.07
(0,0)	R(30)	19248.15	-0.03	*	(1,0)	R(22)	19495.23	0.13
(0,0)	P(32)	19187.78	0.10	*	(1,0)	P(24)	19449.44	0.08
(0,0)	R(32)	19246.24	0.03	*	(1,0)	R(24)	19493.86	0.11
(0,0)	P(34)	19182.17	0.06	*	(1,0)	P(26)	19444.31	0.05
(0,0)	R(34)	19244.01	0.0	*	(1,0)	R(26)	19492.22	0.09
(0,0)	P(36)	19176.31	-0.05	*	(1,0)	P(28)	19438.06	0.03
(0,0)	R(36)	19241.53	-0.06	*	(1,0)	R(28)	19490.29	0.14
(0,0)	P(38)	19170.45	0.01	*	(1,0)	P(30)	19433.42	0.05
(0,0)	P(40)	19164.49	0.14	*	(1,0)	R(30)	19489.16	0.06
(0,0)	P(42)	19158.17	0.07	*	(1,0)	P(32)	19427.70	0.11
(0,0)	P(44)	19151.38	0.19	*	(1,0)	R(32)	19485.30	0.11
(0,0)	P(46)	19145.28	0.14	*	(1,0)	P(34)	19421.59	0.0
(0,0)	P(48)	19138.53	0.07	*	(1,0)	R(34)	19483.13	0.11
(0,1)	P(2)	13993.75	-0.02	*	(1,0)	P(36)	19415.44	0.06
(0,1)	P(4)	13991.59	0.03	*	(1,0)	R(36)	19480.25	0.15
(0,1)	P(6)	19989.20	0.04	*	(1,0)	P(38)	19409.23	0.28
(0,1)	P(8)	19986.37	0.02	*	(1,0)	R(40)	19473.59	0.07
(0,1)	P(10)	19983.78	0.03	*	(1,0)	P(42)	19835.52	0.02
(0,1)	P(10)	19003.23	0.05	*	(1,0)	P(44)	19399.52	0.03
(0,1)	P(12)	19980.74	-0.02	*	(1,0)	P(46)	19391.35	0.06
(0,1)	P(14)	19977.57	-0.01	*	(1,0)	P(48)	19373.99	-0.02
(0,1)	P(16)	19974.21	0.0	*	(1,1)	P(6)	19232.02	-0.06
(0,1)	P(18)	19970.44	-0.02	*	(1,1)	P(8)	19229.32	-0.09
(0,1)	P(20)	19966.92	-0.02	*	(1,1)	P(10)	19226.41	-0.09
(0,1)	P(22)	19962.99	-0.04	*	(1,1)	P(12)	19223.29	-0.10
(0,1)	P(24)	19958.90	-0.06	*	(1,1)	P(14)	19219.95	-0.10
(0,1)	P(26)	19954.66	-0.06	*	(1,1)	P(16)	19216.49	-0.09
(0,1)	P(28)	19950.26	-0.05	*	(1,1)	P(18)	19212.61	-0.15
(0,1)	P(30)	19945.67	-0.05	*	(1,1)	P(20)	19208.63	-0.12
(0,1)	P(32)	19941.02	-0.02	*	(1,1)	P(22)	19204.53	-0.12
(0,1)	P(34)	19936.15	-0.03	*	(1,1)	P(24)	19200.20	-0.09
(0,1)	P(36)	19931.07	-0.01	*	(1,1)	P(26)	19195.60	-0.14
(0,1)	P(38)	19925.83	-0.10	*	(1,1)	P(28)	19190.89	-0.10
(0,1)	P(40)	19920.36	-0.05	*	(1,1)	P(30)	19185.85	-0.12
(0,1)	P(42)	19914.70	-0.06	*	(1,1)	P(32)	19180.82	-0.03

3d sigma

BAND	ROT LINE	OBS FREQ (CM-1)	DEV	*	BAND	ROT LINE	OBS FREQ (CM-1)	DEV
(1,1)	P(32)	19190.99	-0.06	*	(2,0)	P(28)	19674.79	0.17
(1,1)	P(32)	19238.96	-0.09	*	(2,0)	P(28)	19725.70	0.17
(1,1)	P(34)	19175.59	-0.07	*	(2,0)	P(30)	19668.96	0.18
(1,1)	P(34)	19179.14	-0.06	*	(2,0)	P(30)	19723.13	0.19
(1,1)	P(36)	19164.47	-0.10	*	(2,0)	P(32)	19662.68	0.24
(1,1)	P(42)	19152.71	-0.11	*	(2,0)	P(32)	19720.28	0.20
(1,1)	P(44)	19146.64	-0.07	*	(2,0)	P(34)	19656.17	0.18
(1,2)	P(12)	19974.89	-0.15	*	(2,1)	P(4)	19472.67	-0.03
(1,2)	P(14)	19971.92	-0.18	*	(2,1)	P(6)	19470.14	-0.04
(1,2)	P(16)	19968.61	-0.18	*	(2,1)	P(8)	19467.36	-0.06
(1,2)	P(18)	19965.23	-0.19	*	(2,1)	P(10)	19464.46	0.05
(1,2)	P(20)	19961.68	-0.20	*	(2,1)	P(12)	19461.12	-0.04
(1,2)	P(22)	19958.03	-0.15	*	(2,1)	P(14)	19457.61	-0.05
(1,2)	P(24)	19954.21	-0.12	*	(2,1)	P(16)	19453.85	0.02
(1,2)	P(26)	19950.18	-0.14	*	(2,1)	P(18)	19449.91	-0.05
(1,2)	P(28)	19945.96	-0.20	*	(2,1)	P(20)	19445.73	-0.03
(1,2)	P(30)	19941.74	-0.12	*	(2,1)	P(22)	19441.30	-0.03
(1,2)	P(30)	19996.42	-0.16	*	(2,1)	P(24)	19436.44	-0.23
(1,2)	P(32)	19937.29	-0.12	*	(2,1)	R(24)	19490.95	0.13
(1,2)	P(32)	19995.36	-0.15	*	(2,1)	P(26)	19431.75	-0.04
(1,2)	P(34)	19932.69	-0.14	*	(2,1)	P(26)	19479.34	0.05
(1,2)	P(34)	19994.09	-0.17	*	(2,1)	P(28)	19426.74	0.06
(1,2)	P(36)	19928.90	-0.11	*	(2,1)	P(28)	19477.62	0.03
(1,2)	P(36)	19992.74	-0.10	*	(2,1)	P(30)	19421.35	0.0
(1,2)	P(38)	19923.15	-0.11	*	(2,1)	P(30)	19475.57	-0.08
(1,2)	P(38)	19991.13	-0.11	*	(2,1)	P(32)	19415.78	-0.02
(1,2)	P(40)	19918.22	-0.07	*	(2,1)	P(32)	19473.42	-0.02
(1,2)	P(40)	19990.40	-0.08	*	(2,1)	P(34)	19410.07	0.01
(1,2)	P(42)	19913.17	-0.03	*	(2,1)	P(34)	19470.05	-0.04
(1,2)	P(42)	19987.43	-0.11	*	(2,1)	P(36)	19404.19	0.01
(1,2)	P(44)	19907.90	-0.10	*	(2,1)	P(36)	19468.30	0.02
(1,2)	P(44)	19985.31	-0.14	*	(2,1)	P(38)	19397.97	-0.05
(1,2)	P(46)	19902.66	-0.02	*	(2,1)	P(40)	19391.54	-0.01
(1,2)	P(48)	19897.20	-0.06	*	(2,1)	P(40)	19462.03	-0.09
(2,0)	P(10)	19716.19	0.07	*	(2,1)	P(42)	19385.10	0.11
(2,0)	P(12)	19712.77	0.15	*	(2,1)	P(42)	19458.69	0.0
(2,0)	P(14)	19708.20	0.05	*	(2,1)	P(44)	19378.20	0.07
(2,0)	P(16)	19704.80	0.02	*	(2,1)	P(46)	19371.24	-0.03
(2,0)	P(18)	19700.59	0.15	*	(2,2)	P(14)	19206.28	0.06
(2,0)	P(18)	19734.20	0.25	*	(2,2)	P(18)	19202.60	-0.03
(2,0)	P(20)	19695.02	0.12	*	(2,2)	P(20)	19199.05	0.01
(2,0)	P(20)	19733.07	0.20	*	(2,2)	P(22)	19194.99	0.02
(2,0)	P(22)	19690.39	0.19	*	(2,2)	P(24)	19190.75	0.04
(2,0)	P(22)	19731.73	0.25	*	(2,2)	P(26)	19186.32	-0.05
(2,0)	P(24)	19685.97	0.13	*	(2,2)	R(26)	19232.04	0.07
(2,0)	P(24)	19729.96	0.16	*	(2,2)	P(28)	19181.05	0.0
(2,0)	P(26)	19680.48	0.17	*	(2,2)	P(28)	19222.93	0.07
(2,0)	P(26)	19727.97	0.16	*	(2,2)	P(30)	19177.17	0.02

2d sigma

BAND	ROT LINE	OBS FREQ (CM-1)	DEV	*	BAND	ROT LINE	OBS FREQ (CM-1)	DEV
(2,2)	R(20)	19221.40	0.05	*	(3,2)	P(22)	19427.04	-0.08
(2,2)	R(22)	19172.29	0.01	*	(3,2)	R(24)	19422.57	-0.05
(2,2)	R(32)	19229.05	0.05	*	(3,2)	R(24)	19446.27	-0.02
(2,2)	P(34)	19167.27	0.05	*	(3,2)	P(26)	19417.84	-0.06
(2,2)	R(34)	19229.19	0.04	*	(3,2)	R(26)	19444.98	-0.01
(2,2)	P(36)	19162.00	0.08	*	(3,2)	P(28)	19412.94	-0.03
(2,2)	R(36)	19225.17	-0.02	*	(3,2)	P(30)	19407.78	-0.04
(2,2)	P(38)	19156.71	0.09	*	(3,2)	R(30)	19461.60	-0.03
(2,2)	R(38)	19224.07	0.05	*	(3,2)	P(32)	19402.44	-0.02
(2,2)	P(40)	19151.14	0.07	*	(3,2)	R(32)	19459.56	-0.02
(2,2)	R(40)	19221.67	0.02	*	(3,2)	P(34)	19396.90	0.0
(2,2)	P(42)	19145.44	0.07	*	(3,2)	R(34)	19457.25	-0.02
(2,2)	P(44)	19139.57	0.06	*	(3,2)	P(36)	19391.11	-0.01
(2,2)	P(46)	19133.57	0.07	*	(3,2)	R(36)	19454.63	-0.09
(2,2)	P(48)	19127.42	0.08	*	(3,2)	P(38)	19385.17	0.03
(2,2)	P(50)	19121.03	-0.01	*	(3,2)	R(38)	19451.89	-0.02
(2,2)	P(52)	19114.69	0.09	*	(3,2)	P(40)	19379.00	0.04
(3,1)	P(4)	19706.60	-0.01	*	(3,2)	R(40)	19449.92	0.07
(3,1)	P(6)	19704.02	0.0	*	(3,2)	P(42)	19372.55	-0.02
(3,1)	P(8)	19701.20	0.03	*	(3,2)	P(44)	19365.98	-0.01
(3,1)	P(10)	19698.03	0.0	*	(3,2)	R(44)	19441.09	0.0
(3,1)	P(12)	19694.67	0.04	*	(3,2)	P(46)	19359.24	0.03
(3,1)	P(14)	19690.92	-0.03	*	(3,2)	R(46)	19439.05	-0.12
(3,1)	P(16)	19687.00	-0.01	*	(3,2)	P(48)	19352.15	-0.09
(3,1)	P(18)	19682.77	-0.02	*	(3,2)	R(48)	19434.07	-0.04
(3,1)	P(20)	19677.31	-0.01	*	(3,2)	P(50)	19345.07	0.0
(3,1)	P(20)	19714.09	-0.09	*	(4,2)	P(20)	19659.72	-0.05
(3,1)	P(22)	19673.60	0.02	*	(4,2)	R(20)	19696.11	-0.06
(3,1)	P(22)	19710.75	-0.06	*	(4,2)	P(22)	19655.07	-0.07
(3,1)	P(24)	19668.56	-0.02	*	(4,2)	R(22)	19694.06	-0.01
(3,1)	P(24)	19712.27	0.02	*	(4,2)	P(24)	19650.21	-0.04
(3,1)	P(26)	19663.30	0.01	*	(4,2)	R(24)	19693.40	-0.00
(3,1)	P(26)	19710.41	0.0	*	(4,2)	P(26)	19645.06	-0.04
(3,1)	P(28)	19657.83	0.03	*	(4,2)	R(26)	19691.64	-0.00
(3,1)	P(28)	19708.29	0.02	*	(4,2)	P(28)	19639.66	-0.01
(3,1)	P(30)	19652.03	0.0	*	(4,2)	R(28)	19689.57	-0.00
(3,1)	P(30)	19705.92	-0.02	*	(4,2)	P(30)	19633.99	-0.05
(3,1)	P(32)	19703.15	0.03	*	(4,2)	R(30)	19687.26	-0.03
(3,1)	R(34)	19700.15	0.04	*	(4,2)	P(32)	19628.06	-0.06
(3,1)	P(36)	19696.83	0.12	*	(4,2)	R(32)	19684.60	-0.04
(3,1)	P(38)	19692.20	0.08	*	(4,2)	P(34)	19621.91	-0.05
(3,1)	R(40)	19690.40	0.07	*	(4,2)	R(34)	19681.64	-0.06
(3,1)	P(42)	19685.12	-0.03	*	(4,2)	P(36)	19615.53	-0.02
(3,1)	P(44)	19680.62	-0.07	*	(4,2)	R(36)	19678.39	-0.09
(3,2)	P(14)	19442.74	-0.15	*	(4,2)	P(38)	19608.88	0.0
(3,2)	R(16)	19439.22	-0.07	*	(4,2)	P(38)	19674.97	-0.05
(3,2)	P(18)	19435.42	-0.04	*	(4,2)	P(40)	19602.00	0.03
(3,2)	R(20)	19431.39	-0.01	*	(4,2)	R(40)	19671.33	-0.06

3d sigma

BAND	ROT LINE	OBS FREQ (CM-1)	DEV	*	BAND	ROT LINE	OBS FREQ (CM-1)	DEV
(4,2)	P(42)	19504.78	-0.03	*	(5,4)	P(28)	19381.47	-0.04
(4,2)	P(42)	19664.96	0.01	*	(5,4)	R(28)	19430.84	-0.03
(4,2)	P(44)	19597.39	-0.01	*	(5,4)	P(30)	19376.53	0.04
(4,2)	P(44)	19662.46	-0.06	*	(5,4)	R(30)	19429.15	0.04
(4,2)	P(46)	19579.76	0.01	*	(5,4)	P(32)	19371.25	0.0
(4,2)	R(46)	19657.79	0.01	*	(5,4)	R(32)	19427.07	-0.01
(4,2)	P(48)	19571.98	0.13	*	(5,4)	P(34)	19365.81	0.01
(4,2)	P(50)	19563.71	0.01	*	(5,4)	R(34)	19424.82	0.03
(4,4)	P(8)	19194.04	0.15	*	(5,4)	P(36)	19360.19	0.07
(4,4)	P(10)	19191.24	0.02	*	(5,4)	R(36)	19422.34	0.10
(4,4)	P(12)	19188.32	-0.06	*	(5,4)	P(38)	19354.24	0.02
(4,4)	P(14)	19185.30	-0.06	*	(5,4)	R(38)	19419.64	0.23
(4,4)	P(16)	19182.17	0.01	*	(5,4)	P(40)	19348.14	0.04
(4,4)	P(18)	19178.77	-0.01	*	(5,4)	P(42)	19341.75	0.0
(4,4)	P(20)	19175.21	-0.02	*	(5,4)	P(44)	19335.32	0.15
(4,4)	P(22)	19171.46	-0.04	*	(5,4)	P(46)	19329.41	0.04
(4,4)	P(24)	19167.56	-0.04	*	(6,4)	P(10)	19638.24	0.01
(4,4)	P(26)	19163.46	-0.07	*	(6,4)	P(12)	19634.97	0.05
(4,4)	R(26)	19210.12	-0.03	*	(6,4)	P(16)	19627.52	0.0
(4,4)	P(28)	19159.20	-0.08	*	(6,4)	P(18)	19623.29	-0.12
(4,4)	R(28)	19200.15	-0.09	*	(6,4)	P(19)	19655.52	0.0
(4,4)	P(30)	19154.78	-0.08	*	(6,4)	P(20)	19619.04	0.0
(4,4)	R(30)	19209.12	0.0	*	(6,4)	R(20)	19654.53	0.01
(4,4)	P(32)	19150.21	-0.06	*	(6,4)	P(22)	19614.41	0.01
(4,4)	R(32)	19206.75	-0.04	*	(6,4)	R(22)	19652.20	-0.03
(4,4)	P(34)	19145.49	-0.02	*	(6,4)	P(24)	19609.53	0.04
(4,4)	R(34)	19205.23	-0.02	*	(6,4)	P(24)	19651.56	-0.07
(4,4)	P(36)	19140.52	-0.05	*	(6,4)	P(26)	19604.39	0.08
(4,4)	R(36)	19203.46	-0.03	*	(6,4)	P(26)	19649.72	-0.01
(4,4)	P(38)	19135.40	-0.07	*	(6,4)	P(28)	19598.82	-0.04
(4,4)	R(38)	19201.48	-0.03	*	(6,4)	R(28)	19647.46	-0.04
(4,4)	P(40)	19130.16	-0.03	*	(6,4)	P(30)	19593.19	0.05
(4,4)	P(42)	19124.60	-0.14	*	(6,4)	R(30)	19645.01	0.01
(4,4)	P(44)	19119.09	-0.03	*	(6,4)	P(32)	19587.19	0.04
(4,4)	P(46)	19113.22	-0.11	*	(6,4)	R(32)	19642.12	-0.04
(4,4)	P(48)	19107.26	-0.11	*	(6,4)	P(34)	19580.93	0.06
(5,4)	P(10)	19416.96	0.11	*	(6,4)	R(34)	19638.93	-0.02
(5,4)	P(12)	19413.79	-0.01	*	(6,4)	P(36)	19574.41	0.09
(5,4)	P(14)	19410.53	0.01	*	(6,4)	R(36)	19635.53	0.02
(5,4)	P(16)	19407.09	0.06	*	(6,4)	P(38)	19567.52	0.03
(5,4)	P(18)	19403.35	0.03	*	(6,4)	P(40)	19560.46	0.08
(5,4)	P(20)	19399.44	0.04	*	(6,4)	P(42)	19553.00	0.02
(5,4)	P(22)	19395.28	0.03	*	(7,4)	P(16)	19871.33	0.03
(5,4)	R(22)	19434.71	0.09	*	(7,4)	P(18)	19870.04	-0.03
(5,4)	P(24)	19390.93	0.04	*	(7,4)	P(20)	19868.44	-0.05
(5,4)	R(24)	19433.68	0.05	*	(7,4)	P(22)	19866.61	0.06
(5,4)	P(26)	19386.34	0.03	*	(7,4)	R(24)	19864.20	0.05
(5,4)	R(26)	19432.44	0.07	*	(7,4)	P(24)	19816.30	0.05

3d sigma

BAND	ROT LINE	OBS FREQ (CM-1)	DEV	*	BAND	ROT LINE	OBS FREQ (CM-1)	DEV
(7,4)	R(26)	19961.56	-0.02	*	(7,4)	P(32)	19787.25	-0.02
(7,4)	P(28)	19910.72	0.01	*	(7,4)	R(32)	19851.23	-0.00
(7,4)	R(28)	19850.53	-0.01	*	(7,4)	P(34)	19730.89	-0.05
(7,4)	P(30)	19804.17	0.01	*	(7,4)	R(34)	19847.06	-0.08
(7,4)	R(30)	19855.04	-0.08	*				

BAND	ASYM TOP LEVEL	OBS FREQ (CM-1)	OBS-CALC
(0,0)	P(2)	22217.99	0.00
(0,0)	R(2)	22223.00	0.17
(0,0)	P(4)	22210.05	0.14
(0,0)	R(4)	22224.00	0.16
(0,0)	P(6)	22213.90	0.11
(0,0)	R(6)	22226.71	0.10
(0,0)	P(8)	22211.62	0.03
(0,0)	R(8)	22226.53	0.09
(0,0)	P(10)	22209.70	0.07
(0,0)	R(10)	22230.20	0.03
(0,0)	P(12)	22207.80	0.03
(0,0)	R(12)	22232.03	0.06
(0,0)	P(14)	22205.41	-0.01
(0,0)	R(14)	22233.71	0.03
(0,0)	P(16)	22203.23	-0.02
(0,0)	R(16)	22235.39	0.01
(0,0)	P(18)	22201.05	-0.02
(0,0)	R(18)	22237.08	0.07
(0,0)	P(20)	22198.64	-0.02
(0,0)	R(20)	22238.40	0.14
(0,0)	P(22)	22196.00	-0.04
(0,0)	R(22)	22240.33	0.11
(0,0)	P(24)	22194.37	-0.03
(0,0)	R(24)	22241.49	0.14
(0,0)	P(26)	22192.07	-0.06
(0,0)	R(26)	22241.91	-0.07
(0,0)	P(28)	22189.73	-0.10
(0,0)	R(28)	22244.27	-0.21
(0,0)	P(30)	22187.34	-0.07
(0,0)	R(30)	22245.83	-0.19
(0,0)	P(32)	22183.21	-0.11
(0,0)	R(32)	22246.97	-0.14
(0,0)	P(34)	22182.91	-0.10
(0,0)	R(34)	22248.22	-0.12
(0,0)	P(36)	22180.56	-0.12
(0,0)	R(36)	22249.49	-0.02
(0,0)	P(38)	22178.34	-0.02
(0,0)	R(38)	22250.01	0.0
(0,0)	P(40)	22176.05	0.04
(0,0)	R(40)	22251.76	0.12
(0,0)	P(42)	22173.73	0.06
(0,0)	R(42)	22252.73	0.12
(0,0)	R(44)	22253.93	0.07
(1,0)	R(4)	22480.11	-0.02
(1,0)	P(5)	22469.59	0.14
(1,0)	R(5)	22482.24	0.12
(1,0)	P(6)	22467.17	0.10
(1,0)	R(6)	22483.79	0.09

BAND	ASYM TOP LEVEL	OBS FREQ (CM-1)	OBS-CALC
(1,0)	P(10)	22465.17	0.19
(1,0)	R(10)	22485.37	0.12
(1,0)	P(12)	22462.88	0.13
(1,0)	R(12)	22486.79	0.12
(1,0)	P(14)	22460.26	0.10
(1,0)	R(14)	22488.15	0.17
(1,0)	P(16)	22457.91	0.09
(1,0)	R(16)	22489.29	0.16
(1,0)	P(18)	22455.01	0.09
(1,0)	R(18)	22490.51	0.13
(1,0)	P(20)	22452.32	0.10
(1,0)	R(20)	22491.41	0.1
(1,0)	P(22)	22449.51	0.07
(1,0)	R(22)	22492.34	-0.02
(1,0)	P(24)	22446.84	0.06
(1,0)	R(24)	22493.18	-0.02
(1,0)	P(26)	22443.71	0.09
(1,0)	P(28)	22440.74	-0.01
(1,0)	P(30)	22437.77	0.05
(1,1)	R(3)	22221.46	0.02
(1,1)	P(4)	22221.50	-0.02
(1,1)	R(5)	22220.17	0.01
(1,1)	P(6)	22219.48	-0.03
(1,1)	R(6)	22223.21	-0.01
(1,1)	P(7)	22217.47	0.0
(1,1)	R(8)	22220.99	-0.05
(1,1)	P(9)	22215.35	-0.03
(1,1)	R(9)	22221.60	0.0
(1,1)	P(10)	22213.25	-0.01
(1,1)	R(10)	22223.55	0.02
(1,1)	P(12)	22211.05	-0.06
(1,1)	R(12)	22225.17	-0.03
(1,1)	P(14)	22208.84	-0.06
(1,1)	R(14)	22226.60	-0.02
(1,1)	P(16)	22206.54	-0.07
(1,1)	R(16)	22228.31	-0.03
(1,1)	P(18)	22204.21	-0.05
(1,1)	R(18)	22229.82	-0.09
(1,1)	P(20)	22202.09	-0.09
(1,1)	R(20)	22231.30	-0.07
(1,1)	P(22)	22199.75	-0.13
(1,1)	R(22)	22232.07	-0.11
(1,1)	P(24)	22197.42	-0.13
(1,1)	R(24)	22234.02	-0.11
(1,1)	P(26)	22195.06	-0.15
(1,1)	R(26)	22235.34	-0.08
(1,1)	P(28)	22192.71	-0.10
(1,1)	R(28)	22240.55	-0.10

BAND	LINE	OBS FREQ (CM-1)	OBS-CALC	BAND	LINE	OBS FREQ (CM-1)	OBS-CALC
(1,1)	P(30)	22170.30	-0.11	(2,2)	P(2)	22224.94	0.01
(1,1)	R(29)	22207.71	-0.10	(2,2)	P(4)	22216.76	-0.16
(1,1)	P(32)	22187.69	-0.09	(2,2)	R(4)	22227.41	-0.06
(1,1)	R(32)	22245.83	-0.08	(2,2)	P(6)	22219.70	-0.15
(1,1)	P(34)	22185.41	-0.11	(2,2)	P(8)	22214.55	-0.18
(1,1)	R(34)	22249.79	-0.14	(2,2)	R(8)	22230.69	-0.19
(1,1)	P(36)	22182.91	-0.12	(2,2)	P(10)	22212.39	0.04
(1,1)	R(36)	22250.94	0.10	(2,2)	R(10)	22232.44	-0.06
(1,1)	P(38)	22180.56	0.00	(2,2)	P(12)	22210.23	-0.08
(1,1)	R(38)	22251.75	0.0	(2,2)	R(12)	22234.00	-0.01
(1,1)	P(40)	22178.03	0.05	(2,2)	P(14)	22207.89	-0.13
(1,1)	R(40)	22252.70	0.17	(2,2)	R(14)	22235.21	-0.15
(1,1)	P(42)	22175.54	0.15	(2,2)	P(16)	22205.69	0.01
(1,1)	R(42)	22253.60	0.17	(2,2)	R(16)	22236.64	-0.01
(2,1)	R(2)	22474.63	-0.21	(2,2)	P(18)	22203.33	0.34
(2,1)	P(4)	22497.94	-0.05	(2,2)	R(18)	22238.31	0.15
(2,1)	P(6)	22485.74	-0.06	(2,2)	P(20)	22200.95	0.10
(2,1)	R(6)	22483.37	-0.15	(2,2)	R(20)	22239.34	-0.06
(2,1)	R(8)	22479.61	-0.06	(2,2)	P(22)	22198.40	0.04
(2,1)	P(10)	22481.01	-0.12	(2,2)	R(22)	22240.65	0.29
(2,1)	R(10)	22480.92	-0.14	(2,2)	P(24)	22196.04	0.21
(2,1)	P(12)	22476.61	-0.04	(2,2)	P(26)	22193.37	0.12
(2,1)	R(12)	22482.62	0.08	(2,2)	P(28)	22190.64	0.22
(2,1)	P(14)	22476.06	-0.03	(2,2)	P(30)	22188.00	0.12
(2,1)	P(16)	22473.34	-0.06	(2,2)	P(32)	22185.40	0.24
(2,1)	P(18)	22470.66	0.03	(2,2)	P(34)	22182.95	0.20
(2,1)	P(20)	22467.84	0.07	(2,2)	P(36)	22179.77	0.14
(2,1)	R(20)	22486.61	0.09	(2,2)	P(38)	22176.65	0.10
(2,1)	P(22)	22464.66	0.03	(2,2)	P(40)	22173.64	0.02
(2,1)	P(24)	22461.79	0.20	(2,2)	P(42)	22170.70	-0.13
(2,1)	P(26)	22458.97	0.22	(2,2)	P(44)	22167.39	-0.29
(2,1)	P(28)	22432.40	0.25	(2,2)	P(46)	22164.06	-0.60
(2,1)	P(32)	22429.33	0.27				

BAND	ASSIGNMENT	OBS FREQ (CM-1)	DEV		BAND	ASSIGNMENT	OBS FREQ (CM-1)	DEV
(0,0)	P(2)	23776.09	-0.02		(1,0)	R(22)	23962.03	-0.02
(0,0)	P(4)	23766.04	0.14		(1,0)	R(24)	23960.77	-0.10
(0,0)	P(6)	23760.34	0.24		(1,0)	R(26)	23959.27	-0.14
(0,0)	P(8)	23761.49	-0.02		(1,0)	R(28)	23957.57	-0.10
(0,0)	P(10)	23760.65	0.11		(1,0)	R(30)	23955.39	-0.25
(0,0)	P(12)	23757.67	0.10		(1,0)	R(32)	23953.08	-0.23
(0,0)	P(14)	23754.65	0.04		(1,0)	R(34)	23950.54	-0.13
(0,0)	P(16)	23751.32	0.07		(1,0)	R(36)	23947.63	-0.10
(0,0)	P(18)	23747.78	0.10		(1,0)	R(38)	23944.45	-0.01
(0,0)	P(20)	23744.03	0.13		(1,0)	R(40)	23941.17	0.30
(0,0)	P(22)	23733.99	0.10		(1,1)	P(10)	23692.61	0.29
(0,0)	P(24)	23735.77	0.11		(1,1)	P(12)	23689.59	0.26
(0,0)	P(26)	23731.27	0.09		(1,1)	P(14)	23686.37	0.23
(0,0)	P(28)	23726.55	0.10		(1,1)	P(16)	23682.95	0.20
(0,0)	R(24)	23776.43	0.10		(1,1)	P(18)	23679.24	0.07
(0,0)	P(30)	23721.53	0.07		(1,1)	P(20)	23675.42	0.03
(0,0)	R(33)	23770.92	0.23		(1,1)	P(22)	23671.41	0.0
(0,0)	P(32)	23716.24	0.06		(1,1)	P(24)	23667.20	-0.04
(0,0)	R(32)	23774.92	0.21		(1,1)	P(26)	23662.65	-0.21
(0,0)	P(34)	23710.67	0.06		(1,1)	P(28)	23658.08	-0.20
(0,0)	R(34)	23772.31	-0.06		(1,1)	P(30)	23653.23	-0.21
(0,0)	P(36)	23704.71	-0.01		(1,1)	P(32)	23648.36	-0.13
(0,0)	P(38)	23698.29	-0.21		(1,1)	P(34)	23643.11	-0.17
(0,0)	P(40)	23692.03	0.12		(1,1)	P(36)	23637.78	-0.07
(0,0)	P(42)	23685.61	0.06		(1,1)	P(38)	23632.28	0.09
(0,0)	P(44)	23677.53	-0.06		(2,1)	P(4)	23908.28	-0.23
(0,0)	P(4)	23516.10	-0.19		(2,1)	P(6)	23905.44	-0.20
(0,0)	P(6)	23513.75	-0.26		(2,1)	P(8)	23903.06	-0.29
(0,1)	P(8)	23511.45	-0.14		(2,1)	P(10)	23900.26	-0.17
(0,1)	P(10)	23508.85	-0.17		(2,1)	P(12)	23897.18	-0.12
(0,1)	R(10)	23528.61	-0.11		(2,1)	P(14)	23893.78	-0.18
(0,1)	P(12)	23506.20	-0.13		(2,1)	P(16)	23890.30	-0.10
(0,1)	P(14)	23503.33	-0.06		(2,1)	P(18)	23886.48	-0.17
(0,1)	P(16)	23500.27	-0.14		(2,1)	P(20)	23882.61	-0.09
(0,1)	P(18)	23497.07	-0.15		(2,1)	P(22)	23878.52	-0.04
(0,1)	P(20)	23493.83	-0.01		(2,1)	P(24)	23874.18	-0.06
(0,1)	P(22)	23490.17	-0.15		(2,1)	P(26)	23869.68	-0.07
(0,1)	P(24)	23486.57	-0.22		(2,1)	R(26)	23917.71	0.02
(0,1)	P(26)	23482.73	0.04		(2,1)	P(28)	23865.13	0.05
(0,1)	P(28)	23478.38	-0.14		(2,1)	R(28)	23915.50	0.0
(0,1)	P(30)	23474.09	-0.08		(2,1)	P(30)	23860.31	0.06
(0,1)	P(32)	23469.43	-0.11		(2,1)	R(33)	23915.13	0.02
(0,1)	P(34)	23464.60	-0.08		(2,1)	P(32)	23855.36	0.13
(0,1)	P(36)	23459.52	-0.02		(2,1)	R(32)	23913.31	-0.03
(1,0)	P(15)	23933.49	0.30		(2,1)	P(34)	23850.16	0.01
(1,0)	P(18)	23927.73	0.12		(2,1)	R(34)	23911.77	-0.02
(1,0)	R(18)	23993.75	0.17		(2,2)	P(6)	23657.13	0.04
(1,0)	P(20)	23925.46	0.03		(2,2)	P(8)	23654.50	-0.06

5d sigma

BAND	ROT LINE	OBS FREQ (CM-1)	DEV	*	BAND	ROT LINE	OBS FREQ (CM-1)	DEV
(2,2)	P(10)	23651.98	0.13	*	(3,1)	P(22)	24097.80	0.19
(2,2)	P(12)	23648.81	-0.15	*	(3,1)	P(24)	24093.43	0.18
(2,2)	P(14)	23645.87	-0.04	*	(3,1)	P(26)	24088.95	-0.01
(2,2)	P(16)	23642.87	0.18	*	(3,2)	P(2)	23880.22	0.04
(2,2)	P(18)	23639.36	0.05	*	(3,2)	P(4)	23877.94	-0.07
(2,2)	P(20)	23635.88	0.10	*	(3,2)	P(6)	23875.66	0.01
(2,2)	P(22)	23632.23	0.13	*	(3,2)	P(8)	23873.12	0.01
(2,2)	P(24)	23628.24	-0.04	*	(3,2)	P(10)	23870.16	-0.04
(2,2)	P(26)	23624.56	0.23	*	(3,2)	P(12)	23867.72	0.20
(2,2)	P(28)	23620.41	0.16	*	(3,2)	P(14)	23864.59	0.11
(2,2)	P(30)	23616.37	0.32	*	(3,2)	P(16)	23861.38	0.08
(2,2)	P(32)	23611.95	0.22	*	(3,2)	P(18)	23858.05	0.08
(2,2)	R(32)	23670.18	0.18	*	(3,2)	P(20)	23854.60	0.06
(2,2)	P(34)	23607.46	0.14	*	(3,2)	R(20)	23891.87	-0.11
(2,2)	R(34)	23669.13	0.18	*	(3,2)	P(22)	23850.95	0.0
(2,2)	P(36)	23602.81	0.31	*	(3,2)	P(24)	23847.11	-0.18
(2,2)	R(36)	23667.49	-0.28	*	(3,2)	P(26)	23843.26	-0.26
(3,1)	P(20)	24101.64	0.20	*	(3,2)	P(28)	23839.24	-0.49

od sigma

BAND	ROT LINE	OBS FREQ (CM-1)	DEV	*	BAND	ROT LINE	OBS FREQ (CM-1)	DEV
(0,0)	R(0)	24500.50	-0.15	*	(1,1)	P(10)	24483.10	-0.07
(0,0)	R(2)	24502.62	-0.01	*	(1,1)	R(10)	24503.72	0.01
(0,0)	R(4)	24504.69	0.06	*	(1,1)	P(12)	24481.31	0.01
(0,0)	P(6)	24493.73	-0.01	*	(1,1)	R(12)	24505.79	0.07
(0,0)	R(6)	24506.79	0.20	*	(1,1)	P(14)	24479.56	0.11
(0,0)	P(8)	24491.82	0.05	*	(1,1)	R(14)	24507.90	0.16
(0,0)	P(10)	24489.93	0.11	*	(1,1)	P(16)	24477.81	0.19
(0,0)	R(10)	24510.02	0.09	*	(1,1)	R(16)	24509.95	0.19
(0,0)	P(12)	24487.81	-0.06	*	(1,1)	P(18)	24476.05	0.22
(0,0)	R(12)	24512.58	0.09	*	(1,1)	R(18)	24511.95	0.17
(0,0)	P(14)	24485.88	-0.04	*	(1,1)	P(20)	24474.22	0.17
(0,0)	R(14)	24514.40	-0.02	*	(1,1)	R(20)	24513.98	0.18
(0,0)	P(16)	24483.90	-0.07	*	(1,1)	P(22)	24472.53	0.22
(0,0)	R(16)	24516.34	0.0	*	(1,1)	R(22)	24515.52	-0.29
(0,0)	P(18)	24482.30	-0.03	*	(1,1)	P(24)	24470.33	-0.25
(0,0)	R(18)	24518.20	-0.03	*	(1,2)	P(14)	24231.37	-0.33
(0,0)	P(20)	24480.03	-0.05	*	(1,2)	P(16)	24229.91	0.0
(0,0)	R(20)	24520.03	-0.04	*	(1,2)	P(18)	24228.38	-0.11
(0,0)	P(22)	24478.05	-0.07	*	(1,2)	R(18)	24264.37	-0.07
(0,0)	R(22)	24521.78	-0.09	*	(1,2)	P(20)	24227.03	-0.10
(0,0)	P(24)	24476.04	-0.09	*	(1,2)	R(20)	24266.71	-0.17
(0,0)	R(24)	24523.44	-0.16	*	(1,2)	R(22)	24268.62	-0.73
(0,0)	P(26)	24472.04	-0.01	*	(1,2)	P(24)	24223.34	-0.68
(0,0)	P(30)	24470.03	0.10	*	(2,1)	P(34)	24702.90	0.34
(0,0)	P(32)	24469.01	0.30	*	(2,1)	P(36)	24700.83	0.11
(1,0)	P(5)	24736.93	-0.05	*	(2,1)	P(38)	24699.09	0.23
(1,0)	R(6)	24733.67	0.04	*	(2,1)	R(38)	24770.51	0.05
(1,0)	P(10)	24734.89	0.01	*	(2,1)	P(40)	24696.91	-0.07
(1,0)	R(10)	24755.46	0.05	*	(2,1)	R(40)	24772.33	0.15
(1,0)	P(12)	24732.38	0.12	*	(2,1)	P(42)	24694.77	-0.27
(1,0)	R(12)	24757.38	0.19	*	(2,1)	P(44)	24692.79	-0.22
(1,0)	P(14)	24730.77	0.15	*	(2,1)	P(46)	24690.71	-0.13
(1,0)	R(14)	24759.27	0.36	*	(2,1)	P(50)	24686.03	0.13
(1,0)	P(16)	24728.64	0.18	*	(3,2)	P(4)	24724.48	0.16
(1,0)	R(16)	24760.33	0.28	*	(3,2)	P(6)	24720.62	0.24
(1,0)	P(18)	24726.53	0.24	*	(3,2)	R(5)	24730.67	0.13
(1,0)	R(18)	24762.54	0.40	*	(3,2)	P(10)	24716.51	0.10
(1,0)	P(20)	24724.36	0.27	*	(3,2)	P(10)	24713.56	0.25
(1,0)	P(22)	24722.06	0.18	*	(3,2)	R(10)	24738.70	0.09
(1,0)	P(24)	24719.32	-0.24	*	(3,2)	R(10)	24738.35	0.24
(1,1)	P(2)	24499.49	-0.35	*	(3,2)	P(12)	24710.33	-0.11
(1,1)	R(2)	24495.91	-0.11	*	(3,2)	P(12)	24710.43	-0.32
(1,1)	P(4)	24496.97	-0.23	*	(3,2)	R(12)	24740.27	-0.11
(1,1)	R(4)	24497.53	-0.19	*	(3,2)	R(12)	24740.47	-0.01
(1,1)	P(6)	24498.54	-0.11	*	(3,2)	P(14)	24714.26	-0.24
(1,1)	R(6)	24499.02	-0.09	*	(3,2)	P(14)	24714.43	-0.07
(1,1)	P(8)	24498.96	-0.10	*	(3,2)	P(16)	24712.36	-0.22
(1,1)	R(8)	24501.03	-0.06	*	(3,2)	P(16)	24712.49	-0.09

6d sigma

BAND	ROT LINE	OBS FREQ (CM-1)	DEV	*	BAND	ROT LINE	OBS FREQ (CM-1)	DEV
				*				
(3,2)	R(16)	24744.02	-0.23	*	(3,2)	R(20)	24748.15	0.04
(3,2)	R(16)	24744.17	-0.08	*	(3,2)	P(22)	24707.00	-0.08
(3,2)	P(18)	24710.55	-0.14	*	(3,2)	P(22)	24707.08	0.0
(3,2)	R(18)	24745.95	-0.21	*	(3,2)	R(22)	24750.29	0.20
(3,2)	R(18)	24746.21	-0.05	*	(3,2)	R(22)	24750.49	0.40
(3,2)	P(20)	24708.70	-0.16	*	(3,2)	P(24)	24705.33	-0.03
(3,2)	P(20)	24708.82	-0.04	*	(3,2)	P(24)	24705.51	0.15
(3,2)	R(20)	24746.00	-0.11	*				

7d sigma

BAND	ROT LINE	OBS FREQ (CM-1)	DEV	*	BAND	ROT LINE	OBS FREQ (CM-1)	DEV
(0,0)	R(10)	25224.09	-0.58	*	(1,1)	P(22)	25202.74	-0.05
(0,0)	R(12)	25227.00	-0.34	*	(1,1)	R(22)	25247.46	0.06
(0,0)	R(14)	25230.11	0.0	*	(1,1)	R(24)	25250.71	0.14
(0,0)	R(16)	25233.34	0.38	*	(1,1)	R(26)	25253.97	0.18
(0,0)	R(18)	25236.48	0.60	*	(1,1)	R(28)	25257.23	0.18
(0,0)	R(20)	25239.71	0.84	*	(1,1)	R(30)	25260.45	0.12
(0,0)	R(22)	25242.89	0.97	*	(1,1)	R(32)	25263.90	0.26
(0,0)	R(24)	25245.30	0.29	*	(1,1)	R(34)	25267.18	0.22
(0,0)	R(26)	25247.99	-0.16	*	(1,1)	R(36)	25270.59	0.29
(0,0)	R(28)	25250.66	-0.66	*	(1,1)	R(38)	25273.87	0.23
(0,0)	R(30)	25253.32	-0.69	*	(1,1)	R(40)	25277.16	0.18
(0,0)	R(32)	25257.31	-0.41	*	(1,1)	R(42)	25280.41	0.08
(0,0)	R(34)	25260.47	-0.47	*	(1,1)	R(44)	25283.64	-0.05
(0,0)	R(36)	25263.90	-0.26	*	(1,1)	R(46)	25286.89	-0.17
(0,0)	R(38)	25267.26	-0.13	*	(1,1)	R(48)	25290.06	-0.39
(0,0)	R(40)	25270.60	-0.02	*	(2,2)	P(4)	25217.73	0.14
(0,0)	R(42)	25273.86	0.02	*	(2,2)	P(6)	25216.02	0.06
(0,0)	R(44)	25277.24	0.17	*	(2,2)	P(8)	25214.59	0.11
(0,0)	R(46)	25280.49	0.18	*	(2,2)	P(10)	25213.39	0.26
(0,0)	R(48)	25283.86	0.29	*	(2,2)	P(12)	25212.09	0.17
(0,0)	R(50)	25286.90	0.04	*	(2,2)	P(14)	25210.92	0.08
(0,0)	R(52)	25290.16	-0.04	*	(2,2)	P(16)	25209.80	-0.08
(1,1)	R(14)	25234.43	-0.93	*	(2,2)	P(18)	25208.94	-0.10
(1,1)	R(16)	25236.04	-0.22	*	(2,2)	P(20)	25208.25	-0.07
(1,1)	R(18)	25241.12	-0.12	*	(2,2)	R(20)	25248.50	-0.23
(1,1)	R(20)	25244.27	-0.02	*	(2,2)	P(22)	25207.36	-0.34

3d sigma

BAND	ROT LINE	OBS FREQ (CM-1)	DEV	*	BAND	ROT LINE	OBS FREQ (CM-1)	DEV
				*				
(0,0)	R(10)	25747.16	-0.78	*	(1,1)	R(18)	25767.32	0.11
(0,0)	R(12)	25751.29	0.0	*	(1,1)	R(20)	25770.98	0.02
(0,0)	R(14)	25754.82	0.04	*	(1,1)	P(22)	25729.56	0.09
(0,0)	R(16)	25758.54	0.13	*	(1,1)	R(22)	25774.64	-0.11
(0,0)	P(18)	25724.22	0.12	*	(1,1)	R(24)	25778.42	-0.13
(0,0)	R(18)	25762.33	0.20	*	(1,1)	R(26)	25782.17	-0.19
(0,0)	R(20)	25766.09	0.16	*	(1,1)	R(28)	25786.04	-0.09
(0,0)	R(22)	25769.90	0.12	*	(1,1)	R(30)	25789.78	-0.09
(0,0)	R(24)	25773.70	0.05	*	(1,1)	R(32)	25793.47	-0.08
(0,0)	R(26)	25777.62	0.11	*	(1,1)	R(34)	25797.30	0.11
(0,0)	R(28)	25781.36	0.0	*	(2,2)	R(16)	25768.59	0.06
(0,0)	R(30)	25785.13	-0.05	*	(2,2)	R(18)	25772.10	-0.05
(0,0)	R(32)	25788.93	-0.02	*	(2,2)	R(18)	25772.40	0.25
(0,0)	R(36)	25796.17	-0.19	*	(2,2)	R(20)	25775.58	-0.26
(0,0)	R(38)	25800.04	0.01	*	(2,2)	R(20)	25775.98	0.14
(0,0)	R(40)	25803.89	0.17	*	(2,2)	R(22)	25779.55	-0.02
(0,0)	R(42)	25807.53	0.07	*	(2,2)	R(24)	25783.07	-0.24
(0,0)	R(44)	25811.18	-0.14	*	(2,2)	R(26)	25786.94	-0.10
(1,1)	R(10)	25753.35	0.14	*	(2,2)	R(28)	25790.64	-0.10
(1,1)	R(12)	25756.65	0.14	*	(2,2)	R(30)	25794.34	-0.05
(1,1)	R(14)	25760.04	0.08	*	(2,2)	R(32)	25797.97	-0.02
(1,1)	R(16)	25763.55	0.01	*	(2,2)	R(34)	25801.92	0.39

9d sigma

BAND	ROT LINE	OBS FREQ (CM-1)	DEV	*	BAND	ROT LINE	OBS FREQ (CM-1)	DEV
(0,0)	R(10)	26114.02	-0.30	*	(1,1)	R(18)	26135.47	0.14
(0,0)	R(12)	26117.68	-0.19	*	(1,1)	R(20)	26139.17	-0.09
(0,0)	R(14)	26121.66	0.07	*	(1,1)	R(22)	26143.11	-0.10
(0,0)	R(16)	26125.54	0.11	*	(1,1)	R(24)	26146.98	-0.18
(0,0)	R(18)	26129.48	0.10	*	(1,1)	R(26)	26150.95	-0.13
(0,0)	R(20)	26133.49	0.10	*	(1,1)	R(28)	26154.79	-0.18
(0,0)	R(22)	26137.46	0.03	*	(1,1)	R(30)	26158.79	-0.03
(0,0)	R(24)	26141.47	-0.01	*	(1,1)	R(32)	26162.57	-0.07
(0,0)	R(26)	26145.66	0.14	*	(1,1)	R(34)	26166.73	0.28
(0,0)	R(28)	26149.64	0.12	*	(1,1)	R(36)	26170.46	0.17
(0,0)	R(30)	26153.60	0.10	*	(1,1)	R(38)	26174.13	-0.10
(0,0)	R(32)	26157.42	-0.03	*	(2,2)	R(20)	26144.85	0.08
(0,0)	R(34)	26161.21	-0.19	*	(2,2)	R(22)	26148.53	-0.09
(0,0)	R(36)	26165.33	-0.06	*	(2,2)	R(24)	26152.51	0.05
(1,1)	R(10)	26120.67	0.12	*	(2,2)	R(26)	26156.07	-0.21
(1,1)	R(12)	26124.15	0.11	*	(2,2)	R(28)	26160.06	0.01
(1,1)	R(14)	26127.75	0.06	*	(2,2)	R(30)	26163.93	0.16
(1,1)	R(16)	26131.50	0.03	*				

10d sigma

BAND	ROT LINE	OBS FREQ (CM-1)	DEV	*	BAND	ROT LINE	OBS FREQ (CM-1)	DEV
(0,0)	R(6)	26371.29	-0.15	*	(1,1)	R(14)	26393.66	0.27
(0,0)	R(8)	26374.82	-0.11	*	(1,1)	R(16)	26397.58	0.03
(0,0)	R(10)	26378.66	-0.03	*	(1,1)	R(18)	26401.60	-0.11
(0,0)	R(12)	26382.98	0.32	*	(1,1)	R(20)	26405.56	-0.21
(0,0)	R(14)	26386.91	0.13	*	(1,1)	R(22)	26409.41	-0.21
(0,0)	R(16)	26390.94	-0.04	*	(1,1)	R(24)	26413.07	-0.07
(0,0)	R(18)	26395.01	-0.16	*	(2,2)	R(8)	26388.45	-0.15
(0,0)	R(20)	26399.03	-0.23	*	(2,2)	R(10)	26392.34	0.04
(0,0)	R(24)	26407.00	0.29	*	(2,2)	R(16)	26404.52	0.10
(1,1)	R(5)	26377.72	-0.44	*	(2,2)	R(18)	26408.55	0.01
(1,1)	R(8)	26381.61	-0.01	*	(2,2)	R(20)	26412.38	-0.18
(1,1)	R(10)	26385.84	0.49	*	(2,2)	R(22)	26416.26	-0.11
(1,1)	R(12)	26389.55	0.26	*	(2,2)	R(24)	26420.14	0.29

4s sigma

BAND	ROT LINE	OBS FREQ (CM-1)	DEV	*	BAND	ROT LINE	OBS FREQ (CM-1)	DEV
(0,0)	R(0)	20233.56	-0.02	*	(0,1)	P(24)	19950.34	-0.19
(0,0)	P(2)	20230.57	-0.04	*	(0,1)	R(24)	19996.46	-0.04
(0,0)	R(2)	20235.56	0.19	*	(0,1)	P(26)	19947.39	-0.18
(0,0)	P(4)	20228.57	0.12	*	(0,1)	P(28)	19944.33	-0.22
(0,0)	R(4)	20237.11	0.09	*	(0,1)	P(30)	19941.33	-0.15
(0,0)	P(6)	20226.23	0.08	*	(0,1)	P(32)	19938.24	-0.14
(0,0)	R(6)	20238.53	0.01	*	(0,1)	P(34)	19935.26	0.02
(0,0)	P(8)	20223.77	0.06	*	(0,1)	P(36)	19932.05	-0.02
(0,0)	R(8)	20240.10	0.22	*	(0,1)	P(38)	19928.87	-0.01
(0,0)	P(10)	20221.22	0.09	*	(0,1)	P(40)	19925.79	0.12
(0,0)	P(12)	20218.48	0.06	*	(0,1)	P(42)	19922.60	0.16
(0,0)	P(14)	20215.68	0.10	*	(0,1)	P(44)	19919.51	0.30
(0,0)	P(16)	20212.60	-0.02	*	(0,1)	P(46)	19916.36	0.39
(0,0)	P(18)	20209.69	0.16	*	(1,0)	P(8)	20488.11	0.16
(0,0)	P(20)	20206.37	0.04	*	(1,0)	P(10)	20485.32	0.18
(0,0)	P(22)	20203.10	0.08	*	(1,0)	P(12)	20482.35	0.21
(0,0)	P(24)	20199.66	0.05	*	(1,0)	P(14)	20479.21	0.25
(0,0)	P(26)	20196.10	0.01	*	(1,0)	P(16)	20475.78	0.18
(0,0)	P(28)	20192.58	0.09	*	(1,0)	P(18)	20472.33	0.27
(0,0)	P(30)	20188.83	0.04	*	(1,0)	P(20)	20468.49	0.13
(0,0)	P(32)	20185.08	0.06	*	(1,0)	P(22)	20464.61	0.13
(0,0)	P(34)	20181.30	0.13	*	(1,0)	P(24)	20460.59	0.14
(0,0)	P(36)	20177.44	0.19	*	(1,0)	P(26)	20456.31	0.04
(0,0)	P(38)	20173.52	0.25	*	(1,0)	P(28)	20451.97	0.03
(0,0)	P(40)	20169.45	0.23	*	(1,0)	P(30)	20447.51	0.05
(0,0)	P(42)	20165.39	0.26	*	(1,0)	P(32)	20442.84	-0.01
(0,0)	P(44)	20157.34	0.54	*	(1,0)	P(34)	20438.03	-0.08
(0,1)	R(2)	19983.06	-0.03	*	(1,0)	P(36)	20433.18	-0.07
(0,1)	P(4)	19976.12	-0.12	*	(1,0)	P(38)	20428.20	-0.07
(0,1)	R(4)	19984.75	-0.07	*	(1,0)	P(40)	20422.99	-0.18
(0,1)	P(6)	19973.97	-0.09	*	(1,0)	P(42)	20417.67	-0.30
(0,1)	R(6)	19986.28	-0.16	*	(1,1)	P(2)	20243.12	0.18
(0,1)	P(8)	19971.68	-0.11	*	(1,1)	R(2)	20247.86	0.23
(0,1)	R(8)	19987.81	-0.14	*	(1,1)	P(4)	20241.01	0.22
(0,1)	P(10)	19969.29	-0.12	*	(1,1)	R(4)	20249.47	0.24
(0,1)	R(10)	19989.25	-0.12	*	(1,1)	P(6)	20238.67	0.19
(0,1)	P(12)	19966.82	-0.13	*	(1,1)	R(6)	20250.89	0.21
(0,1)	R(12)	19990.49	-0.19	*	(1,1)	P(8)	20236.20	0.17
(0,1)	P(14)	19964.22	-0.19	*	(1,1)	P(10)	20233.59	0.17
(0,1)	R(14)	19991.77	-0.12	*	(1,1)	P(12)	20230.79	0.12
(0,1)	P(16)	19961.60	-0.16	*	(1,1)	P(14)	20227.91	0.12
(0,1)	R(16)	19992.80	-0.20	*	(1,1)	P(16)	20224.87	0.11
(0,1)	P(18)	19958.35	-0.12	*	(1,1)	P(18)	20221.66	0.09
(0,1)	R(18)	19993.91	-0.09	*	(1,1)	P(20)	20218.36	0.05
(0,1)	P(20)	19956.15	-0.14	*	(1,1)	P(22)	20214.94	0.03
(0,1)	R(20)	19994.76	-0.10	*	(1,1)	P(24)	20211.39	0.01
(0,1)	P(22)	19953.16	-0.26	*	(1,1)	P(26)	20207.66	-0.08
(0,1)	R(22)	19995.01	-0.16	*	(1,1)	P(28)	20203.93	-0.07

4s sigma

BAND	ROT LINE	OBS FREQ (CM-1)	DEV	*	BAND	ROT LINE	OBS FREQ (CM-1)	DEV
(1,1)	P(30)	20200.02	-0.13	*	(2,0)	R(30)	20754.16	0.11
(1,1)	P(32)	20196.07	-0.14	*	(2,0)	R(32)	20752.20	0.26
(1,1)	P(34)	20192.08	-0.10	*	(2,1)	P(4)	20498.66	-0.08
(1,1)	P(36)	20187.66	-0.21	*	(2,1)	P(6)	20496.22	-0.08
(1,1)	P(38)	20183.64	-0.24	*	(2,1)	P(8)	20493.58	-0.07
(1,1)	P(40)	20179.41	-0.20	*	(2,1)	P(10)	20490.76	-0.04
(1,1)	P(42)	20175.00	-0.28	*	(2,1)	P(12)	20487.72	-0.02
(1,2)	R(6)	20001.76	0.03	*	(2,1)	P(14)	20484.43	-0.05
(1,2)	P(8)	19987.33	0.09	*	(2,1)	P(16)	20481.00	-0.02
(1,2)	R(8)	20003.26	0.09	*	(2,1)	P(18)	20477.37	-0.01
(1,2)	P(10)	19984.90	0.06	*	(2,1)	P(20)	20473.54	0.0
(1,2)	R(10)	20004.52	0.02	*	(2,1)	P(22)	20469.49	-0.03
(1,2)	P(12)	19982.36	0.02	*	(2,1)	P(24)	20465.33	0.0
(1,2)	R(12)	20005.72	0.0	*	(2,1)	P(26)	20460.94	-0.03
(1,2)	P(14)	19979.75	0.01	*	(2,1)	P(28)	20456.44	0.0
(1,2)	P(16)	19977.07	0.02	*	(2,1)	P(30)	20451.74	-0.01
(1,2)	R(16)	20007.77	-0.05	*	(2,1)	P(32)	20446.88	-0.02
(1,2)	P(18)	19974.29	0.03	*	(2,1)	P(34)	20441.86	-0.05
(1,2)	R(18)	20008.63	-0.02	*	(2,1)	R(34)	20503.63	-0.04
(1,2)	P(20)	19971.42	0.03	*	(2,1)	P(36)	20436.73	-0.05
(1,2)	P(22)	19968.39	-0.06	*	(2,1)	R(36)	20501.70	-0.16
(1,2)	P(24)	19965.33	-0.09	*	(2,1)	P(38)	20431.36	-0.14
(1,2)	P(26)	19962.22	-0.11	*	(2,1)	R(38)	20499.53	-0.34
(1,2)	P(28)	19959.03	-0.14	*	(2,1)	P(40)	20426.00	-0.10
(1,2)	P(30)	19955.70	-0.25	*	(2,2)	P(8)	20244.80	-0.06
(1,2)	P(32)	19952.45	-0.22	*	(2,2)	P(10)	20242.15	-0.06
(1,2)	P(34)	19949.09	-0.26	*	(2,2)	P(12)	20239.33	-0.07
(1,2)	P(36)	19942.27	-0.31	*	(2,2)	P(14)	20236.36	-0.07
(1,2)	P(38)	19938.79	-0.38	*	(2,2)	P(16)	20233.14	-0.17
(1,2)	P(40)	19935.29	-0.33	*	(2,2)	P(18)	20230.00	-0.04
(1,2)	P(42)	19931.90	-0.27	*	(2,2)	P(20)	20226.59	-0.03
(1,2)	P(44)	19928.40	-0.25	*	(2,2)	P(22)	20223.06	0.0
(2,0)	P(8)	20745.79	0.21	*	(2,2)	P(24)	20219.33	-0.04
(2,0)	P(10)	20742.69	0.13	*	(2,2)	P(26)	20215.54	-0.01
(2,0)	P(12)	20739.35	0.14	*	(2,2)	P(28)	20211.58	-0.03
(2,0)	P(14)	20735.83	0.21	*	(2,2)	P(30)	20207.48	-0.06
(2,0)	P(16)	20732.13	0.27	*	(2,2)	P(32)	20203.35	-0.01
(2,0)	P(18)	20728.09	0.25	*	(2,2)	R(32)	20261.61	-0.15
(2,0)	P(20)	20723.77	0.19	*	(2,2)	P(34)	20199.01	-0.07
(2,0)	P(22)	20719.29	0.19	*	(2,2)	R(34)	20260.63	-0.16
(2,0)	R(22)	20780.60	0.52	*	(2,2)	P(36)	20194.98	-0.01
(2,0)	P(24)	20714.84	0.24	*	(2,2)	R(36)	20259.60	-0.17
(2,0)	R(24)	20779.38	0.40	*	(2,2)	P(38)	20190.11	-0.09
(2,0)	P(26)	20709.70	0.27	*	(2,2)	P(40)	20185.54	-0.08
(2,0)	R(26)	20757.95	0.38	*	(2,2)	R(40)	20256.95	-0.27
(2,0)	P(28)	20704.57	0.19	*	(2,2)	P(42)	20180.82	-0.13
(2,0)	R(28)	20759.10	0.17	*	(2,2)	R(42)	20255.35	-0.19
(2,0)	P(30)	20699.15	0.12	*	(2,2)	P(44)	20175.04	-0.15

4s sigma

BAND	ROT LINE	OBS FREQ (CM-1)	DEV	*	BAND	ROT LINE	OBS FREQ (CM-1)	DEV
(3,1)	P(4)	20749.20	-0.42	*	(3,2)	P(40)	20424.43	0.28
(3,1)	P(6)	20746.58	-0.47	*	(3,2)	R(40)	20494.79	0.33
(3,1)	P(8)	20743.79	-0.39	*	(3,2)	R(42)	20491.95	0.33
(3,1)	P(10)	20740.72	-0.33	*	(3,4)	P(8)	20006.64	-0.50
(3,1)	P(12)	20737.33	-0.33	*	(3,4)	R(10)	20023.36	-0.29
(3,1)	P(14)	20733.72	-0.28	*	(3,4)	P(12)	20001.64	-0.33
(3,1)	P(16)	20729.90	-0.18	*	(3,4)	R(12)	20024.31	-0.27
(3,1)	P(18)	20725.79	-0.12	*	(3,4)	P(14)	19998.92	-0.26
(3,1)	P(20)	20721.40	-0.08	*	(3,4)	P(16)	19996.06	-0.19
(3,1)	P(22)	20716.66	-0.15	*	(3,4)	P(18)	19993.00	-0.20
(3,1)	R(22)	20757.25	0.12	*	(3,4)	P(20)	19989.91	-0.11
(3,1)	R(24)	20755.88	0.19	*	(3,4)	P(22)	19986.63	-0.09
(3,1)	P(26)	20706.84	0.09	*	(3,4)	P(24)	19983.26	-0.04
(3,1)	R(26)	20754.16	0.17	*	(3,4)	P(26)	19979.72	-0.05
(3,1)	P(28)	20701.56	0.18	*	(3,4)	P(28)	19976.21	0.07
(3,1)	P(28)	20701.45	0.07	*	(3,4)	P(30)	19972.55	0.15
(3,1)	R(28)	20752.09	0.07	*	(3,4)	P(34)	19964.89	0.24
(3,1)	P(30)	20696.05	0.27	*	(3,4)	P(36)	19960.93	0.30
(3,1)	R(30)	20750.01	0.21	*	(5,4)	P(6)	20485.35	0.42
(3,1)	P(32)	20690.18	0.22	*	(5,4)	P(10)	20482.24	0.43
(3,1)	P(34)	20684.17	0.24	*	(5,4)	P(12)	20478.68	0.26
(3,2)	P(16)	20482.02	-0.35	*	(5,4)	P(14)	20475.08	0.34
(3,2)	P(18)	20478.29	-0.28	*	(5,4)	P(16)	20470.93	0.14
(3,2)	P(20)	20474.33	-0.23	*	(5,4)	P(18)	20466.65	0.08
(3,2)	P(22)	20470.21	-0.14	*	(5,4)	R(18)	20498.70	0.13
(3,2)	P(24)	20465.86	-0.08	*	(5,4)	P(20)	20462.09	0.0
(3,2)	P(26)	20461.36	0.02	*	(5,4)	R(20)	20497.48	0.02
(3,2)	R(26)	20506.64	0.07	*	(5,4)	P(22)	20457.17	-0.17
(3,2)	P(28)	20456.62	0.07	*	(5,4)	R(22)	20495.96	-0.11
(3,2)	R(28)	20507.26	0.07	*	(5,4)	P(24)	20452.22	-0.11
(3,2)	P(30)	20451.73	0.16	*	(5,4)	R(24)	20494.03	-0.36
(3,2)	R(30)	20505.75	0.16	*	(5,4)	P(26)	20446.81	-0.27
(3,2)	P(32)	20446.63	0.21	*	(5,4)	R(28)	20490.59	0.39
(3,2)	R(32)	20503.91	0.13	*	(5,4)	P(30)	20436.10	0.23
(3,2)	P(34)	20441.36	0.26	*	(5,4)	R(30)	20487.32	0.13
(3,2)	R(34)	20501.93	0.17	*	(5,4)	P(32)	20429.82	-0.02
(3,2)	P(36)	20435.63	0.22	*	(5,4)	R(32)	20484.56	-0.34
(3,2)	R(36)	20499.71	0.18	*	(5,4)	P(34)	20423.24	-0.38
(3,2)	P(38)	20430.15	0.19	*	(5,4)	R(34)	20481.02	-0.62
(3,2)	R(38)	20497.39	0.29	*				

5s sigma

BAND	ROT LINE	OBS FREQ (CM-1)	DEV	*	BAND	ROT LINE	OBS FREQ (CM-1)	DEV
(0,0)	R(2)	22763.71	-0.10	*	(0,2)	R(12)	22272.01	-0.13
(0,0)	P(4)	22757.01	0.13	*	(0,2)	R(14)	22274.10	0.02
(0,0)	R(4)	22765.56	-0.04	*	(0,2)	R(16)	22276.09	0.07
(0,0)	P(6)	22754.62	-0.11	*	(0,2)	R(18)	22277.96	0.01
(0,0)	R(6)	22767.30	-0.02	*	(0,2)	R(20)	22279.68	0.02
(0,0)	P(8)	22752.43	-0.07	*	(0,2)	R(22)	22281.71	-0.05
(0,0)	R(8)	22766.96	0.01	*	(0,2)	R(24)	22283.63	-0.01
(0,0)	P(10)	22750.07	-0.13	*	(0,2)	R(26)	22285.51	0.02
(0,0)	R(10)	22770.48	-0.01	*	(0,2)	R(30)	22289.08	-0.02
(0,0)	P(12)	22747.86	0.04	*	(0,2)	R(32)	22290.79	-0.06
(0,0)	R(12)	22771.96	0.02	*	(0,2)	R(34)	22292.51	-0.05
(0,0)	P(14)	22745.37	0.0	*	(0,2)	R(36)	22294.13	-0.08
(0,0)	R(14)	22773.32	0.02	*	(0,2)	R(38)	22295.76	-0.04
(0,0)	R(18)	22775.65	-0.10	*	(0,2)	R(40)	22297.27	-0.05
(0,1)	P(2)	22506.72	0.04	*	(0,2)	R(42)	22298.77	0.01
(0,1)	R(2)	22511.53	0.01	*	(0,2)	R(44)	22300.09	-0.03
(0,1)	P(4)	22504.78	0.10	*	(0,2)	R(46)	22301.40	0.03
(0,1)	R(4)	22513.46	0.06	*	(0,2)	R(48)	22302.46	-0.05
(0,1)	P(6)	22502.70	0.06	*	(1,1)	R(2)	22754.95	-0.02
(0,1)	R(6)	22515.28	0.05	*	(1,1)	P(4)	22748.02	-0.10
(0,1)	P(8)	22500.64	0.06	*	(1,1)	R(4)	22756.71	0.05
(0,1)	R(8)	22517.10	0.08	*	(1,1)	P(6)	22745.79	-0.12
(0,1)	P(10)	22498.51	0.03	*	(1,1)	R(6)	22758.18	-0.05
(0,1)	R(10)	22518.77	0.0	*	(1,1)	P(8)	22743.53	-0.05
(0,1)	P(12)	22496.36	0.0	*	(1,1)	R(8)	22759.79	0.11
(0,1)	R(12)	22520.51	0.04	*	(1,1)	P(10)	22741.09	-0.05
(0,1)	P(14)	22494.21	0.01	*	(1,1)	R(10)	22761.03	0.02
(0,1)	R(14)	22522.16	0.03	*	(1,1)	P(12)	22738.57	-0.03
(0,1)	P(16)	22492.05	0.04	*	(1,1)	R(12)	22762.25	0.04
(0,1)	R(16)	22523.73	0.0	*	(1,1)	R(14)	22763.37	0.08
(0,1)	P(18)	22489.80	0.0	*	(1,1)	R(16)	22764.41	0.18
(0,1)	R(18)	22525.34	0.05	*	(1,1)	R(18)	22765.15	0.10
(0,1)	R(20)	22526.79	0.01	*	(1,2)	R(2)	22505.60	-0.22
(0,1)	R(22)	22528.19	-0.03	*	(1,2)	P(4)	22498.72	-0.33
(0,1)	R(24)	22529.59	-0.01	*	(1,2)	R(4)	22507.30	-0.29
(0,1)	R(25)	22530.65	-0.06	*	(1,2)	P(6)	22496.50	-0.15
(0,1)	R(26)	22532.13	-0.02	*	(1,2)	R(6)	22509.02	-0.26
(0,1)	P(30)	22475.90	-0.01	*	(1,2)	P(8)	22494.79	0.0
(0,1)	R(30)	22533.27	-0.04	*	(1,2)	R(8)	22510.90	0.01
(0,1)	P(32)	22473.44	-0.04	*	(1,2)	P(10)	22492.51	-0.05
(0,1)	R(32)	22534.41	0.01	*	(1,2)	R(10)	22512.36	-0.07
(0,1)	P(34)	22470.97	-0.04	*	(1,2)	P(12)	22490.21	-0.05
(0,1)	R(34)	22535.37	-0.02	*	(1,2)	R(12)	22513.38	0.0
(0,1)	R(36)	22536.32	0.02	*	(1,2)	P(14)	22487.93	0.04
(0,1)	R(38)	22537.03	-0.07	*	(1,2)	R(14)	22515.25	0.01
(0,2)	R(2)	22266.46	0.12	*	(1,2)	P(16)	22485.52	0.06
(0,2)	R(6)	22268.36	0.13	*	(1,2)	R(16)	22516.46	-0.04
(0,2)	R(10)	22270.22	0.13	*	(1,2)	P(18)	22482.97	0.01

5s sigma

BAND	ROT LINE	OBS FREQ (CM-1)	DEV	*	BAND	ROT LINE	OBS FREQ (CM-1)	DEV
(1,2)	P(20)	22480.40	0.0	*	(2,1)	P(24)	22953.05	-0.15
(1,2)	R(20)	22518.82	0.02	*	(2,4)	R(0)	22257.92	0.08
(1,2)	P(22)	22477.31	0.04	*	(2,4)	P(8)	22245.31	0.14
(1,2)	R(22)	22519.84	0.04	*	(2,4)	R(8)	22259.56	0.12
(1,2)	P(24)	22475.11	0.04	*	(2,4)	P(10)	22241.67	0.16
(1,2)	R(24)	22520.78	0.08	*	(2,4)	R(10)	22261.20	0.24
(1,2)	P(26)	22469.47	0.01	*	(2,4)	P(12)	22239.39	0.11
(1,2)	P(30)	22466.39	-0.16	*	(2,4)	R(12)	22262.46	0.06
(1,2)	P(32)	22463.66	0.09	*	(2,4)	P(14)	22237.07	0.06
(1,2)	P(34)	22460.66	0.15	*	(2,4)	R(14)	22263.87	0.11
(1,2)	P(36)	22457.59	0.23	*	(2,4)	P(16)	22234.70	0.06
(1,2)	P(38)	22454.74	0.61	*	(2,4)	R(16)	22265.17	0.14
(2,1)	R(2)	22992.37	-0.17	*	(2,4)	P(18)	22232.36	0.14
(2,1)	R(4)	22994.03	-0.02	*	(2,4)	R(18)	22266.23	0.06
(2,1)	P(6)	22983.19	-0.11	*	(2,4)	P(20)	22229.64	-0.10
(2,1)	R(6)	22995.40	0.04	*	(2,4)	R(20)	22267.38	0.05
(2,1)	P(8)	22980.68	-0.03	*	(2,4)	P(22)	22227.38	0.18
(2,1)	P(10)	22977.86	-0.08	*	(2,4)	R(22)	22268.36	0.03
(2,1)	R(10)	22997.47	0.09	*	(2,4)	P(24)	22224.50	-0.10
(2,1)	P(12)	22975.05	0.08	*	(2,4)	R(24)	22269.16	-0.08
(2,1)	P(14)	22971.68	0.07	*	(2,4)	P(26)	22221.85	-0.07
(2,1)	P(16)	22966.45	-0.02	*	(2,4)	P(28)	22219.30	-0.18
(2,1)	P(18)	22964.91	-0.02	*	(2,4)	R(28)	22270.43	-0.32
(2,1)	P(20)	22961.16	-0.05	*	(2,4)	P(30)	22215.95	-0.42
(2,1)	P(22)	22957.19	-0.11	*				

6s sigma

BAND	ROT LINE	OBS FREQ (C.M-1)	DEV	*	BAND	ROT LINE	OBS FREQ (C.M-1)	DEV
(0,0)	P(10)	24047.27	0.04	*	(0,1)	R(14)	23816.43	-0.07
(0,0)	P(12)	24044.68	0.01	*	(0,1)	P(16)	23788.30	-0.09
(0,0)	P(14)	24042.10	0.09	*	(0,1)	R(16)	23819.71	-0.09
(0,0)	P(16)	24039.33	0.10	*	(0,1)	P(18)	23785.98	0.11
(0,0)	P(18)	24036.40	0.07	*	(0,1)	R(18)	23820.90	-0.11
(0,0)	P(20)	24033.40	0.08	*	(0,1)	P(20)	23783.24	-0.04
(0,0)	P(22)	24030.21	0.02	*	(1,1)	P(14)	24032.76	0.11
(0,0)	P(24)	24026.90	-0.02	*	(1,1)	P(16)	24029.65	0.02
(0,0)	P(26)	24023.62	0.09	*	(1,1)	P(18)	24026.65	0.17
(0,0)	P(28)	24020.03	0.03	*	(1,1)	P(22)	24019.77	0.12
(0,0)	P(30)	24016.29	-0.03	*	(1,1)	R(22)	24061.10	-0.14
(0,0)	P(32)	24012.54	0.05	*	(1,1)	P(24)	24015.65	-0.16
(0,1)	P(6)	23799.92	0.0	*	(1,1)	P(26)	24012.17	-0.02
(0,1)	P(10)	23795.52	0.01	*	(1,1)	P(28)	24008.13	-0.10
(0,1)	R(10)	23815.61	-0.01	*	(2,2)	P(18)	24011.14	-0.40
(0,1)	P(12)	23793.16	-0.02	*	(2,2)	P(20)	24007.90	0.0
(0,1)	R(12)	23816.99	-0.12	*	(2,2)	R(20)	24045.59	0.40
(0,1)	P(14)	23790.74	-0.09	*				

7a sigma

BAND	ROT LINE	OBS FREQ (CM-1)	DEV		BAND	ROT LINE	OBS FREQ (CM-1)	DEV
(0,0)	R(2)	24944.77	0.35	*	(0,0)	R(58)	24987.35	-0.03
(0,0)	R(4)	24949.06	0.31	*	(1,1)	R(5)	24951.98	-0.72
(0,0)	R(6)	24946.60	0.28	*	(1,1)	R(6)	24954.05	-0.59
(0,0)	R(8)	24950.50	0.26	*	(1,1)	R(10)	24956.20	-0.37
(0,0)	R(10)	24952.38	0.23	*	(1,1)	R(12)	24958.22	-0.26
(0,0)	R(12)	24954.23	0.19	*	(1,1)	R(14)	24960.15	-0.23
(0,0)	R(14)	24956.04	0.14	*	(1,1)	R(16)	24962.18	-0.08
(0,0)	R(16)	24957.82	0.08	*	(1,1)	R(16)	24962.79	0.53
(0,0)	P(18)	24923.43	0.05	*	(1,1)	R(18)	24963.98	-0.14
(0,0)	R(18)	24959.62	0.07	*	(1,1)	R(18)	24964.57	0.45
(0,0)	P(20)	24921.29	-0.11	*	(1,1)	P(20)	24926.40	0.01
(0,0)	R(20)	24961.33	0.01	*	(1,1)	R(20)	24965.84	-0.11
(0,0)	P(22)	24919.17	-0.20	*	(1,1)	R(20)	24966.32	0.37
(0,0)	R(22)	24963.01	-0.05	*	(1,1)	P(22)	24924.31	-0.15
(0,0)	P(24)	24917.12	-0.20	*	(1,1)	R(22)	24967.37	-0.38
(0,0)	R(24)	24964.95	-0.11	*	(1,1)	R(22)	24967.69	0.14
(0,0)	P(26)	24915.10	-0.17	*	(1,1)	R(24)	24969.49	-0.03
(0,0)	R(26)	24966.28	-0.13	*	(1,1)	R(24)	24970.05	0.53
(0,0)	P(28)	24912.93	-0.24	*	(1,1)	P(26)	24920.66	0.08
(0,0)	R(28)	24967.94	-0.09	*	(1,1)	R(26)	24971.18	-0.07
(0,0)	P(30)	24910.86	-0.30	*	(1,1)	R(26)	24971.80	0.55
(0,0)	R(30)	24969.47	-0.12	*	(1,1)	P(28)	24918.65	0.01
(0,0)	P(32)	24908.89	-0.20	*	(1,1)	P(28)	24919.01	0.37
(0,0)	R(32)	24971.01	-0.10	*	(1,1)	R(28)	24972.82	-0.13
(0,0)	P(34)	24906.73	-0.29	*	(1,1)	R(28)	24973.40	0.45
(0,0)	R(34)	24972.51	-0.08	*	(1,1)	P(30)	24916.62	-0.38
(0,0)	P(36)	24904.66	-0.23	*	(1,1)	P(30)	24917.09	0.39
(0,0)	R(36)	24973.97	-0.04	*	(1,1)	R(30)	24974.47	-0.13
(0,0)	P(38)	24902.56	-0.26	*	(1,1)	R(30)	24975.08	0.48
(0,0)	R(38)	24975.29	-0.10	*	(1,1)	P(32)	24914.67	-0.09
(0,0)	P(40)	24900.50	-0.29	*	(1,1)	P(32)	24915.09	0.33
(0,0)	R(40)	24976.77	0.04	*	(1,1)	R(32)	24976.01	-0.20
(0,0)	P(42)	24898.57	-0.15	*	(1,1)	R(32)	24976.56	0.35
(0,0)	R(42)	24978.23	0.20	*	(1,1)	P(34)	24912.85	-0.17
(0,0)	P(44)	24896.37	-0.10	*	(1,1)	P(34)	24913.03	0.21
(0,0)	R(44)	24979.43	0.14	*	(1,1)	R(34)	24977.55	-0.23
(0,0)	P(46)	24894.02	-0.01	*	(1,1)	R(34)	24978.15	0.37
(0,0)	R(46)	24980.03	0.17	*	(1,1)	P(36)	24910.81	-0.06
(0,0)	P(48)	24891.32	-0.10	*	(1,1)	P(36)	24911.12	0.23
(0,0)	R(48)	24981.99	0.26	*	(1,1)	R(36)	24979.03	-0.28
(0,0)	P(50)	24888.93	-0.03	*	(1,1)	R(36)	24979.61	0.30
(0,0)	R(50)	24982.34	0.42	*	(1,1)	P(38)	24906.97	-0.26
(0,0)	P(52)	24886.72	-0.01	*	(1,1)	P(38)	24907.14	0.19
(0,0)	R(52)	24983.49	0.34	*	(1,1)	R(38)	24980.48	-0.22
(0,0)	P(54)	24884.39	0.03	*	(1,1)	R(38)	24981.09	0.39
(0,0)	R(54)	24983.36	0.20	*	(1,1)	P(40)	24903.79	-0.24
(0,0)	P(56)	24882.04	-0.14	*	(1,1)	P(40)	24903.14	0.11
(0,0)	R(56)	24980.83	0.21	*	(1,1)	R(40)	24981.96	-0.29

7s s1jaa

BAND	ROT LINE	OBS FREQ (CM-1)	DEV	*	BAND	ROT LINE	OBS FREQ (CM-1)	DEV
(1,1)	R(40)	24982.58	0.33	*	(1,1)	R(54)	24991.49	-0.22
(1,1)	P(42)	24904.99	-0.12	*	(2,2)	R(20)	24970.20	0.34
(1,1)	P(42)	24905.30	0.19	*	(2,2)	R(22)	24971.68	-0.04
(1,1)	R(42)	24983.27	-0.39	*	(2,2)	R(22)	24971.27	-0.45
(1,1)	R(42)	24983.93	0.27	*	(2,2)	R(24)	24973.oo	0.11
(1,1)	P(44)	24903.30	0.09	*	(2,2)	R(24)	24973.15	-0.40
(1,1)	R(44)	24984.66	-0.37	*	(2,2)	R(26)	24975.47	0.11
(1,1)	R(44)	24985.28	0.25	*	(2,2)	R(26)	24974.97	-0.39
(1,1)	P(46)	24901.47	0.14	*	(2,2)	R(28)	24977.26	0.13
(1,1)	R(46)	24986.07	-0.31	*	(2,2)	R(28)	24976.76	-0.37
(1,1)	R(46)	24986.59	0.21	*	(2,2)	R(30)	24979.07	0.20
(1,1)	P(48)	24899.55	0.08	*	(2,2)	R(30)	24978.62	-0.25
(1,1)	R(48)	24987.27	-0.45	*	(2,2)	R(32)	24980.32	0.25
(1,1)	R(48)	24987.64	0.12	*	(2,2)	R(32)	24980.37	-0.20
(1,1)	P(50)	24897.03	-0.03	*	(2,2)	R(34)	24982.59	0.35
(1,1)	R(50)	24988.57	-0.47	*	(2,2)	R(34)	24982.00	-0.24
(1,1)	R(50)	24989.13	0.09	*	(2,2)	R(36)	24984.21	0.35
(1,1)	P(52)	24895.85	-0.05	*	(2,2)	R(36)	24983.oo	-0.20
(1,1)	R(52)	24989.93	-0.44	*	(2,2)	R(38)	24986.02	0.37
(1,1)	R(52)	24990.37	0.0	*	(2,2)	R(38)	24985.o1	0.16

3s sigma

BAND	ROT LINE	OBS FREQ (CM-1)	DEV	*	BAND	ROT LINE	OBS FREQ (CM-1)	DEV
(0,0)	R(6)	25566.17	0.0	*	(1,1)	R(28)	25589.86	0.08
(0,0)	R(8)	25567.99	0.05	*	(1,1)	R(30)	25591.06	0.02
(0,0)	R(10)	25569.61	-0.06	*	(1,1)	P(32)	25531.30	0.10
(0,0)	R(12)	25571.27	-0.06	*	(1,1)	R(32)	25592.23	-0.02
(0,0)	R(14)	25572.95	-0.03	*	(1,1)	P(34)	25528.91	0.05
(0,0)	R(16)	25574.55	-0.01	*	(1,1)	R(34)	25593.42	0.0
(0,0)	R(18)	25576.14	0.05	*	(1,1)	P(36)	25526.44	-0.08
(0,0)	R(20)	25577.57	-0.01	*	(1,1)	R(36)	25594.54	-0.01
(0,0)	R(22)	25579.06	0.04	*	(1,1)	P(38)	25524.23	0.04
(0,0)	R(24)	25580.49	0.07	*	(1,1)	R(38)	25595.61	-0.03
(0,0)	R(26)	25581.81	0.03	*	(1,1)	P(40)	25521.80	-0.07
(0,0)	R(28)	25583.14	0.04	*	(1,1)	R(40)	25596.60	-0.09
(0,0)	R(30)	25584.45	0.08	*	(1,1)	R(42)	25597.63	-0.07
(0,0)	R(32)	25585.67	0.06	*	(1,1)	R(44)	25598.59	-0.07
(0,0)	R(34)	25587.96	-0.01	*	(1,1)	R(46)	25599.69	0.11
(0,0)	R(36)	25589.05	-0.04	*	(1,1)	R(48)	25600.67	0.23
(0,0)	R(40)	25590.17	0.0	*	(2,2)	R(2)	25576.17	-0.02
(0,0)	R(42)	25591.20	-0.02	*	(2,2)	R(4)	25578.09	0.06
(0,0)	R(44)	25592.15	-0.07	*	(2,2)	R(6)	25579.86	0.05
(0,0)	R(46)	25593.07	-0.11	*	(2,2)	R(8)	25581.44	-0.11
(1,1)	R(4)	25571.18	-0.07	*	(2,2)	R(10)	25583.21	-0.03
(1,1)	R(6)	25572.85	-0.20	*	(2,2)	R(12)	25585.06	0.18
(1,1)	R(8)	25574.75	-0.06	*	(2,2)	R(14)	25586.45	-0.02
(1,1)	R(10)	25576.47	-0.05	*	(2,2)	R(16)	25588.18	0.16
(1,1)	R(12)	25578.13	-0.05	*	(2,2)	R(18)	25589.61	0.10
(1,1)	R(14)	25579.80	0.01	*	(2,2)	R(20)	25591.08	0.11
(1,1)	R(16)	25581.33	-0.02	*	(2,2)	P(22)	25549.92	-0.01
(1,1)	R(18)	25582.89	0.02	*	(2,2)	R(22)	25592.28	-0.09
(1,1)	P(20)	25545.13	-0.01	*	(2,2)	P(24)	25547.64	0.0
(1,1)	R(20)	25584.37	0.03	*	(2,2)	R(24)	25593.63	-0.10
(1,1)	P(22)	25542.90	0.05	*	(2,2)	R(26)	25594.95	-0.10
(1,1)	R(22)	25585.82	0.05	*	(2,2)	R(28)	25596.30	-0.02
(1,1)	P(24)	25540.55	0.01	*	(2,2)	R(30)	25597.50	-0.04
(1,1)	R(24)	25587.15	0.0	*	(2,2)	R(32)	25598.70	-0.03
(1,1)	P(26)	25538.30	0.09	*	(2,2)	R(34)	25599.72	-0.15
(1,1)	R(26)	25588.51	0.02	*	(2,2)	R(36)	25601.02	0.05
(1,1)	P(28)	25536.85	-0.03	*				

9s sigma

BAND	ROT LINE	OBS FREQ (CM-1)	DEV	*	BAND	ROT LINE	OBS FREQ (CM-1)	DEV
				*				
(0,0)	R(6)	25987.23	-0.15	*	(1,1)	P(24)	25959.49	0.14
(0,0)	R(10)	25988.95	-0.11	*	(1,1)	R(24)	26005.83	0.07
(0,0)	R(12)	25990.66	0.02	*	(1,1)	P(26)	25956.74	-0.09
(0,0)	P(14)	25964.37	0.27	*	(1,1)	R(26)	26006.92	0.03
(0,0)	R(14)	25992.17	-0.02	*	(1,1)	P(28)	25954.34	0.06
(0,0)	P(16)	25961.84	0.10	*	(1,1)	R(28)	26007.87	-0.08
(0,0)	R(16)	25993.07	0.03	*	(1,1)	P(30)	25951.85	0.14
(0,0)	P(18)	25959.37	0.04	*	(1,1)	R(30)	26008.95	-0.03
(0,0)	R(18)	25994.95	-0.05	*	(1,1)	P(32)	25948.93	-0.22
(0,0)	P(20)	25956.89	0.04	*	(1,1)	P(34)	25946.30	-0.30
(0,0)	R(20)	25996.26	-0.02	*	(1,1)	R(34)	26010.63	-0.35
(0,0)	P(22)	25954.30	-0.02	*	(1,1)	P(36)	25943.92	-0.16
(0,0)	R(22)	25997.42	-0.05	*	(1,1)	P(38)	25941.74	0.11
(0,0)	R(24)	25998.56	-0.03	*	(1,1)	P(40)	25939.49	0.24
(0,0)	R(26)	25999.49	-0.14	*	(1,1)	P(44)	25935.24	0.47
(0,0)	R(28)	26000.51	-0.10	*	(1,1)	P(46)	25933.14	0.45
(0,0)	R(30)	26001.59	0.05	*	(1,1)	P(48)	25930.82	0.14
(0,0)	R(32)	26002.44	-0.01	*	(1,1)	P(50)	25928.79	0.06
(0,1)	R(12)	25739.24	0.04	*	(1,1)	P(52)	25926.46	-0.30
(0,1)	R(14)	25740.97	-0.05	*	(1,1)	P(54)	25924.25	-0.43
(0,1)	R(16)	25742.85	0.05	*	(1,1)	P(56)	25922.14	-0.21
(0,1)	R(18)	25744.57	0.03	*	(1,1)	P(58)	25919.93	0.36
(0,1)	R(20)	25746.26	0.02	*	(1,2)	R(8)	25744.98	-0.40
(0,1)	R(22)	25747.87	-0.02	*	(1,2)	R(10)	25747.06	-0.21
(0,1)	R(24)	25749.54	0.03	*	(1,2)	R(12)	25749.03	-0.14
(0,1)	R(26)	25751.11	0.01	*	(1,2)	R(14)	25751.00	-0.03
(0,1)	R(28)	25752.76	0.09	*	(1,2)	R(16)	25752.85	0.0
(0,1)	R(30)	25754.19	-0.05	*	(1,2)	R(18)	25754.63	-0.01
(1,1)	R(6)	25991.94	-0.47	*	(1,2)	R(20)	25756.36	-0.04
(1,1)	R(8)	25993.99	-0.18	*	(1,2)	R(22)	25757.99	-0.13
(1,1)	R(10)	25996.04	0.17	*	(1,2)	R(24)	25759.59	-0.21
(1,1)	R(12)	25997.68	0.17	*	(1,2)	R(26)	25761.24	-0.23
(1,1)	R(14)	25999.41	0.34	*	(1,2)	R(28)	25762.74	-0.38
(1,1)	R(16)	26000.93	0.36	*	(2,2)	R(18)	26009.31	0.21
(1,1)	P(18)	25960.92	0.29	*	(2,2)	P(20)	25971.70	-0.39
(1,1)	R(18)	26002.33	0.35	*	(2,2)	P(22)	25969.60	0.14
(1,1)	P(20)	25964.47	0.22	*	(2,2)	R(22)	26011.86	0.04
(1,1)	R(20)	26003.63	0.31	*	(2,2)	P(24)	25967.34	-0.05
(1,1)	R(22)	26004.89	0.11	*	(2,2)	R(26)	26014.01	-0.26

10s sigma

BAND	ROT LINE	OBS FREQ (CM-1)	DEV	*	BAND	ROT LINE	OBS FREQ (CM-1)	DEV
				*				
(0,0)	R(8)	26282.15	-0.03	*	(1,1)	P(18)	26259.36	-0.01
(0,0)	R(10)	26283.47	-0.01	*	(1,1)	P(20)	26256.36	-0.05
(0,0)	R(12)	26284.68	0.02	*	(1,1)	R(20)	26294.85	-0.07
(0,0)	R(14)	26285.81	0.05	*	(1,1)	P(22)	26253.53	0.11
(0,0)	R(16)	26286.75	-0.03	*	(1,1)	R(24)	26296.35	-0.07
(1,1)	R(10)	26290.36	0.04	*	(1,1)	P(26)	26247.55	0.06
(1,1)	R(12)	26291.33	-0.06	*	(2,2)	P(22)	26259.99	-0.03
(1,1)	R(14)	26292.47	0.07	*	(2,2)	R(22)	26301.69	0.03
(1,1)	R(16)	26293.23	-0.02	*				

4d pi

BAND	ROT LINE	OBS FREQ (CM-1)	DEV	*	BAND	ROT LINE	OBS FREQ (CM-1)	DEV
(0,0)	R(6)	21277.68	0.08	*	(0,1)	P(30)	20981.90	-0.07
(0,0)	R(8)	21276.96	0.08	*	(0,1)	P(32)	20977.93	0.04
(0,0)	R(10)	21276.06	0.09	*	(0,1)	P(34)	20973.69	0.04
(0,0)	P(12)	21264.35	0.32	*	(1,0)	Q(3)	21501.04	0.05
(0,0)	R(12)	21274.89	0.02	*	(1,0)	R(10)	21499.31	0.01
(0,0)	P(14)	21260.75	0.13	*	(1,0)	Q(12)	21498.41	0.05
(0,0)	R(14)	21273.70	0.13	*	(1,0)	R(14)	21496.61	-0.06
(0,0)	P(16)	21257.46	0.12	*	(1,0)	P(16)	21490.20	-0.01
(0,0)	R(16)	21272.15	0.08	*	(1,0)	R(16)	21494.67	-0.05
(0,0)	P(18)	21253.84	-0.03	*	(1,0)	P(18)	21475.20	-0.06
(0,0)	P(20)	21250.28	0.05	*	(1,0)	R(18)	21492.56	0.05
(0,0)	R(20)	21268.64	0.15	*	(1,0)	P(20)	21472.04	-0.03
(0,0)	P(22)	21246.42	0.02	*	(1,0)	R(20)	21490.29	0.25
(0,0)	R(22)	21266.67	0.17	*	(1,0)	P(22)	21467.65	0.0
(0,0)	P(24)	21242.42	0.02	*	(1,0)	R(22)	21487.38	0.06
(0,0)	R(24)	21264.05	-0.05	*	(1,0)	R(22)	21508.64	-0.07
(0,0)	P(26)	21238.24	0.03	*	(1,0)	P(24)	21462.96	-0.02
(0,0)	R(26)	21261.63	0.03	*	(1,0)	R(24)	21507.46	-0.09
(0,0)	P(28)	21233.84	0.0	*	(1,0)	P(26)	21458.03	-0.04
(0,0)	R(28)	21258.96	0.07	*	(1,0)	R(26)	21481.09	0.01
(0,0)	P(30)	21229.23	0.0	*	(1,0)	R(26)	21506.00	-0.11
(0,0)	R(30)	21256.05	0.09	*	(1,0)	P(28)	21452.90	-0.02
(0,0)	R(30)	21284.62	-0.41	*	(1,0)	R(28)	21477.60	0.05
(0,0)	P(32)	21224.45	-0.08	*	(1,0)	R(28)	21504.27	-0.12
(0,0)	R(32)	21283.28	-0.40	*	(1,0)	P(30)	21447.45	-0.07
(0,0)	P(34)	21219.49	-0.09	*	(1,0)	R(30)	21473.30	0.05
(0,0)	R(34)	21281.72	-0.36	*	(1,0)	P(32)	21441.80	-0.07
(0,0)	P(36)	21214.25	-0.19	*	(1,0)	R(32)	21469.84	0.17
(0,0)	R(36)	21279.67	-0.57	*	(1,0)	P(34)	21435.81	-0.15
(0,0)	P(38)	21208.88	-0.21	*	(1,0)	R(34)	21465.45	0.14
(0,0)	P(40)	21203.31	-0.21	*	(1,0)	P(36)	21429.68	-0.12
(0,0)	P(42)	21197.49	-0.25	*	(1,0)	R(36)	21460.80	0.14
(0,0)	P(44)	21191.61	-0.12	*	(1,0)	R(38)	21453.91	0.20
(0,0)	P(46)	21185.14	-0.35	*	(1,0)	R(40)	21450.79	0.34
(0,1)	R(2)	21029.12	0.11	*	(1,0)	R(42)	21445.23	0.35
(0,1)	R(4)	21030.79	0.14	*	(1,1)	P(3)	21241.86	0.14
(0,1)	R(6)	21032.26	0.12	*	(1,1)	P(10)	21238.87	-0.03
(0,1)	P(10)	21015.08	0.14	*	(1,1)	P(12)	21235.61	-0.12
(0,1)	R(10)	21034.83	0.15	*	(1,1)	P(14)	21232.66	-0.09
(0,1)	P(12)	21013.42	0.16	*	(1,1)	P(16)	21229.43	0.06
(0,1)	P(14)	21009.52	0.07	*	(1,1)	P(20)	21222.11	0.08
(0,1)	P(16)	21006.46	-0.02	*	(1,1)	P(22)	21218.06	-0.01
(0,1)	P(18)	21003.46	0.05	*	(1,1)	P(24)	21213.91	0.0
(0,1)	P(20)	21000.36	0.17	*	(1,1)	P(26)	21209.53	-0.01
(0,1)	P(22)	20996.92	0.09	*	(1,1)	P(28)	21204.90	-0.08
(0,1)	P(24)	20993.32	-0.01	*	(1,1)	P(30)	21200.11	-0.10
(0,1)	P(26)	20989.53	-0.05	*	(1,1)	R(30)	21255.01	-0.06
(0,1)	P(28)	20985.57	-0.23	*	(1,1)	P(32)	21195.29	0.06

BAND	ROT LINE	OBS FREQ (CM-1)	DEV	*	BAND	ROT LINE	OBS FREQ (CM-1)	DEV
(1,1)	R(32)	21253.47	0.04	*	(2,2)	R(32)	21221.72	-0.05
(1,1)	P(34)	21190.34	0.0	*	(2,2)	P(34)	21159.05	-0.03
(1,2)	P(18)	20978.54	0.08	*	(2,2)	R(34)	21219.65	0.09
(1,2)	P(20)	20975.08	-0.03	*	(2,2)	P(36)	21153.46	0.06
(1,2)	P(22)	20971.56	-0.05	*	(2,2)	R(36)	21217.13	0.12
(1,2)	P(24)	20967.89	-0.06	*	(2,2)	P(38)	21147.51	0.03
(1,2)	P(26)	20964.08	-0.05	*	(2,2)	P(40)	21141.43	0.12
(1,2)	P(28)	20960.13	-0.02	*	(2,2)	P(42)	21135.11	0.24
(1,2)	P(30)	20956.04	0.04	*	(2,2)	P(44)	21128.45	0.28
(1,2)	R(30)	21010.91	0.05	*	(2,2)	P(46)	21121.36	0.17
(1,2)	P(32)	20951.68	-0.01	*	(3,1)	P(8)	21676.33	-0.19
(1,2)	Q(32)	20979.65	0.16	*	(3,1)	P(10)	21672.99	-0.23
(1,2)	R(32)	21009.63	-0.05	*	(3,1)	Q(10)	21681.97	-0.12
(1,2)	P(34)	20947.13	-0.07	*	(3,1)	R(10)	21691.78	-0.25
(1,2)	Q(34)	20976.71	0.16	*	(3,1)	P(12)	21669.42	-0.20
(1,2)	R(34)	21008.68	-0.01	*	(3,1)	P(14)	21665.58	-0.12
(1,2)	P(36)	20942.43	-0.11	*	(3,1)	Q(14)	21677.83	-0.19
(1,2)	Q(36)	20973.58	0.19	*	(3,1)	P(16)	21661.43	-0.03
(1,2)	P(38)	20937.69	0.0	*	(3,1)	Q(16)	21675.26	-0.24
(1,2)	Q(38)	20970.30	0.28	*	(3,1)	P(18)	21656.83	-0.09
(1,2)	P(40)	20932.30	0.15	*	(3,1)	P(20)	21652.05	-0.01
(1,2)	Q(40)	20966.31	0.45	*	(3,1)	P(22)	21646.67	-0.22
(2,1)	Q(4)	21470.13	-0.28	*	(3,1)	P(24)	21641.36	-0.04
(2,1)	Q(6)	21466.43	-0.25	*	(3,1)	P(26)	21635.55	-0.05
(2,1)	P(10)	21458.26	-0.14	*	(3,4)	Q(22)	20935.78	-0.04
(2,1)	Q(10)	21467.28	-0.14	*	(3,4)	P(24)	20912.75	-0.05
(2,1)	P(12)	21454.97	-0.13	*	(3,4)	Q(24)	20933.34	-0.11
(2,1)	Q(12)	21465.77	-0.12	*	(3,4)	P(26)	20906.57	-0.05
(2,1)	Q(14)	21463.98	-0.11	*	(3,4)	Q(26)	20930.74	-0.12
(2,1)	P(16)	21447.61	-0.14	*	(3,4)	P(28)	20904.25	0.02
(2,1)	Q(16)	21459.47	-0.20	*	(3,4)	Q(28)	20928.01	-0.03
(2,1)	P(20)	21439.38	0.0	*	(3,4)	R(28)	20954.02	0.0
(2,1)	Q(20)	21457.04	-0.01	*	(3,4)	P(30)	20899.81	0.16
(2,1)	P(22)	21434.80	-0.01	*	(3,4)	Q(30)	20925.05	0.05
(2,1)	Q(22)	21454.22	0.06	*	(3,4)	P(32)	20894.79	-0.07
(2,1)	R(22)	21475.00	-0.22	*	(4,2)	P(20)	21612.94	-0.06
(2,1)	P(24)	21429.93	-0.05	*	(4,2)	P(22)	21607.66	-0.03
(2,1)	R(24)	21473.72	-0.12	*	(4,2)	P(26)	21596.41	0.35
(2,1)	P(26)	21424.87	-0.03	*	(4,2)	P(30)	21583.47	0.40
(2,1)	R(26)	21472.09	-0.07	*	(4,2)	P(32)	21576.17	0.11
(2,1)	P(28)	21419.52	-0.04	*	(4,2)	P(34)	21568.92	0.21
(2,1)	P(30)	21413.90	-0.05	*	(4,2)	P(36)	21561.91	-0.09
(2,1)	P(32)	21408.14	0.07	*	(4,2)	R(26)	21622.42	-0.38
(2,1)	P(34)	21402.00	0.08	*	(4,2)	P(38)	21552.94	0.02
(2,1)	P(36)	21395.50	0.11	*	(4,2)	R(38)	21617.68	0.25
(2,1)	P(38)	21388.95	0.17	*	(4,2)	P(40)	21544.60	0.12
(2,2)	R(30)	21223.60	0.10	*	(4,2)	R(40)	21611.90	-0.04
(2,2)	P(32)	21164.64	0.11	*	(4,2)	P(42)	21535.57	-0.09

4d pi

BAND	ROT LINE	OBS FREQ (CM-1)	DEV	*	BAND	ROT LINE	OBS FREQ (CM-1)	DEV
(4,2)	R(42)	21605.90	-0.10	*	(5,4)	R(30)	21354.35	-0.09
(4,2)	P(44)	21526.40	-0.06	*	(5,4)	P(32)	21296.65	0.06
(4,2)	R(44)	21599.63	0.01	*	(5,4)	P(34)	21289.61	-0.06
(4,4)	R(24)	21161.81	0.0	*	(5,4)	P(36)	21282.50	0.03
(4,4)	P(26)	21114.73	0.24	*	(5,4)	P(38)	21275.02	0.19
(4,4)	Q(26)	21136.35	0.0	*	(6,4)	P(16)	21539.41	0.20
(4,4)	R(26)	21160.30	0.11	*	(6,4)	P(18)	21534.43	0.15
(4,4)	P(28)	21109.42	0.09	*	(6,4)	R(18)	21565.60	0.04
(4,4)	Q(28)	21132.71	-0.01	*	(6,4)	P(20)	21529.30	0.22
(4,4)	R(28)	21156.37	0.09	*	(6,4)	R(20)	21563.79	0.11
(4,4)	P(30)	21104.05	0.15	*	(6,4)	P(22)	21523.68	0.21
(4,4)	Q(30)	21128.70	-0.11	*	(6,4)	R(22)	21561.37	0.15
(4,4)	R(30)	21156.29	0.23	*	(6,4)	P(24)	21517.90	0.41
(4,4)	P(32)	21098.35	0.14	*	(6,4)	R(24)	21558.41	-0.04
(4,4)	Q(32)	21124.36	-0.25	*	(6,4)	Q(26)	21532.19	-0.04
(5,4)	Q(22)	21344.75	0.04	*	(6,4)	R(26)	21555.40	0.12
(5,4)	R(22)	21364.71	-0.04	*	(6,4)	P(28)	21504.58	0.17
(5,4)	Q(24)	21340.88	-0.07	*	(6,4)	Q(28)	21526.96	-0.02
(5,4)	R(24)	21362.79	0.09	*	(6,4)	R(28)	21551.96	0.28
(5,4)	P(26)	21315.47	0.09	*	(6,4)	P(30)	21497.32	0.01
(5,4)	Q(26)	21336.72	-0.14	*	(6,4)	Q(30)	21521.09	-0.24
(5,4)	R(26)	21360.37	0.07	*	(6,4)	R(30)	21547.82	0.15
(5,4)	P(28)	21309.51	0.07	*	(6,4)	P(32)	21489.89	0.07
(5,4)	Q(28)	21332.39	-0.04	*	(6,4)	Q(32)	21514.99	-0.28
(5,4)	R(28)	21357.67	0.12	*	(6,4)	Q(34)	21508.33	-0.46
(5,4)	P(30)	21303.28	0.10	*	(6,4)	Q(36)	21501.16	-0.73
(5,4)	Q(30)	21327.42	-0.22	*	(6,4)	Q(38)	21493.74	-0.81

3d $^1\Pi$

BAND	ROT LINE	OBS FREQ (CM-1)	DEV	*	BAND	ROT LINE	OBS FREQ (CM-1)	DEV
(0,0)	R(2)	23182.64	0.0	*	(1,0)	P(30)	23365.68	0.13
(0,0)	R(4)	23184.37	0.05	*	(1,0)	Q(30)	23391.41	-0.10
(0,0)	R(5)	23185.91	0.04	*	(1,0)	P(32)	23361.37	0.16
(0,0)	R(6)	23187.51	0.23	*	(1,0)	Q(32)	23388.51	0.07
(0,0)	P(14)	23163.09	-0.04	*	(1,0)	P(34)	23356.66	0.16
(0,0)	P(16)	23160.31	0.07	*	(1,0)	Q(34)	23385.14	-0.03
(0,0)	P(18)	23157.41	0.17	*	(1,0)	P(36)	23351.71	0.08
(0,0)	P(22)	23151.01	0.13	*	(1,0)	P(40)	23341.23	-0.15
(0,0)	P(24)	23147.66	0.13	*	(1,0)	P(42)	23336.05	0.06
(0,0)	P(26)	23144.16	0.10	*	(1,1)	R(4)	23166.04	-0.07
(0,0)	P(28)	23140.63	0.15	*	(1,1)	R(6)	23167.58	-0.04
(0,0)	P(30)	23136.87	0.09	*	(1,1)	P(10)	23150.32	-0.13
(0,0)	P(32)	23133.09	0.12	*	(1,1)	R(10)	23170.19	-0.04
(0,0)	P(34)	23129.14	0.10	*	(1,1)	P(12)	23147.89	0.08
(0,0)	P(36)	23125.27	0.28	*	(1,1)	P(14)	23144.96	-0.08
(0,0)	P(38)	23120.92	0.10	*	(1,1)	P(16)	23142.00	-0.14
(0,0)	P(40)	23116.73	0.19	*	(1,1)	P(18)	23139.00	-0.12
(0,0)	P(42)	23112.27	0.15	*	(1,1)	P(20)	23136.02	0.04
(0,1)	R(6)	22935.21	-0.15	*	(1,1)	P(24)	23129.36	0.03
(0,1)	P(10)	22916.64	-0.18	*	(1,1)	P(26)	23125.79	-0.03
(0,1)	R(10)	22936.65	-0.19	*	(1,1)	P(28)	23122.19	0.0
(0,1)	P(12)	22914.03	-0.39	*	(1,1)	P(30)	23118.27	-0.17
(0,1)	R(12)	22938.03	-0.20	*	(1,1)	P(32)	23114.44	-0.13
(0,1)	P(14)	22911.73	-0.22	*	(1,1)	P(34)	23110.53	-0.04
(0,1)	R(16)	22940.59	-0.12	*	(1,1)	P(36)	23106.40	-0.05
(0,1)	P(18)	22906.66	-0.12	*	(1,1)	P(38)	23101.89	-0.31
(0,1)	P(20)	22903.85	-0.23	*	(1,1)	P(44)	23088.41	-0.24
(0,1)	R(20)	22942.64	-0.16	*	(2,1)	P(8)	23383.98	0.39
(0,1)	P(22)	22901.17	-0.13	*	(2,1)	P(10)	23380.91	0.04
(0,1)	P(26)	22895.44	-0.09	*	(2,1)	P(12)	23377.97	-0.01
(0,1)	P(28)	22892.46	-0.08	*	(2,1)	P(14)	23375.14	0.23
(0,1)	P(30)	22889.37	-0.10	*	(2,1)	P(16)	23372.05	0.38
(0,1)	P(32)	22886.19	-0.14	*	(2,1)	P(18)	23368.47	0.22
(1,0)	R(12)	23410.36	0.10	*	(2,1)	P(20)	23364.82	0.16
(1,0)	R(14)	23409.17	0.21	*	(2,1)	P(22)	23361.01	0.10
(1,0)	P(16)	23393.24	0.26	*	(2,1)	P(24)	23356.98	0.0
(1,0)	R(16)	23407.60	0.14	*	(2,1)	P(26)	23353.07	0.18
(1,0)	P(18)	23389.83	0.25	*	(2,1)	P(28)	23348.60	-0.03
(1,0)	R(18)	23405.93	0.17	*	(2,2)	P(30)	23160.34	0.35
(1,0)	R(19)	23422.98	-0.19	*	(2,2)	P(32)	23096.00	-0.05
(1,0)	P(20)	23386.13	0.11	*	(2,2)	P(34)	23091.67	-0.11
(1,0)	R(20)	23403.97	0.10	*	(2,2)	P(36)	23087.63	-0.15
(1,0)	P(22)	23382.01	-0.28	*	(2,2)	P(38)	23083.24	-0.10
(1,0)	R(22)	23402.09	0.30	*	(2,2)	P(40)	23078.98	0.01
(1,0)	R(24)	23399.59	0.08	*	(2,2)	P(42)	23074.34	0.0
(1,0)	P(26)	23374.53	0.18	*	(2,2)	P(44)	23069.19	-0.38
(1,0)	P(28)	23370.24	0.11	*	(2,2)	P(46)	23064.56	-0.09
(1,0)	R(28)	23394.29	-0.08	*	(2,2)	P(48)	23059.44	-0.12

3d pi

BAND	ROT LINE	OBS FREQ (CM-1)	DEV	*	BAND	ROT LINE	OBS FREQ (CM-1)	DEV
(3,2)	P(50)	23054.37	0.07	*	(3,4)	Q(30)	22868.32	-0.07
(3,2)	P(26)	23331.48	0.16	*	(3,4)	P(32)	22839.63	-0.32
(3,2)	Q(26)	23353.46	0.06	*	(3,4)	Q(32)	22866.39	-0.08
(3,2)	P(28)	23327.18	0.17	*	(3,4)	P(34)	22836.49	-0.07
(3,2)	Q(28)	23350.53	-0.05	*	(3,4)	Q(34)	22864.23	-0.19
(3,2)	R(28)	23378.19	0.05	*	(4,4)	Q(14)	23102.44	0.03
(3,2)	P(30)	23322.53	0.01	*	(4,4)	R(16)	23101.03	-0.09
(3,2)	Q(30)	23347.38	-0.18	*	(4,4)	Q(18)	23099.67	0.0
(3,2)	R(30)	23377.01	-0.01	*	(4,4)	R(20)	23098.07	0.02
(3,2)	P(32)	23317.92	0.07	*	(4,4)	P(22)	23077.48	-0.07
(3,2)	Q(32)	23344.10	-0.22	*	(4,4)	Q(22)	23096.08	-0.18
(3,2)	R(32)	23375.56	-0.13	*	(4,4)	P(24)	23073.94	-0.10
(3,2)	P(34)	23313.10	0.09	*	(4,4)	Q(24)	23094.13	-0.16
(3,2)	Q(34)	23340.79	-0.08	*	(4,4)	P(26)	23070.34	-0.05
(3,2)	R(34)	23373.91	-0.22	*	(4,4)	Q(26)	23092.06	-0.09
(3,2)	P(36)	23307.99	0.01	*	(4,4)	P(28)	23066.56	-0.04
(3,2)	Q(36)	23337.11	-0.08	*	(4,4)	Q(28)	23089.79	-0.05
(3,2)	R(36)	23372.80	0.26	*	(4,4)	P(30)	23062.58	-0.09
(3,2)	P(38)	23303.16	0.39	*	(4,4)	Q(30)	23087.29	-0.06
(3,2)	Q(38)	23333.32	0.03	*	(4,4)	P(32)	23058.84	0.25
(3,2)	P(40)	23297.46	0.09	*	(4,4)	Q(32)	23084.46	-0.22
(3,2)	Q(40)	23329.10	-0.06	*	(4,4)	P(34)	23054.41	0.04
(3,2)	P(42)	23291.89	0.11	*	(4,4)	P(36)	23050.07	0.08
(3,2)	Q(42)	23325.16	0.36	*	(4,4)	Q(36)	23073.94	0.17
(3,4)	P(22)	22853.74	-0.05	*	(4,4)	P(38)	23045.48	0.02
(3,4)	Q(22)	22874.03	-0.13	*	(4,4)	Q(38)	23076.15	0.62
(3,4)	P(24)	22852.84	-0.18	*	(4,4)	P(40)	23040.49	-0.29
(3,4)	Q(24)	22873.23	-0.13	*	(5,4)	P(20)	23299.90	-0.05
(3,4)	P(26)	22849.62	-0.14	*	(5,4)	P(22)	23296.04	-0.05
(3,4)	Q(26)	22871.80	-0.23	*	(5,4)	P(24)	23291.98	-0.06
(3,4)	P(28)	22846.56	-0.10	*	(5,4)	P(26)	23287.87	0.06
(3,4)	Q(28)	22869.99	-0.19	*	(5,4)	P(28)	23283.50	0.12
(3,4)	P(30)	22843.26	-0.09	*	(5,4)	P(30)	23279.15	0.32

oc pi

BAND	ROT LINE	OBS FREQ (CM-1)	DEV	*	BAND	ROT LINE	OBS FREQ (CM-1)	DEV
(0,0)	R(2)	24391.69	-0.17	*	(1,1)	P(22)	24356.73	0.06
(0,0)	R(4)	24393.45	-0.19	*	(1,1)	R(22)	24398.98	-0.12
(0,0)	R(6)	24395.23	-0.09	*	(1,1)	P(24)	24353.90	0.03
(0,0)	P(8)	24380.50	0.0	*	(1,1)	P(26)	24350.98	-0.04
(0,0)	R(8)	24396.84	-0.06	*	(1,1)	P(28)	24348.05	-0.06
(0,0)	P(10)	24378.11	-0.05	*	(1,1)	P(32)	24342.12	-0.05
(0,0)	R(10)	24396.37	-0.03	*	(1,1)	P(34)	24339.09	-0.05
(0,0)	P(12)	24375.60	-0.07	*	(1,1)	P(36)	24336.07	0.0
(0,0)	R(12)	24399.77	-0.02	*	(2,2)	P(20)	24353.49	-0.03
(0,0)	P(14)	24373.14	-0.09	*	(2,2)	P(24)	24347.92	-0.11
(0,0)	P(16)	24370.66	0.01	*	(2,2)	P(26)	24345.04	-0.17
(0,0)	P(18)	24367.96	-0.05	*	(2,2)	P(28)	24342.23	-0.10
(0,0)	R(18)	24403.44	0.0	*	(2,2)	Q(28)	24368.46	0.23
(0,0)	P(20)	24365.36	0.06	*	(2,2)	P(30)	24339.26	-0.14
(0,0)	P(22)	24362.57	0.04	*	(2,2)	Q(30)	24367.24	0.18
(0,0)	P(24)	24359.73	0.03	*	(2,2)	P(32)	24336.27	-0.16
(0,0)	P(26)	24356.80	-0.01	*	(2,2)	Q(32)	24366.00	0.17
(0,0)	P(28)	24353.91	0.03	*	(2,2)	P(34)	24333.30	-0.12
(0,0)	P(30)	24350.98	0.08	*	(2,2)	Q(34)	24364.62	0.08
(0,0)	P(32)	24347.95	0.07	*	(2,2)	P(36)	24330.27	-0.10
(0,0)	P(34)	24344.94	0.12	*	(2,2)	Q(36)	24363.24	0.05
(0,0)	P(36)	24341.75	0.02	*	(2,2)	R(36)	24396.78	-0.07
(0,0)	P(38)	24338.65	0.04	*	(2,2)	P(38)	24327.25	-0.03
(0,0)	P(40)	24335.48	0.02	*	(2,2)	Q(38)	24361.72	-0.07
(0,0)	P(42)	24332.21	-0.08	*	(2,2)	P(40)	24324.19	0.03
(0,0)	P(44)	24329.09	-0.01	*	(2,2)	Q(40)	24360.27	-0.04
(0,0)	P(46)	24325.85	-0.03	*	(2,2)	P(42)	24321.11	0.10
(1,0)	P(18)	24612.00	0.10	*	(2,2)	Q(42)	24358.70	-0.09
(1,0)	P(20)	24609.62	0.16	*	(2,2)	P(44)	24317.89	0.06
(1,0)	P(22)	24606.30	0.05	*	(3,2)	Q(24)	24607.23	0.13
(1,0)	P(24)	24603.16	0.21	*	(3,2)	Q(26)	24605.59	0.06
(1,0)	P(26)	24599.50	-0.04	*	(3,2)	Q(28)	24603.92	0.07
(1,0)	P(28)	24596.05	0.0	*	(3,2)	P(30)	24574.37	-0.34
(1,0)	P(30)	24592.52	0.05	*	(3,2)	Q(30)	24602.07	0.01
(1,1)	R(2)	24385.85	0.17	*	(3,2)	P(32)	24570.73	-0.37
(1,1)	R(4)	24387.50	0.00	*	(3,2)	Q(32)	24600.56	-0.10
(1,1)	R(6)	24389.18	0.08	*	(3,2)	P(34)	24567.01	-0.39
(1,1)	P(8)	24374.54	0.09	*	(3,2)	Q(34)	24598.21	0.05
(1,1)	R(8)	24390.74	0.07	*	(3,2)	P(36)	24563.71	0.09
(1,1)	P(10)	24372.19	0.06	*	(3,2)	R(36)	24596.10	0.04
(1,1)	R(10)	24392.10	-0.05	*	(3,2)	P(38)	24559.34	0.06
(1,1)	P(12)	24369.70	-0.03	*	(3,2)	R(38)	24593.94	0.06
(1,1)	R(12)	24393.65	0.12	*	(3,2)	P(40)	24556.05	0.22
(1,1)	P(14)	24367.21	0.05	*	(3,2)	Q(40)	24591.41	-0.15
(1,1)	P(16)	24364.73	0.02	*	(4,4)	P(24)	24346.23	-0.01
(1,1)	R(16)	24390.03	0.0	*	(4,4)	P(26)	24343.19	-0.27
(1,1)	P(18)	24362.12	0.02	*	(4,4)	P(28)	24340.55	-0.06
(1,1)	P(20)	24359.42	0.0	*	(4,4)	R(26)	24362.12	0.02

od pi

BAND	ROT LINE	OBS FREQ (CM-1)	DEV	*	BAND	ROT LINE	OBS FREQ (CM-1)	DEV
				*				
(4,4)	P(30)	24327.81	0.09	*	(4,4)	P(34)	24322.11	0.31
(4,4)	P(32)	24325.02	0.24	*				

7d pi-

BAND	ROT LINE	OBS FREQ (CM-1)	DEV	*	BAND	ROT LINE	OBS FREQ (CM-1)	DEV
(0,0)	Q(4)	25179.72	-0.17	*	(1,1)	Q(40)	25170.59	-0.05
(0,0)	Q(18)	25178.19	0.17	*	(2,2)	Q(8)	25178.81	-0.01
(1,1)	Q(10)	25178.73	0.14	*	(2,2)	Q(20)	25176.83	-0.02
(1,1)	Q(22)	25176.28	-0.09	*	(2,2)	Q(46)	25168.05	0.03

8d pi-

BAND	ROT LINE	OBS FREQ (CM-1)	DEV	*	BAND	ROT LINE	OBS FREQ (CM-1)	DEV
(0,0)	Q(4)	25711.37	-0.05	*	(1,1)	Q(40)	25712.44	-0.05
(0,0)	Q(18)	25710.85	0.05	*	(2,2)	Q(8)	25716.75	0.09
(1,1)	Q(10)	25713.63	-0.07	*	(2,2)	Q(20)	25716.38	-0.11
(1,1)	Q(22)	25713.38	0.12	*	(2,2)	Q(46)	25716.35	0.03

9d pi-

BAND	ROT LINE	OBS FREQ (CM-1)	DEV	*	BAND	ROT LINE	OBS FREQ (CM-1)	DEV
(0,0)	Q(4)	26081.33	0.0	*	(1,1)	Q(40)	26082.83	0.0
(0,0)	Q(18)	26080.87	0.0	*	(2,2)	Q(8)	26085.05	0.0
(1,1)	Q(10)	26082.03	0.0	*	(2,2)	Q(20)	26085.57	0.0
(1,1)	Q(22)	26082.08	0.0	*				

10d pi-

BAND	ROT LINE	OBS FREQ (CM-1)	DEV	*	BAND	ROT LINE	OBS FREQ (CM-1)	DEV
(0,0)	Q(4)	26350.95	-0.10	*	(1,1)	Q(22)	26356.81	-0.16
(0,0)	Q(18)	26350.49	0.10	*	(2,2)	Q(8)	26365.48	-0.09
(1,1)	Q(10)	26358.57	0.16	*	(2,2)	Q(20)	26363.79	0.09

11d pi-

BAND	ROT LINE	OBS FREQ (CM-1)	DEV	*	BAND	ROT LINE	OBS FREQ (CM-1)	DEV
(0,0)	Q(4)	26543.06	-0.03	*	(1,1)	Q(22)	26548.10	-0.05
(0,0)	Q(18)	26543.08	0.03	*	(2,2)	Q(8)	26552.58	-0.03
(1,1)	Q(10)	26547.64	0.05	*	(2,2)	Q(20)	26553.64	0.03

7d pi+

BAND	ROT LINE	OBS FREQ (CM-1)	DEV	*	BAND	ROT LINE	OBS FREQ (CM-1)	DEV
(0,0)	R(4)	25183.99	0.24	*	(1,1)	P(20)	25152.28	-0.13
(0,0)	R(6)	25185.18	0.06	*	(1,1)	R(20)	25190.74	0.0
(0,0)	P(8)	25170.56	0.26	*	(1,1)	P(22)	25149.20	-0.04
(0,0)	R(8)	25186.43	0.12	*	(1,1)	P(24)	25146.10	0.02
(0,0)	P(10)	25167.59	0.03	*	(1,1)	P(26)	25142.95	0.0
(0,0)	R(10)	25187.34	-0.01	*	(1,1)	R(26)	25192.56	0.09
(0,0)	P(12)	25164.63	-0.06	*	(1,1)	P(28)	25139.95	0.08
(0,0)	P(14)	25161.58	-0.11	*	(1,1)	R(28)	25193.06	-0.02
(0,0)	P(16)	25158.45	-0.15	*	(1,1)	P(30)	25136.94	0.10
(0,0)	P(18)	25155.34	-0.10	*	(1,1)	R(30)	25193.74	0.02
(0,0)	P(20)	25152.08	-0.15	*	(1,1)	P(32)	25133.96	0.08
(0,0)	P(22)	25148.93	-0.08	*	(1,1)	R(32)	25194.42	0.02
(0,0)	P(24)	25145.75	-0.03	*	(1,1)	P(34)	25131.06	0.05
(0,0)	P(26)	25142.56	-0.03	*	(1,1)	R(34)	25195.13	0.02
(0,0)	P(28)	25139.48	0.05	*	(1,1)	P(36)	25128.29	0.08
(0,0)	P(30)	25136.40	0.06	*	(1,1)	R(36)	25195.79	-0.06
(0,0)	P(32)	25133.40	0.09	*	(1,1)	P(38)	25125.42	-0.07
(0,0)	P(34)	25130.39	0.03	*	(1,1)	P(40)	25122.79	-0.05
(0,0)	P(36)	25127.53	0.04	*	(1,1)	P(42)	25120.20	-0.06
(0,0)	P(38)	25124.64	-0.05	*	(1,1)	P(44)	25117.72	-0.02
(0,0)	P(40)	25121.90	-0.07	*	(1,1)	P(46)	25115.20	-0.08
(0,0)	P(42)	25119.17	-0.15	*	(1,1)	P(48)	25112.91	0.03
(0,0)	P(44)	25116.68	-0.04	*	(1,1)	P(50)	25110.64	0.08
(0,0)	P(46)	25114.09	-0.10	*	(1,1)	P(52)	25108.56	0.21
(0,0)	P(48)	25111.70	-0.02	*	(2,2)	R(2)	25191.93	0.12
(0,0)	R(48)	25200.34	-0.07	*	(2,2)	P(4)	25175.15	0.11
(0,0)	P(50)	25109.43	0.09	*	(2,2)	R(4)	25183.40	0.07
(0,0)	R(50)	25201.06	-0.20	*	(2,2)	P(6)	25172.69	-0.01
(0,0)	P(52)	25107.17	0.11	*	(2,2)	P(8)	25170.12	-0.07
(0,0)	R(52)	25202.23	0.02	*	(2,2)	R(10)	25186.74	-0.16
(0,0)	P(54)	25105.08	0.13	*	(2,2)	P(12)	25164.65	-0.09
(0,0)	R(54)	25203.50	0.16	*	(2,2)	R(12)	25187.76	-0.06
(0,0)	P(56)	25103.06	-0.02	*	(2,2)	P(14)	25161.74	-0.09
(0,0)	R(56)	25204.97	0.21	*	(2,2)	R(14)	25188.41	-0.21
(0,0)	R(58)	25206.39	-0.26	*	(2,2)	P(16)	25158.69	-0.15
(1,1)	R(2)	25182.18	0.23	*	(2,2)	R(16)	25189.23	-0.11
(1,1)	R(4)	25183.63	0.15	*	(2,2)	P(18)	25155.72	-0.06
(1,1)	R(6)	25185.06	0.22	*	(2,2)	P(20)	25152.68	-0.01
(1,1)	P(8)	25170.43	0.25	*	(2,2)	P(22)	25149.60	0.02
(1,1)	R(8)	25185.96	-0.07	*	(2,2)	P(24)	25146.58	0.10
(1,1)	P(10)	25167.52	0.03	*	(2,2)	P(26)	25143.60	0.19
(1,1)	R(10)	25186.97	-0.10	*	(2,2)	P(28)	25140.59	0.20
(1,1)	P(12)	25164.55	-0.10	*	(2,2)	P(30)	25137.65	0.22
(1,1)	R(12)	25187.76	-0.22	*	(2,2)	R(30)	25193.76	0.05
(1,1)	P(14)	25161.51	-0.19	*	(2,2)	P(32)	25134.78	0.24
(1,1)	R(14)	25188.57	-0.21	*	(2,2)	P(34)	25131.93	0.20
(1,1)	P(16)	25158.50	-0.16	*	(2,2)	P(36)	25129.15	0.15
(1,1)	P(18)	25155.37	-0.19	*	(2,2)	P(38)	25126.35	0.0

7d pi+

BAND	ROT LINE	OBS FREQ (CM-1)	DEV	*	BAND	ROT LINE	OBS FREQ (CM-1)	DEV
(2,2)	P(40)	25123.63	-0.14	*	(2,2)	P(46)	25116.30	-0.11
(2,2)	P(42)	25121.24	-0.02	*	(2,2)	P(48)	25114.04	-0.04
(2,2)	P(44)	25118.61	-0.20	*	(2,2)	P(50)	25111.70	-0.13

8d pi+

BAND	ROT LINE	OBS FREQ (CM-1)	DEV	*	BAND	ROT LINE	OBS FREQ (CM-1)	DEV
(0,0)	P(4)	25707.11	0.04	*	(1,1)	P(40)	25660.23	0.03
(0,0)	P(6)	25704.66	0.10	*	(1,1)	R(40)	25735.18	-0.21
(0,0)	P(8)	25701.63	-0.21	*	(1,1)	P(42)	25658.15	-0.11
(0,0)	P(22)	25679.37	-0.33	*	(1,1)	R(42)	25737.01	0.18
(0,0)	P(24)	25676.46	-0.09	*	(1,1)	P(44)	25656.35	-0.03
(0,0)	P(26)	25673.56	0.06	*	(2,2)	R(2)	25719.37	0.25
(0,0)	P(28)	25670.76	0.18	*	(2,2)	R(4)	25720.58	0.02
(0,0)	P(30)	25668.00	0.20	*	(2,2)	P(6)	25709.89	-0.04
(0,0)	P(32)	25665.30	0.15	*	(2,2)	R(6)	25721.65	-0.14
(0,0)	R(32)	25726.79	0.04	*	(2,2)	P(8)	25707.21	-0.09
(0,0)	P(34)	25662.79	0.14	*	(2,2)	R(8)	25722.64	-0.21
(0,0)	R(34)	25727.92	0.01	*	(2,2)	P(10)	25704.41	-0.11
(0,0)	P(36)	25660.25	-0.02	*	(2,2)	P(12)	25701.58	-0.01
(0,0)	R(36)	25729.13	-0.02	*	(2,2)	R(12)	25724.73	0.18
(0,0)	P(38)	25657.94	-0.06	*	(2,2)	P(14)	25698.85	0.28
(0,0)	R(38)	25730.39	-0.03	*	(2,2)	R(14)	25725.78	0.51
(0,0)	P(40)	25655.79	-0.03	*	(2,2)	P(16)	25696.06	0.58
(0,0)	P(42)	25653.71	0.0	*	(2,2)	R(20)	25726.82	-0.48
(0,0)	R(42)	25732.85	-0.19	*	(2,2)	P(22)	25685.87	-0.40
(0,0)	P(44)	25651.74	0.06	*	(2,2)	P(24)	25683.12	-0.21
(1,1)	P(4)	25709.68	0.07	*	(2,2)	P(26)	25680.45	-0.06
(1,1)	R(4)	25717.87	-0.03	*	(2,2)	R(26)	25729.62	-0.23
(1,1)	P(6)	25707.29	0.15	*	(2,2)	P(28)	25677.98	0.05
(1,1)	R(6)	25718.97	-0.16	*	(2,2)	R(28)	25730.92	0.01
(1,1)	P(8)	25704.50	0.03	*	(2,2)	P(30)	25675.28	-0.02
(1,1)	R(8)	25719.99	-0.18	*	(2,2)	R(30)	25732.06	-0.03
(1,1)	P(10)	25701.58	-0.05	*	(2,2)	P(32)	25672.89	-0.03
(1,1)	P(12)	25698.49	-0.15	*	(2,2)	R(32)	25733.41	0.04
(1,1)	P(14)	25695.60	0.05	*	(2,2)	P(34)	25670.69	0.01
(1,1)	R(20)	25724.39	0.0	*	(2,2)	P(36)	25668.47	-0.12
(1,1)	P(22)	25682.73	-0.17	*	(2,2)	P(38)	25666.29	-0.32
(1,1)	P(24)	25679.84	-0.01	*	(2,2)	P(40)	25664.92	0.19
(1,1)	P(26)	25677.01	0.09	*	(2,2)	R(40)	25739.19	-0.02
(1,1)	P(28)	25674.30	0.18	*	(2,2)	P(42)	25662.94	0.0
(1,1)	R(28)	25727.98	0.28	*	(2,2)	R(42)	25740.83	0.06
(1,1)	P(30)	25671.61	0.15	*	(2,2)	P(44)	25661.30	0.08
(1,1)	P(32)	25669.18	0.23	*	(2,2)	R(44)	25742.56	0.21
(1,1)	P(34)	25666.69	0.10	*	(2,2)	P(46)	25659.64	0.06
(1,1)	P(36)	25664.29	-0.06	*	(2,2)	R(46)	25744.05	0.04
(1,1)	R(36)	25732.50	-0.09	*	(2,2)	P(48)	25658.21	0.14
(1,1)	P(38)	25662.21	-0.02	*	(2,2)	P(50)	25656.57	-0.19
(1,1)	R(38)	25733.71	-0.27	*				

9d pi+

BAND	ROT LINE	OBS FREQ (CM-1)	DEV	*	BAND	ROT LINE	OBS FREQ (CM-1)	DEV
(0,0)	P(16)	26058.65	0.96	*	(1,1)	R(32)	26105.47	0.07
(0,0)	P(18)	26055.61	0.52	*	(1,1)	P(34)	26041.95	-0.06
(0,0)	P(20)	26052.62	0.14	*	(1,1)	R(34)	26106.73	-0.18
(0,0)	P(22)	26049.81	-0.05	*	(1,1)	P(36)	26039.92	-0.09
(0,0)	P(24)	26047.00	-0.26	*	(1,1)	R(36)	26108.29	-0.18
(0,0)	P(26)	26044.35	-0.34	*	(1,1)	P(38)	26038.10	-0.01
(0,0)	R(26)	26094.90	-0.46	*	(1,1)	R(38)	26110.02	-0.05
(0,0)	P(28)	26041.78	-0.39	*	(1,1)	P(40)	26036.36	0.06
(0,0)	R(28)	26096.27	-0.30	*	(1,1)	P(42)	26034.80	0.23
(0,0)	P(30)	26039.40	-0.30	*	(1,1)	P(44)	26033.14	0.22
(0,0)	R(30)	26097.57	-0.24	*	(2,2)	R(4)	26089.59	-0.16
(0,0)	P(32)	26037.11	-0.20	*	(2,2)	P(6)	26078.91	-0.21
(0,0)	R(32)	26098.87	-0.22	*	(2,2)	R(6)	26091.27	-0.17
(0,0)	P(34)	26034.93	-0.06	*	(2,2)	P(8)	26076.76	-0.19
(0,0)	R(34)	26100.33	-0.08	*	(2,2)	R(8)	26092.69	-0.37
(0,0)	P(36)	26032.81	0.05	*	(2,2)	P(10)	26074.20	-0.52
(0,0)	R(36)	26101.89	0.11	*	(2,2)	R(10)	26094.20	-0.41
(0,0)	R(38)	26103.52	0.34	*	(2,2)	P(12)	26072.23	-0.22
(0,0)	R(40)	26105.38	0.78	*	(2,2)	R(12)	26095.97	-0.15
(1,1)	P(4)	26077.42	0.37	*	(2,2)	P(14)	26069.96	-0.17
(1,1)	R(4)	26085.80	0.14	*	(2,2)	R(14)	26097.52	-0.06
(1,1)	P(6)	26075.19	0.29	*	(2,2)	P(16)	26067.79	-0.01
(1,1)	R(6)	26087.38	0.06	*	(2,2)	R(16)	26099.15	0.14
(1,1)	P(8)	26072.87	0.20	*	(2,2)	P(18)	26065.42	-0.03
(1,1)	R(8)	26089.08	0.17	*	(2,2)	R(18)	26100.69	0.27
(1,1)	P(10)	26070.59	0.22	*	(2,2)	P(20)	26063.63	0.51
(1,1)	R(10)	26090.43	0.01	*	(2,2)	R(20)	26102.17	0.34
(1,1)	P(12)	26068.02	0.02	*	(2,2)	P(22)	26061.17	0.37
(1,1)	R(12)	26091.78	-0.08	*	(2,2)	P(24)	26058.97	0.45
(1,1)	P(14)	26065.37	-0.22	*	(2,2)	P(26)	26056.63	0.33
(1,1)	R(14)	26093.13	-0.13	*	(2,2)	R(26)	26106.17	0.01
(1,1)	P(16)	26063.15	0.01	*	(2,2)	P(28)	26054.43	0.29
(1,1)	R(16)	26094.45	-0.15	*	(2,2)	P(30)	26052.57	0.51
(1,1)	P(18)	26060.52	-0.15	*	(2,2)	P(32)	26050.32	0.24
(1,1)	R(18)	26095.81	-0.11	*	(2,2)	P(34)	26048.48	0.28
(1,1)	P(20)	26058.04	-0.16	*	(2,2)	P(36)	26046.42	0.0
(1,1)	P(22)	26055.63	-0.10	*	(2,2)	P(38)	26044.72	-0.03
(1,1)	P(24)	26053.14	-0.16	*	(2,2)	P(40)	26043.00	-0.18
(1,1)	P(26)	26050.70	-0.20	*	(2,2)	P(42)	26041.52	-0.18
(1,1)	P(28)	26048.53	-0.03	*	(2,2)	P(44)	26039.84	-0.47
(1,1)	P(30)	26046.33	0.04	*	(2,2)	P(46)	26038.78	-0.19
(1,1)	R(30)	26103.92	-0.02	*	(2,2)	R(46)	26123.56	-0.02
(1,1)	P(32)	26044.08	-0.03	*				

10d pi+

BAND	ROT LINE	OBS FREQ (CM-1)	DEV	*	BAND	ROT LINE	OBS FREQ (CM-1)	DEV
(0,0)	P(4)	26346.20	1.48	*	(1,1)	P(24)	26320.66	0.29
(0,0)	P(8)	26339.26	0.18	*	(1,1)	P(26)	26318.20	0.20
(0,0)	P(10)	26335.47	-0.44	*	(1,1)	R(26)	26368.76	0.27
(0,0)	P(14)	26328.58	-0.61	*	(1,1)	P(28)	26315.99	0.11
(0,0)	P(16)	26325.22	-0.58	*	(1,1)	P(30)	26313.82	-0.15
(0,0)	P(18)	26322.17	-0.31	*	(1,1)	R(30)	26371.69	-0.29
(0,0)	R(18)	26357.21	-0.24	*	(1,1)	P(32)	26311.90	-0.24
(0,0)	P(20)	26319.25	-0.05	*	(1,1)	P(34)	26310.34	0.11
(0,0)	P(22)	26316.53	0.19	*	(2,2)	P(6)	26354.97	0.13
(0,0)	R(22)	26359.60	0.23	*	(2,2)	P(8)	26352.06	0.10
(0,0)	P(24)	26313.81	0.18	*	(2,2)	R(8)	26366.82	-0.38
(0,0)	P(26)	26311.11	-0.08	*	(2,2)	P(10)	26348.69	-0.18
(0,0)	R(26)	26362.32	0.12	*	(2,2)	P(12)	26345.20	-0.44
(0,0)	P(28)	26309.02	0.02	*	(2,2)	P(16)	26338.94	-0.10
(0,0)	R(28)	26363.79	-0.10	*	(2,2)	P(18)	26335.78	-0.05
(0,0)	P(30)	26306.83	-0.19	*	(2,2)	P(20)	26333.04	0.27
(0,0)	R(30)	26365.56	-0.07	*	(2,2)	R(20)	26371.29	0.33
(0,0)	P(32)	26304.96	-0.16	*	(2,2)	P(22)	26330.37	0.45
(0,0)	R(32)	26367.15	-0.09	*	(2,2)	P(24)	26327.62	0.28
(0,0)	P(34)	26303.01	-0.13	*	(2,2)	R(24)	26373.64	0.22
(0,0)	R(34)	26369.10	0.62	*	(2,2)	P(26)	26325.11	0.08
(1,1)	P(10)	26342.42	0.16	*	(2,2)	R(26)	26375.07	0.07
(1,1)	R(10)	26361.36	-0.04	*	(2,2)	P(28)	26323.06	0.08
(1,1)	P(12)	26338.72	-0.27	*	(2,2)	R(28)	26376.58	-0.17
(1,1)	P(14)	26335.33	-0.31	*	(2,2)	P(30)	26320.97	-0.16
(1,1)	P(18)	26328.95	-0.08	*	(2,2)	R(30)	26378.27	-0.27
(1,1)	P(20)	26325.97	0.05	*	(2,2)	P(32)	26319.12	-0.25
(1,1)	P(22)	26323.20	0.18	*				

11d pi+

BAND	ROT LINE	OBS FREQ (CM-1)	DEV	*	BAND	ROT LINE	OBS FREQ (CM-1)	DEV
(0,0)	P(10)	26530.26	0.50	*	(1,1)	P(14)	26531.31	-0.04
(0,0)	P(12)	26527.41	0.16	*	(1,1)	P(16)	26528.76	-0.10
(0,0)	P(14)	26524.59	-0.10	*	(1,1)	P(18)	26526.24	-0.14
(0,0)	P(16)	26521.78	-0.32	*	(1,1)	P(20)	26523.97	0.01
(0,0)	R(16)	26553.70	-0.13	*	(1,1)	R(20)	26563.16	0.05
(0,0)	P(18)	26519.20	-0.32	*	(1,1)	P(22)	26521.68	0.06
(0,0)	R(18)	26554.95	-0.18	*	(1,1)	R(22)	26564.65	0.01
(0,0)	P(20)	26516.76	-0.22	*	(1,1)	P(24)	26519.48	0.07
(0,0)	R(20)	26556.50	0.02	*	(1,1)	R(24)	26566.32	0.0
(0,0)	P(22)	26514.49	-0.03	*	(1,1)	P(26)	26517.37	-0.01
(0,0)	R(22)	26558.05	0.13	*	(1,1)	R(26)	26568.13	-0.05
(0,0)	P(24)	26512.12	-0.06	*	(1,1)	P(28)	26515.32	-0.25
(0,0)	R(24)	26559.61	0.12	*	(2,2)	P(8)	26544.63	-0.46
(0,0)	P(26)	26510.08	0.07	*	(2,2)	P(10)	26542.74	-0.03
(0,0)	R(26)	26561.50	0.26	*	(2,2)	P(12)	26540.35	-0.06
(0,0)	P(28)	26508.08	0.03	*	(2,2)	P(14)	26537.98	-0.03
(0,0)	R(28)	26563.39	0.16	*	(2,2)	P(16)	26535.60	-0.01
(0,0)	R(30)	26565.39	-0.11	*	(2,2)	P(18)	26533.39	0.15
(1,1)	R(4)	26551.75	0.05	*	(2,2)	P(20)	26531.11	0.19
(1,1)	P(6)	26541.11	0.17	*	(2,2)	R(20)	26569.91	0.17
(1,1)	R(6)	26553.31	0.01	*	(2,2)	P(22)	26528.92	0.22
(1,1)	P(8)	26538.80	0.15	*	(2,2)	P(24)	26526.90	0.28
(1,1)	R(8)	26554.83	0.02	*	(2,2)	R(24)	26573.07	-0.05
(1,1)	P(10)	26536.31	0.04	*	(2,2)	P(26)	26524.69	-0.04
(1,1)	R(10)	26556.22	-0.03	*	(2,2)	R(26)	26574.76	-0.33
(1,1)	P(12)	26533.82	-0.01	*				

12d pi

BAND	ROT LINE	OBS FREQ (CM-1)
(0,0)	Q(18)	26693.44
(1,1)	Q(20)	26700.13
(2,2)	Q(20)	26706.66

13d pi

BAND	ROT LINE	OBS FREQ (CM-1)
(0,0)	Q(18)	26810.99
(1,1)	Q(20)	26818.37
(2,2)	Q(20)	26826.40

14d pi

BAND	ROT LINE	OBS FREQ (CM-1)
(0,0)	Q(18)	26902.65
(1,1)	Q(20)	26909.33
(2,2)	Q(20)	26915.39

15d pi

BAND	ROT LINE	OBS FREQ (CM-1)
(0,0)	Q(18)	26977.12
(1,1)	Q(20)	26984.27
(2,2)	Q(20)	26990.36

Extra pi state (dissociation products undetermined)

BAND	ROT LINE	OBS FREQ (CM-1)	DEV	*	BAND	ROT LINE	OBS FREQ (CM-1)	DEV
(0,0)	P(12)	24772.26	0.16	*	(1,1)	P(32)	24762.98	-0.08
(0,0)	R(12)	24796.90	-0.14	*	(1,1)	R(32)	24825.43	0.07
(0,0)	P(14)	24770.52	0.05	*	(1,1)	P(34)	24761.83	-0.14
(0,0)	R(14)	24799.56	0.20	*	(1,1)	R(34)	24827.95	0.11
(0,0)	P(16)	24768.95	0.04	*	(1,1)	P(36)	24760.83	-0.11
(0,0)	R(16)	24801.83	0.11	*	(1,1)	R(36)	24830.40	0.08
(0,0)	P(18)	24767.39	-0.02	*	(1,1)	P(38)	24760.05	0.09
(0,0)	Q(18)	24785.11	-0.16	*	(1,1)	R(38)	24832.80	0.01
(0,0)	R(18)	24804.22	0.11	*	(1,1)	P(40)	24759.22	0.20
(0,0)	P(20)	24765.87	-0.10	*	(1,1)	Q(40)	24796.92	0.21
(0,0)	R(20)	24806.63	0.08	*	(1,1)	R(40)	24835.36	0.11
(0,0)	R(22)	24809.08	0.07	*	(1,1)	P(42)	24758.30	0.19
(0,0)	R(24)	24811.57	0.05	*	(1,1)	R(42)	24837.81	0.11
(0,0)	R(26)	24813.98	-0.07	*	(1,1)	R(44)	24840.24	0.12
(0,0)	R(28)	24816.72	0.12	*	(1,1)	R(46)	24842.50	0.0
(0,0)	R(30)	24819.13	-0.06	*	(1,1)	R(48)	24844.83	-0.01
(0,0)	R(32)	24821.66	-0.13	*	(1,1)	R(50)	24846.72	-0.39
(0,0)	R(34)	24824.32	-0.08	*	(2,2)	R(12)	24806.02	0.05
(0,0)	R(36)	24826.91	-0.12	*	(2,2)	P(14)	24780.07	0.08
(0,0)	R(38)	24829.58	-0.09	*	(2,2)	R(14)	24808.03	-0.12
(0,0)	R(40)	24832.19	-0.11	*	(2,2)	P(16)	24778.25	-0.12
(0,0)	R(42)	24834.87	-0.05	*	(2,2)	R(16)	24810.52	0.15
(0,0)	R(44)	24837.48	-0.05	*	(2,2)	P(18)	24776.61	-0.20
(0,0)	R(46)	24839.98	-0.14	*	(2,2)	R(18)	24812.66	0.06
(0,0)	R(48)	24842.68	0.01	*	(2,2)	P(20)	24775.24	-0.06
(0,0)	R(50)	24845.19	0.02	*	(2,2)	Q(20)	24794.75	0.14
(0,0)	R(52)	24847.91	0.30	*	(2,2)	R(20)	24814.92	0.06
(1,1)	P(14)	24775.28	-0.03	*	(2,2)	P(22)	24773.75	-0.08
(1,1)	R(14)	24803.78	-0.06	*	(2,2)	R(22)	24817.18	0.04
(1,1)	P(16)	24773.60	-0.12	*	(2,2)	P(24)	24772.37	-0.04
(1,1)	R(16)	24806.16	0.04	*	(2,2)	R(24)	24819.45	0.01
(1,1)	P(18)	24772.09	-0.10	*	(2,2)	P(26)	24771.04	-0.01
(1,1)	P(20)	24770.62	-0.10	*	(2,2)	R(26)	24821.84	0.09
(1,1)	R(20)	24810.80	0.01	*	(2,2)	P(28)	24769.72	-0.01
(1,1)	P(22)	24769.41	0.11	*	(2,2)	R(28)	24824.22	0.14
(1,1)	Q(22)	24790.75	-0.01	*	(2,2)	P(30)	24768.48	0.02
(1,1)	R(22)	24813.14	-0.03	*	(2,2)	R(30)	24826.51	0.10
(1,1)	P(24)	24767.86	-0.07	*	(2,2)	P(32)	24767.17	-0.07
(1,1)	R(24)	24815.53	-0.04	*	(2,2)	R(32)	24828.89	0.15
(1,1)	P(26)	24766.58	-0.05	*	(2,2)	P(34)	24766.01	-0.05
(1,1)	R(26)	24818.05	0.06	*	(2,2)	R(34)	24831.21	0.14
(1,1)	P(28)	24765.32	-0.06	*	(2,2)	P(36)	24764.81	-0.11
(1,1)	R(28)	24820.43	0.0	*	(2,2)	R(36)	24833.35	-0.05
(1,1)	P(30)	24764.10	-0.09	*	(2,2)	R(38)	24835.66	-0.05
(1,1)	R(30)	24822.85	-0.04	*	(2,2)	R(40)	24837.75	-0.24

Observed transitions not used in the final Dunham fits

4d sigma

BAND	ROT LINE	OBS FREQ (CM-1)	DEV	*	BAND	ROT LINE	OBS FREQ (CM-1)	DEV
(3,2)	R(6)	22466.01	0.28	*	(4,2)	P(24)	22635.36	-0.06
(3,2)	P(8)	22451.47	0.23	*	(4,2)	P(26)	22629.64	-0.06
(3,2)	R(8)	22467.24	0.08	*	(4,2)	P(28)	22623.47	-0.10
(3,2)	P(10)	22448.99	0.17	*	(4,2)	P(30)	22616.87	-0.12
(3,2)	R(10)	22468.49	0.05	*	(4,2)	P(32)	22609.73	-0.22
(3,2)	P(12)	22446.37	0.09	*	(4,2)	P(34)	22601.99	-0.41
(3,2)	R(12)	22469.63	0.05	*	(4,4)	P(8)	22180.46	0.01
(3,2)	P(14)	22443.51	-0.09	*	(4,4)	P(10)	22177.95	0.18
(3,2)	R(14)	22470.51	-0.05	*	(4,4)	P(12)	22174.86	-0.03
(3,2)	P(16)	22440.62	-0.15	*	(4,4)	P(14)	22171.82	0.02
(3,2)	P(18)	22437.55	-0.24	*	(4,4)	P(16)	22168.51	0.01
(3,2)	P(20)	22434.37	-0.26	*	(4,4)	P(18)	22164.91	-0.05
(3,2)	P(22)	22431.00	-0.28	*	(4,4)	P(20)	22161.48	0.31
(3,2)	P(24)	22427.46	-0.26	*	(4,4)	P(22)	22157.29	0.17
(3,2)	P(26)	22423.74	-0.19	*	(4,4)	R(22)	22196.72	0.20
(3,2)	P(28)	22419.82	-0.06	*	(4,4)	P(24)	22152.93	0.15
(3,2)	P(30)	22415.76	0.21	*	(4,4)	R(24)	22195.82	0.37
(3,2)	P(32)	22411.32	0.42	*	(4,4)	P(26)	22148.26	0.12
(4,2)	P(8)	22668.56	-0.13	*	(4,4)	R(26)	22194.21	0.19
(4,2)	P(10)	22665.45	-0.16	*	(4,4)	P(28)	22143.26	0.10
(4,2)	P(12)	22662.05	-0.19	*	(4,4)	R(28)	22192.25	0.05
(4,2)	P(14)	22658.42	-0.16	*	(4,4)	P(30)	22137.89	0.07
(4,2)	P(16)	22654.43	-0.18	*	(4,4)	R(30)	22189.98	0.03
(4,2)	P(18)	22650.08	-0.25	*	(4,4)	P(32)	22132.05	-0.05
(4,2)	P(20)	22645.82	0.10	*	(4,4)	R(32)	22187.28	0.05
(4,2)	P(22)	22640.77	0.02	*				

Observed transitions not used in the final Dunham fits

5d sigma

BAND	ROT LINE	OBS FREQ (CM-1)
(3,1)	P(20)	24101.64
(3,1)	P(22)	24097.60
(3,1)	P(24)	24093.43
(3,1)	P(26)	24088.95
(3,2)	P(2)	23880.22
(3,2)	P(4)	23877.94
(3,2)	P(6)	23875.66
(3,2)	P(8)	23873.12
(3,2)	P(10)	23870.36
(3,2)	P(12)	23867.72
(3,2)	P(14)	23864.59
(3,2)	P(16)	23861.38
(3,2)	P(18)	23858.05
(3,2)	P(20)	23854.60
(3,2)	R(20)	23891.87
(3,2)	P(22)	23850.95
(3,2)	P(24)	23847.11
(3,2)	P(26)	23843.26
(3,2)	P(28)	23839.24

Observed Transitions Not Used in the Final Dunham Fits

8d pi

BAND	ROT LINE	OBS FREQ (CM-1)
(0,0)	P(18)	25685.62
(0,0)	P(20)	25682.59
(1,1)	R(16)	25722.47
(1,1)	P(18)	25688.62
(1,1)	P(20)	25685.72
(2,2)	P(20)	25688.67

9d pi

BAND	ROT LINE	OBS FREQ (CM-1)
(0,0)	P(4)	26077.03
(0,0)	R(4)	26084.99
(0,0)	P(6)	26074.04
(0,0)	P(8)	26071.03
(0,0)	R(8)	26086.94
(0,0)	P(10)	26068.01
(0,0)	R(10)	26087.80
(0,0)	R(12)	26088.63
(0,0)	P(14)	26061.78

11d pi

BAND	ROT LINE	OBS FREQ (CM-1)
(0,0)	P(4)	26539.03
(0,0)	P(6)	26536.17
(0,0)	P(8)	26533.30

APPENDIX II. Assigned spectral lines for the $E^1\Sigma_g^+$ state of $^7Li_2$. All of the spectral transitions given in the following list originated from the $A^1\Sigma_u^+$ state, and all were used in the final Dunham fit of the observed $E^1\Sigma_g^+$ state energy levels. The format of this listing is identical to that used in Appendix I.

BAND	ROT LINE	OBS FREQ (CM-1)	DEV	*	BAND	ROT LINE	OBS FREQ (CM-1)	DEV
(0,0)	P(2)	13335.07	0.34	*	(0,0)	R(28)	13368.42	0.17
(0,0)	R(2)	13339.73	0.0	*	(0,0)	P(30)	13311.45	0.07
(0,0)	R(2)	13339.85	0.12	*	(0,0)	P(30)	13311.51	0.13
(0,0)	P(4)	13332.89	0.09	*	(0,0)	R(30)	13370.48	0.06
(0,0)	R(4)	13341.99	0.20	*	(0,0)	R(30)	13370.57	0.15
(0,0)	R(4)	13341.93	0.14	*	(0,0)	P(32)	13310.00	0.08
(0,0)	P(6)	13331.06	0.14	*	(0,0)	P(32)	13310.05	0.13
(0,0)	P(6)	13331.02	0.10	*	(0,0)	R(32)	13372.70	0.14
(0,0)	R(6)	13343.93	0.03	*	(0,0)	R(32)	13372.82	0.26
(0,0)	R(6)	13344.01	0.11	*	(0,0)	P(34)	13308.56	0.10
(0,0)	P(8)	13329.15	0.07	*	(0,0)	P(34)	13308.57	0.11
(0,0)	P(8)	13329.23	0.15	*	(0,0)	R(34)	13374.78	0.12
(0,0)	R(8)	13346.09	0.06	*	(0,0)	R(34)	13374.79	0.15
(0,0)	R(8)	13346.14	0.11	*	(0,0)	P(36)	13307.05	0.06
(0,0)	P(10)	13327.28	0.0	*	(0,0)	P(36)	13307.11	0.12
(0,0)	P(10)	13327.43	0.15	*	(0,0)	R(36)	13376.73	0.07
(0,0)	R(10)	13348.30	0.11	*	(0,0)	R(36)	13376.82	0.16
(0,0)	R(10)	13348.37	0.18	*	(0,0)	P(38)	13305.64	0.13
(0,0)	P(12)	13325.66	0.13	*	(0,0)	R(38)	13378.67	0.07
(0,0)	P(12)	13325.64	0.11	*	(0,0)	R(38)	13378.74	0.14
(0,0)	R(12)	13350.36	-0.03	*	(0,0)	P(40)	13304.06	0.06
(0,0)	R(12)	13350.52	0.13	*	(0,0)	P(42)	13302.57	0.12
(0,0)	P(14)	13323.81	-0.01	*	(0,0)	P(44)	13300.91	0.06
(0,0)	P(14)	13323.92	0.10	*	(0,0)	P(46)	13299.25	0.07
(0,0)	R(14)	13352.70	0.10	*	(0,0)	P(48)	13297.67	0.25
(0,0)	R(14)	13352.74	0.14	*	(0,1)	R(0)	13085.60	0.22
(0,0)	P(16)	13322.25	0.10	*	(0,1)	R(2)	13087.22	-0.23
(0,0)	R(16)	13354.95	0.12	*	(0,1)	R(2)	13087.62	0.17
(0,0)	R(16)	13355.06	0.23	*	(0,1)	P(4)	13080.42	-0.18
(0,0)	P(18)	13320.64	0.12	*	(0,1)	P(4)	13080.64	0.04
(0,0)	R(18)	13357.28	0.21	*	(0,1)	R(4)	13089.39	-0.20
(0,0)	R(18)	13357.18	0.11	*	(0,1)	R(4)	13089.69	0.10
(0,0)	P(20)	13319.01	0.09	*	(0,1)	P(6)	13078.60	-0.23
(0,0)	R(20)	13359.35	0.03	*	(0,1)	P(6)	13078.90	0.07
(0,0)	R(20)	13359.51	0.19	*	(0,1)	R(5)	13090.77	0.08
(0,0)	P(22)	13317.42	0.06	*	(0,1)	P(7)	13077.90	-0.09
(0,0)	P(22)	13317.45	0.09	*	(0,1)	R(6)	13091.63	-0.18
(0,0)	R(22)	13361.63	0.06	*	(0,1)	R(6)	13091.91	0.10
(0,0)	R(22)	13361.74	0.17	*	(0,1)	P(8)	13076.95	-0.21
(0,0)	P(24)	13315.92	0.09	*	(0,1)	P(8)	13077.24	0.08
(0,0)	P(24)	13315.93	0.10	*	(0,1)	R(7)	13092.95	0.0
(0,0)	R(24)	13363.96	0.15	*	(0,1)	P(9)	13076.21	-0.14
(0,0)	R(24)	13364.02	0.21	*	(0,1)	R(8)	13094.03	-0.08
(0,0)	P(26)	13314.39	0.06	*	(0,1)	R(8)	13093.93	-0.18
(0,0)	P(26)	13314.43	0.10	*	(0,1)	R(8)	13094.28	0.17
(0,0)	R(26)	13366.12	0.08	*	(0,1)	P(10)	13075.37	-0.20
(0,0)	R(26)	13366.22	0.18	*	(0,1)	P(10)	13075.36	-0.21
(0,0)	P(28)	13312.94	0.10	*	(0,1)	P(10)	13075.64	0.07
(0,0)	P(28)	13312.97	0.13	*	(0,1)	R(9)	13095.21	-0.07
(0,0)	R(28)	13368.32	0.07	*	(0,1)	P(11)	13074.63	-0.17

BAND	ROT LINE	OBS FREQ (CM-1)	DEV	*	BAND	ROT LINE	OBS FREQ (CM-1)	DEV
(0,1)	R(10)	13096.40	-0.08	*	(0,1)	R(24)	13114.60	-0.14
(0,1)	R(10)	13096.31	-0.17	*	(0,1)	R(24)	13114.91	0.17
(0,1)	R(10)	13096.59	0.11	*	(0,1)	P(26)	13065.59	-0.21
(0,1)	P(12)	13073.90	-0.16	*	(0,1)	P(26)	13065.91	0.11
(0,1)	P(12)	13073.86	-0.20	*	(0,1)	P(27)	13065.20	-0.15
(0,1)	P(12)	13074.20	0.14	*	(0,1)	R(26)	13117.32	-0.19
(0,1)	R(11)	13097.63	-0.06	*	(0,1)	R(26)	13117.64	0.13
(0,1)	P(13)	13073.17	-0.17	*	(0,1)	P(28)	13064.69	-0.22
(0,1)	R(12)	13098.72	-0.20	*	(0,1)	P(28)	13065.07	0.16
(0,1)	R(12)	13099.00	0.08	*	(0,1)	R(28)	13120.13	-0.18
(0,1)	P(14)	13072.42	-0.22	*	(0,1)	P(30)	13063.65	-0.22
(0,1)	P(14)	13072.72	0.08	*	(0,1)	P(31)	13063.54	-0.13
(0,1)	R(13)	13100.05	-0.11	*	(0,1)	R(30)	13122.95	-0.16
(0,1)	P(15)	13071.76	-0.21	*	(0,1)	P(32)	13063.12	-0.16
(0,1)	R(14)	13101.24	-0.18	*	(0,1)	P(32)	13063.10	-0.18
(0,1)	R(14)	13101.56	0.14	*	(0,1)	P(33)	13062.71	-0.19
(0,1)	P(16)	13071.08	-0.23	*	(0,1)	R(32)	13125.73	-0.19
(0,1)	P(16)	13071.11	-0.20	*	(0,1)	P(34)	13062.32	-0.21
(0,1)	P(16)	13071.44	0.13	*	(0,1)	P(34)	13062.33	-0.20
(0,1)	R(15)	13102.65	-0.05	*	(0,1)	R(34)	13128.59	-0.12
(0,1)	P(17)	13070.51	-0.16	*	(0,1)	P(36)	13061.68	-0.14
(0,1)	R(16)	13104.04	0.05	*	(0,1)	R(36)	13131.35	-0.13
(0,1)	R(16)	13103.80	-0.19	*	(0,1)	P(38)	13060.86	-0.26
(0,1)	R(16)	13104.11	0.12	*	(0,1)	R(38)	13134.03	-0.19
(0,1)	P(18)	13069.80	-0.26	*	(0,1)	P(40)	13060.31	-0.13
(0,1)	P(18)	13069.86	-0.20	*	(0,1)	R(40)	13136.89	-0.21
(0,1)	P(18)	13070.14	0.08	*	(0,1)	P(42)	13059.62	-0.14
(0,1)	R(17)	13105.30	0.01	*	(0,1)	P(44)	13058.93	-0.14
(0,1)	P(19)	13069.28	-0.18	*	(1,0)	R(0)	13575.45	-0.17
(0,1)	R(18)	13106.69	0.08	*	(1,0)	P(2)	13572.57	-0.08
(0,1)	R(18)	13106.44	-0.17	*	(1,0)	P(3)	13571.74	0.10
(0,1)	R(18)	13106.72	0.11	*	(1,0)	R(2)	13577.43	-0.11
(0,1)	P(20)	13068.69	-0.19	*	(1,0)	P(4)	13570.54	-0.08
(0,1)	P(20)	13068.68	-0.20	*	(1,0)	R(3)	13578.36	-0.13
(0,1)	P(20)	13068.93	0.05	*	(1,0)	P(5)	13569.71	0.12
(0,1)	R(19)	13107.88	-0.06	*	(1,0)	R(4)	13579.38	-0.04
(0,1)	P(21)	13068.14	-0.18	*	(1,0)	P(6)	13568.39	-0.15
(0,1)	R(20)	13109.14	-0.14	*	(1,0)	R(5)	13580.30	-0.04
(0,1)	R(20)	13109.55	0.27	*	(1,0)	P(7)	13567.56	0.07
(0,1)	P(22)	13067.65	-0.13	*	(1,0)	R(6)	13581.16	-0.06
(0,1)	P(22)	13067.56	-0.20	*	(1,0)	P(8)	13566.31	-0.12
(0,1)	P(22)	13067.87	0.09	*	(1,0)	R(7)	13582.04	-0.09
(0,1)	R(21)	13110.65	0.02	*	(1,0)	P(9)	13565.39	0.04
(0,1)	P(23)	13067.17	-0.09	*	(1,0)	R(8)	13582.92	-0.09
(0,1)	R(22)	13111.63	-0.16	*	(1,0)	P(10)	13564.18	-0.06
(0,1)	R(22)	13112.17	0.18	*	(1,0)	R(9)	13583.76	-0.12
(0,1)	P(24)	13066.55	-0.21	*	(1,0)	P(11)	13563.26	0.09
(0,1)	P(24)	13066.94	0.18	*	(1,0)	R(10)	13584.67	-0.05
(0,1)	R(23)	13113.35	-0.01	*	(1,0)	P(12)	13562.03	-0.03
(0,1)	P(25)	13066.11	-0.16	*	(1,0)	R(11)	13585.44	-0.12

BAND	ROT LINE	OBS FREQ (CM-1)	DEV	*	BAND	ROT LINE	OBS FREQ (CM-1)	DEV
(1,0)	P(13)	13560.99	0.05	*	(1,1)	P(6)	13316.45	-0.01
(1,0)	R(12)	13566.29	-0.08	*	(1,1)	R(5)	13328.21	0.03
(1,0)	P(14)	13559.72	-0.09	*	(1,1)	P(7)	13315.52	0.04
(1,0)	R(13)	13567.08	-0.09	*	(1,1)	R(6)	13329.16	0.0
(1,0)	P(15)	13558.69	0.03	*	(1,1)	R(6)	13329.15	-0.01
(1,0)	R(14)	13567.66	-0.06	*	(1,1)	R(6)	13329.17	0.01
(1,0)	P(16)	13557.40	-0.11	*	(1,1)	P(8)	13314.60	0.10
(1,0)	R(15)	13568.63	-0.09	*	(1,1)	P(8)	13314.51	0.01
(1,0)	P(17)	13556.37	0.03	*	(1,1)	P(8)	13314.47	-0.03
(1,0)	R(16)	13569.37	-0.09	*	(1,1)	R(7)	13330.17	0.05
(1,0)	P(18)	13555.13	-0.02	*	(1,1)	P(9)	13313.55	0.02
(1,0)	R(17)	13570.06	-0.13	*	(1,1)	R(8)	13331.09	0.0
(1,0)	P(19)	13553.97	0.02	*	(1,1)	R(8)	13331.11	0.02
(1,0)	R(18)	13590.65	-0.04	*	(1,1)	P(10)	13312.53	-0.02
(1,0)	P(20)	13552.66	-0.08	*	(1,1)	P(10)	13312.54	-0.01
(1,0)	R(20)	13592.08	-0.15	*	(1,1)	P(10)	13312.63	0.08
(1,0)	P(22)	13550.19	-0.08	*	(1,1)	R(9)	13332.09	0.04
(1,0)	P(23)	13549.01	0.0	*	(1,1)	P(11)	13311.65	0.08
(1,0)	R(22)	13593.46	-0.01	*	(1,1)	R(10)	13333.00	-0.01
(1,0)	P(24)	13547.63	-0.10	*	(1,1)	R(10)	13333.01	0.0
(1,0)	P(25)	13546.43	-0.01	*	(1,1)	R(10)	13333.03	0.02
(1,0)	R(24)	13594.50	-0.10	*	(1,1)	P(12)	13310.61	0.02
(1,0)	P(26)	13545.01	-0.11	*	(1,1)	P(12)	13310.58	-0.01
(1,0)	P(27)	13543.82	0.03	*	(1,1)	R(11)	13334.01	0.05
(1,0)	R(26)	13595.54	-0.08	*	(1,1)	P(13)	13309.65	0.04
(1,0)	P(28)	13542.37	-0.06	*	(1,1)	R(12)	13334.91	0.0
(1,0)	P(29)	13541.06	0.01	*	(1,1)	R(12)	13334.92	0.01
(1,0)	R(28)	13596.47	-0.05	*	(1,1)	R(12)	13334.94	0.03
(1,0)	P(30)	13539.54	-0.10	*	(1,1)	P(14)	13308.63	0.0
(1,0)	P(31)	13538.22	0.0	*	(1,1)	P(14)	13308.62	-0.01
(1,0)	R(30)	13597.09	-0.18	*	(1,1)	P(14)	13308.66	0.03
(1,0)	P(32)	13536.68	-0.08	*	(1,1)	R(13)	13335.69	0.04
(1,0)	P(33)	13535.28	0.0	*	(1,1)	P(15)	13307.70	0.05
(1,0)	R(32)	13597.76	-0.11	*	(1,1)	R(14)	13336.79	0.01
(1,0)	P(34)	13533.67	-0.10	*	(1,1)	R(14)	13336.76	-0.02
(1,0)	R(34)	13598.23	-0.07	*	(1,1)	R(14)	13336.81	0.03
(1,0)	P(36)	13530.57	-0.08	*	(1,1)	P(16)	13306.67	0.0
(1,0)	R(36)	13598.43	-0.12	*	(1,1)	P(16)	13306.68	0.01
(1,0)	P(38)	13527.29	-0.11	*	(1,1)	P(16)	13306.71	0.04
(1,1)	P(2)	13320.38	0.01	*	(1,1)	R(15)	13337.73	0.02
(1,1)	R(2)	13325.32	0.06	*	(1,1)	P(17)	13305.69	0.01
(1,1)	P(4)	13318.44	0.03	*	(1,1)	R(16)	13338.60	-0.02
(1,1)	P(4)	13318.42	0.01	*	(1,1)	R(16)	13338.64	0.02
(1,1)	R(3)	13326.26	0.02	*	(1,1)	R(16)	13338.66	0.04
(1,1)	P(5)	13317.47	0.03	*	(1,1)	P(18)	13304.74	0.05
(1,1)	R(4)	13327.33	0.12	*	(1,1)	P(18)	13304.69	0.0
(1,1)	R(4)	13327.19	-0.02	*	(1,1)	P(18)	13304.69	0.0
(1,1)	R(4)	13327.25	0.04	*	(1,1)	R(17)	13339.55	0.02
(1,1)	P(6)	13316.49	0.03	*	(1,1)	P(19)	13303.74	0.04
(1,1)	P(6)	13316.52	0.06	*	(1,1)	P(19)	13303.74	0.04

BAND	ROT LINE	OBS FREQ (CM-1)	DEV	*	BAND	ROT LINE	OBS FREQ (CM-1)	DEV
(1,1)	R(18)	13340.47	0.04	*	(1,1)	P(34)	13287.68	0.04
(1,1)	R(18)	13340.46	0.05	*	(1,1)	R(33)	13351.89	0.07
(1,1)	R(18)	13340.45	0.02	*	(1,1)	P(35)	13286.70	0.03
(1,1)	P(20)	13302.70	0.0	*	(1,1)	R(34)	13352.41	0.04
(1,1)	P(20)	13302.69	-0.01	*	(1,1)	P(36)	13285.49	0.01
(1,1)	R(19)	13341.34	0.03	*	(1,1)	R(35)	13352.92	0.03
(1,1)	P(21)	13301.76	0.06	*	(1,1)	R(36)	13353.40	0.02
(1,1)	P(21)	13301.70	0.0	*	(1,1)	R(36)	13353.40	0.02
(1,1)	R(20)	13342.12	-0.07	*	(1,1)	P(38)	13283.07	0.05
(1,1)	R(20)	13342.21	0.02	*	(1,1)	R(37)	13353.84	0.02
(1,1)	P(22)	13300.60	0.11	*	(1,1)	P(39)	13281.80	0.06
(1,1)	P(22)	13300.69	0.0	*	(1,1)	P(40)	13280.45	0.01
(1,1)	R(21)	13343.14	0.09	*	(1,1)	R(39)	13354.59	0.02
(1,1)	P(23)	13299.70	0.02	*	(1,1)	P(41)	13279.09	-0.02
(1,1)	P(23)	13299.67	-0.01	*	(1,1)	P(42)	13277.75	0.0
(1,1)	R(22)	13343.94	0.05	*	(1,1)	P(43)	13276.31	-0.03
(1,1)	R(22)	13343.91	0.02	*	(1,1)	P(44)	13274.79	-0.11
(1,1)	R(22)	13343.91	0.02	*	(1,2)	R(10)	13084.33	-0.09
(1,1)	P(24)	13298.73	0.07	*	(1,2)	P(12)	13062.07	-0.18
(1,1)	P(24)	13298.69	0.03	*	(1,2)	P(12)	13062.26	0.03
(1,1)	R(23)	13344.81	0.09	*	(1,2)	R(12)	13086.48	-0.09
(1,1)	P(25)	13297.66	0.03	*	(1,2)	P(14)	13060.34	-0.25
(1,1)	P(25)	13297.64	0.01	*	(1,2)	P(14)	13060.64	0.05
(1,1)	R(24)	13345.62	0.09	*	(1,2)	R(14)	13088.65	-0.08
(1,1)	R(24)	13345.51	-0.02	*	(1,2)	P(16)	13058.76	-0.19
(1,1)	R(24)	13345.55	0.02	*	(1,2)	P(16)	13059.04	0.09
(1,1)	P(26)	13296.67	0.07	*	(1,2)	R(16)	13090.76	-0.13
(1,1)	P(26)	13296.58	-0.02	*	(1,2)	P(18)	13057.35	0.0
(1,1)	R(25)	13346.34	0.02	*	(1,2)	P(18)	13057.40	0.05
(1,1)	P(27)	13295.61	0.06	*	(1,2)	R(18)	13092.95	-0.14
(1,1)	R(26)	13347.12	0.02	*	(1,2)	P(20)	13055.55	-0.23
(1,1)	R(26)	13347.08	-0.02	*	(1,2)	P(20)	13055.83	0.05
(1,1)	R(26)	13347.07	-0.03	*	(1,2)	R(20)	13095.22	-0.05
(1,1)	P(28)	13294.58	0.09	*	(1,2)	P(22)	13054.01	-0.22
(1,1)	P(28)	13294.47	-0.02	*	(1,2)	P(22)	13054.27	0.04
(1,1)	R(27)	13347.91	0.06	*	(1,2)	R(22)	13097.41	-0.02
(1,1)	P(29)	13293.44	0.02	*	(1,2)	P(24)	13052.46	-0.22
(1,1)	R(28)	13348.81	0.03	*	(1,2)	P(24)	13052.77	0.07
(1,1)	R(28)	13348.57	-0.01	*	(1,2)	R(24)	13099.34	-0.03
(1,1)	R(28)	13348.53	-0.05	*	(1,2)	P(26)	13051.22	0.04
(1,1)	R(29)	13349.33	0.05	*	(1,2)	R(26)	13101.62	-0.06
(1,1)	P(31)	13291.32	0.08	*	(1,2)	P(28)	13049.70	0.04
(1,1)	R(30)	13350.02	0.06	*	(1,2)	R(28)	13103.79	0.04
(1,1)	R(30)	13349.94	-0.02	*	(1,2)	P(30)	13048.18	0.05
(1,1)	R(30)	13350.01	0.05	*	(1,2)	R(30)	13105.76	0.01
(1,1)	P(32)	13290.32	0.20	*	(1,2)	P(32)	13046.65	0.07
(1,1)	R(31)	13350.08	0.07	*	(1,2)	R(32)	13107.70	0.01
(1,1)	P(33)	13289.04	0.05	*	(1,2)	P(34)	13044.97	-0.04
(1,1)	R(32)	13351.20	-0.03	*	(1,2)	R(34)	13109.53	-0.01
(1,1)	R(32)	13351.25	0.02	*	(1,2)	P(36)	13043.50	0.11

BAND	ROT LINE	OBS FREQ (CM-1)	DEV	*	BAND	ROT LINE	OBS FREQ (CM-1)	DEV
(1,2)	R(36)	13111.36	0.07	*	(2,2)	R(22)	13316.04	0.02
(1,2)	P(38)	13041.75	0.04	*	(2,2)	P(24)	13273.32	0.03
(1,2)	R(38)	13112.92	0.01	*	(2,2)	P(26)	13270.58	0.07
(1,2)	P(40)	13039.90	-0.07	*	(2,2)	P(28)	13267.67	0.05
(1,2)	R(40)	13114.35	-0.06	*	(2,2)	P(30)	13264.67	0.09
(1,2)	P(42)	13038.07	-0.06	*	(2,2)	P(32)	13261.47	0.06
(1,2)	P(44)	13036.15	-0.04	*	(2,2)	P(34)	13258.21	0.15
(1,2)	P(46)	13033.93	-0.19	*	(2,2)	R(34)	13320.82	0.13
(1,2)	P(48)	13031.74	-0.16	*	(2,2)	P(36)	13254.66	0.14
(2,1)	P(2)	13547.76	0.04	*	(2,2)	R(36)	13320.56	0.17
(2,1)	R(2)	13552.60	0.11	*	(2,2)	P(38)	13251.04	0.23
(2,1)	P(4)	13545.63	-0.02	*	(2,2)	P(40)	13247.09	0.23
(2,1)	R(4)	13554.31	0.08	*	(2,2)	P(42)	13242.88	0.21
(2,1)	P(6)	13543.47	-0.01	*	(3,4)	P(12)	13014.94	0.18
(2,1)	R(6)	13555.88	0.02	*	(3,4)	P(14)	13012.61	0.20
(2,1)	P(8)	13541.25	0.04	*	(3,4)	P(16)	13010.02	0.05
(2,1)	R(8)	13557.48	0.09	*	(3,4)	P(18)	13007.39	-0.04
(2,1)	P(10)	13538.97	0.12	*	(3,4)	P(20)	13004.69	-0.09
(2,1)	R(10)	13558.84	0.03	*	(3,4)	P(22)	13001.98	-0.04
(2,1)	P(12)	13536.44	0.05	*	(3,4)	P(24)	12998.95	-0.16
(2,1)	R(12)	13560.07	-0.03	*	(3,4)	P(26)	12995.91	-0.16
(2,1)	P(14)	13533.66	0.03	*	(3,4)	P(28)	12992.67	-0.19
(2,1)	R(14)	13561.30	0.03	*	(4,2)	P(34)	13647.21	-0.16
(2,1)	P(16)	13531.13	-0.02	*	(4,2)	P(36)	13639.61	-0.25
(2,1)	R(16)	13562.31	0.01	*	(4,2)	R(36)	13701.41	-0.03
(2,1)	P(18)	13528.37	0.0	*	(4,2)	R(36)	13701.31	-0.13
(2,1)	R(18)	13563.17	-0.02	*	(4,4)	R(26)	13237.59	-0.17
(2,1)	P(20)	13525.43	-0.03	*	(4,4)	R(26)	13236.09	-0.19
(2,1)	P(22)	13522.40	-0.03	*	(6,7)	P(20)	12869.38	0.09
(2,1)	P(24)	13519.21	-0.04	*	(6,7)	P(22)	12864.39	-0.21
(2,1)	P(26)	13515.87	-0.06	*	(6,7)	P(24)	12859.66	0.07
(2,1)	P(28)	13512.45	0.0	*	(6,7)	R(24)	12899.84	-0.13
(2,1)	P(30)	13508.83	0.04	*	(6,7)	P(26)	12854.05	-0.19
(2,1)	P(32)	13504.92	-0.03	*	(6,7)	P(28)	12848.42	-0.10
(2,1)	P(34)	13500.97	0.07	*	(6,7)	R(28)	12895.24	0.27
(2,2)	P(2)	13298.73	0.15	*	(7,7)	P(8)	13070.40	-0.29
(2,2)	P(2)	13298.71	0.13	*	(7,7)	P(10)	13064.14	-0.21
(2,2)	P(4)	13296.67	0.09	*	(7,7)	P(12)	13058.49	-0.05
(2,2)	P(6)	13294.59	0.07	*	(7,7)	R(12)	13080.10	-0.12
(2,2)	P(8)	13292.43	0.01	*	(7,7)	P(16)	13051.94	-0.14
(2,2)	P(10)	13290.32	0.05	*	(7,7)	P(18)	13047.22	-0.01
(2,2)	P(12)	13286.07	0.02	*	(7,7)	R(18)	13077.19	-0.05
(2,2)	P(14)	13285.80	0.02	*	(7,7)	P(20)	13041.91	-0.08
(2,2)	P(16)	13283.43	-0.01	*	(7,7)	R(20)	13075.08	-0.04
(2,2)	R(16)	13314.80	0.01	*	(7,7)	P(22)	13036.30	-0.04
(2,2)	P(18)	13281.05	0.02	*	(7,7)	R(22)	13072.49	-0.06
(2,2)	R(18)	13315.85	0.0	*	(7,7)	P(24)	13030.29	0.01
(2,2)	P(20)	13278.52	-0.02	*	(7,7)	R(24)	13069.56	0.04
(2,2)	R(20)	13317.05	0.05	*	(7,7)	P(26)	13023.78	-0.01
(2,2)	P(22)	13275.99	0.02	*	(7,7)	R(26)	13066.14	0.13

BAND	ROT LINE	OBS FREQ (CM-1)	DEV	*	BAND	ROT LINE	OBS FREQ (CM-1)	DEV
(7,7)	P(28)	13016.94	0.08	*	(10,7)	R(14)	13562.64	0.06
(7,7)	P(32)	13001.75	0.15	*	(10,7)	P(16)	13534.45	0.01
(8,7)	P(10)	13233.50	-0.23	*	(10,7)	R(16)	13558.90	-0.04
(8,7)	P(12)	13229.41	-0.13	*	(10,7)	P(18)	13527.15	-0.08
(8,7)	R(12)	13249.50	0.06	*	(10,7)	P(20)	13519.23	-0.08
(8,7)	P(14)	13224.80	-0.08	*	(10,7)	R(20)	13549.34	-0.11
(8,7)	R(14)	13247.90	-0.01	*	(10,7)	P(22)	13510.57	-0.11
(8,7)	P(16)	13219.70	-0.07	*	(10,7)	R(22)	13543.41	-0.15
(8,7)	R(16)	13245.88	-0.01	*	(10,7)	P(24)	13501.17	-0.12
(8,7)	P(18)	13214.19	0.01	*	(10,7)	R(24)	13536.72	-0.14
(8,7)	R(18)	13243.39	0.03	*	(10,7)	P(26)	13490.96	-0.18
(8,7)	P(20)	13208.23	0.13	*	(10,7)	R(26)	13529.11	-0.23
(8,7)	R(20)	13240.48	0.16	*	(10,7)	P(28)	13480.03	-0.16
(8,7)	P(22)	13201.69	0.15	*	(10,7)	R(28)	13520.75	-0.20
(8,7)	R(22)	13236.94	0.20	*	(10,9)	P(4)	13105.76	0.17
(8,7)	P(24)	13194.65	0.17	*	(10,9)	P(6)	13102.69	0.13
(8,7)	R(24)	13232.84	0.21	*	(10,9)	P(8)	13099.10	0.12
(8,7)	P(26)	13187.12	0.22	*	(10,9)	R(10)	13110.61	0.0
(8,7)	R(26)	13227.97	0.02	*	(10,9)	R(11)	13109.64	0.04
(8,7)	P(28)	13179.03	0.24	*	(10,9)	R(12)	13108.85	0.01
(8,7)	R(28)	13222.64	0.15	*	(10,9)	R(12)	13108.74	-0.10
(8,7)	P(30)	13170.33	0.19	*	(10,9)	P(14)	13084.90	0.06
(8,7)	R(30)	13216.66	0.03	*	(10,9)	R(13)	13107.62	-0.11
(8,7)	P(32)	13161.14	0.21	*	(10,9)	R(14)	13106.36	-0.11
(8,7)	R(32)	13210.40	0.04	*	(10,9)	R(14)	13106.38	-0.09
(8,7)	P(34)	13151.12	-0.03	*	(10,9)	P(16)	13078.63	-0.14
(9,7)	R(10)	13413.09	0.27	*	(10,9)	R(15)	13104.97	-0.08
(9,7)	R(12)	13411.46	0.25	*	(10,9)	R(15)	13105.09	0.04
(9,7)	R(14)	13409.22	0.20	*	(10,9)	P(17)	13075.75	-0.05
(9,7)	P(16)	13381.15	0.27	*	(10,9)	P(17)	13075.91	0.11
(9,7)	R(16)	13406.42	0.17	*	(10,9)	R(16)	13103.31	-0.16
(9,7)	P(18)	13374.73	0.20	*	(10,9)	P(18)	13072.26	-0.22
(9,7)	R(18)	13403.06	0.19	*	(10,9)	R(17)	13101.62	-0.11
(9,7)	P(20)	13367.84	0.23	*	(10,9)	R(17)	13101.84	0.11
(9,7)	R(20)	13399.03	0.16	*	(10,9)	P(19)	13068.97	-0.04
(9,7)	P(22)	13360.26	0.16	*	(10,9)	R(18)	13099.62	-0.20
(9,7)	R(22)	13394.38	0.13	*	(10,9)	P(20)	13065.17	-0.20
(9,7)	R(24)	13389.06	0.09	*	(10,9)	R(19)	13097.61	-0.14
(9,7)	P(26)	13343.33	0.09	*	(10,9)	P(21)	13061.72	0.14
(9,7)	R(26)	13383.01	-0.02	*	(10,9)	R(20)	13095.36	-0.15
(9,7)	P(28)	13333.95	0.08	*	(10,9)	P(22)	13057.42	-0.20
(9,7)	R(28)	13376.39	0.0	*	(10,9)	R(21)	13092.62	-0.28
(9,7)	R(30)	13366.89	-0.15	*	(10,9)	R(21)	13092.94	-0.16
(9,7)	R(32)	13360.74	-0.22	*	(10,9)	P(23)	13053.47	-0.03
(10,7)	P(8)	13556.71	0.18	*	(10,9)	P(23)	13053.21	-0.29
(10,7)	R(8)	13569.42	0.10	*	(10,9)	R(22)	13090.26	-0.24
(10,7)	P(10)	13552.11	0.12	*	(10,9)	P(24)	13049.01	-0.19
(10,7)	P(12)	13546.88	0.07	*	(10,9)	R(23)	13087.53	-0.20
(10,7)	R(12)	13565.58	0.06	*	(10,9)	R(23)	13087.70	-0.03
(10,7)	P(14)	13541.07	0.11	*	(10,9)	P(25)	13044.62	-0.12

BAND	ROT LINE	OBS FREQ (CM-1)	DEV	*	BAND	ROT LINE	OBS FREQ (CM-1)	DEV
(10,9)	P(25)	13044.58	-0.16	*	(11,9)	P(20)	13206.56	-0.13
(10,9)	R(24)	13084.54	-0.24	*	(11,9)	R(19)	13238.29	-0.05
(10,9)	P(26)	13039.93	-0.17	*	(11,9)	P(21)	13202.21	0.04
(10,9)	R(25)	13081.49	-0.14	*	(11,9)	P(21)	13202.16	-0.01
(10,9)	R(26)	13078.05	-0.25	*	(11,9)	R(20)	13235.43	0.11
(10,9)	P(28)	13029.93	-0.35	*	(11,9)	P(22)	13197.36	-0.05
(10,9)	R(28)	13070.69	-0.36	*	(11,9)	R(21)	13232.15	0.09
(10,9)	R(30)	13062.59	-0.38	*	(11,9)	P(23)	13192.43	-0.03
(11,7)	P(8)	13703.26	0.0	*	(11,9)	P(23)	13192.39	-0.07
(11,7)	P(10)	13698.18	-0.02	*	(11,9)	R(22)	13228.62	0.04
(11,7)	P(12)	13692.49	0.14	*	(11,9)	P(24)	13187.34	0.06
(11,7)	R(12)	13710.15	-0.10	*	(11,9)	R(23)	13225.12	0.27
(11,7)	P(14)	13685.71	0.02	*	(11,9)	P(25)	13182.09	0.23
(11,7)	R(14)	13706.45	0.10	*	(11,9)	R(24)	13221.00	0.12
(11,7)	P(16)	13678.21	0.0	*	(11,9)	P(26)	13176.45	0.24
(11,7)	R(16)	13701.67	0.09	*	(11,9)	P(27)	13170.48	0.17
(11,7)	P(18)	13669.87	0.0	*	(11,9)	R(26)	13212.41	0.22
(11,7)	R(18)	13695.95	0.06	*	(11,9)	P(28)	13164.36	0.20
(11,7)	P(20)	13660.69	0.06	*	(11,9)	R(28)	13202.70	0.27
(11,7)	R(20)	13689.35	0.09	*	(11,9)	P(30)	13151.35	0.26
(11,7)	P(22)	13650.58	0.10	*	(11,9)	R(30)	13191.83	0.28
(11,7)	R(22)	13681.77	0.14	*	(11,9)	P(32)	13137.21	0.27
(11,7)	P(24)	13639.45	0.09	*	(11,9)	R(32)	13179.65	0.15
(11,7)	R(24)	13673.19	0.22	*	(11,9)	P(34)	13121.73	0.08
(11,7)	R(26)	13663.45	0.23	*	(11,9)	R(34)	13165.75	-0.45
(11,7)	P(28)	13614.33	0.26	*	(11,9)	P(36)	13104.79	-0.37
(11,7)	R(28)	13652.68	0.34	*	(12,7)	P(14)	13817.37	-0.02
(11,7)	P(30)	13600.17	0.38	*	(12,7)	P(16)	13808.46	-0.07
(11,7)	R(30)	13640.62	0.37	*	(12,7)	R(16)	13830.30	0.03
(11,7)	P(32)	13584.70	0.35	*	(12,7)	P(18)	13796.62	0.06
(11,7)	P(34)	13567.68	0.18	*	(12,7)	R(18)	13822.64	0.16
(11,9)	R(12)	13253.43	-0.15	*	(12,7)	P(20)	13787.50	0.08
(11,9)	R(14)	13250.06	-0.18	*	(12,7)	R(20)	13814.01	0.17
(11,9)	P(16)	13222.65	-0.09	*	(12,7)	P(22)	13775.16	0.12
(11,9)	R(15)	13246.11	-0.17	*	(12,7)	R(22)	13803.74	0.07
(11,9)	P(17)	13218.97	-0.06	*	(12,7)	P(24)	13761.49	0.09
(11,9)	R(16)	13246.08	-0.03	*	(12,7)	R(24)	13792.02	-0.07
(11,9)	P(18)	13214.85	-0.27	*	(12,7)	P(26)	13746.22	-0.14
(11,9)	R(17)	13243.06	-0.07	*	(12,7)	R(26)	13778.39	-0.64
(11,9)	P(19)	13210.91	-0.10	*	(12,7)	P(28)	13729.17	-0.70
(11,9)	R(18)	13241.00	-0.15	*				

VITA

Terence Lamar Tipton, son of Lamar and Sylvia Tipton, was born October 13, 1953 in Annapolis, Maryland. He graduated from Fort Lee High School, Fort Lee, New Jersey in 1972. He received a B.A. in chemistry with high distinction from Rutgers University in 1976, and entered the graduate program in chemistry at The Pennsylvania State University in 1977.

DISTRIBUTION LIST FOR TM 82-181

Commander (NSEA 0342)
Naval Sea Systems Command
Department of the Navy
Washington, DC 20362 — Copies 1 and 2

Commander (NSEA 9961)
Naval Sea Systems Command
Department of the Navy
Washington, DC 20362 — Copies 3 and 4

Defense Technical Information Center
5010 Duke Street
Cameron Station
Alexandria, VA 22314 — Copies 5 through 10